PETROCHEMICAL CONTRAINTS ON GENERATION OF THE PEACH SPRING TUFF SUPERERUPTION MAGMA, ARIZONA, NEVADA, CALIFORNIA

By

William Oliver Frazier

Thesis

Submitted to the Faculty of the

Graduate School of Vanderbilt University

in partial fulfillment of the requirements for

the degree of

MASTER OF SCIENCE

in

Earth and Environmental Sciences

August 2013

Nashville, Tennessee

Approved:

Professor Calvin F. Miller

Professor Guil Gualda

To my family, whose love makes all things possible.

ACKNOWLEDGEMENTS

I owe a deep debt of gratitude to Professors Calvin Miller and Guil Gualda for guiding me through the Master's Thesis process; I will forever cherish their wisdom and support that has helped me grow, personally and professionally. I would also like to thank the rest of the Earth and Environmental Science department for making my experience at Vanderbilt University an unforgettable one, specifically Professor David Furbish for uncountable ah-hah moments, Shelly Donohue, Siobhan Fathel and Tyler Doane for their constant support (and putting up with my antics in the cubicle farm), and Ayla Pamukcu, Abraham Padilla, Tamara Carley, and especially Susanne McDowell for their work with or related to the Peach Spring Tuff and northern Colorado River extensional corridor. I also appreciate the efforts of Teri Sparkman, Jewell Beasley-Stanley, and Aaron Covey, who do all the little things that keep the department running.

I would also like extend my thanks to Chris Fisher and Jeff Vervoort for their invaluable assistance at the Washington State geoanalytical lab, without whose efforts, we would never have been able to obtain such a beautiful and complete isotopic dataset, to Charles Ferguson for his field expertise and humor, to Professor Jonathan Miller, Marsha Lidzbarski, and Sarah Overton for sharing their Peach Spring Tuff and Mojave data, to Professor Rod Metcalf for providing an extensive set of volcanic data from the northern Colorado River extensional corridor, and to Mark Ghiorso for help executing the MELTS modeling.

This research was made possible by National Science Foundation Grant NSF-EAR-0911726.

TABLE OF CONTENTS

Page

DEDICATION ii

ACKNOWLEDGEMENTS iii

LIST OF TABLES vi

LIST OF FIGURES vii

CHAPTER I: INTRODUCTION 1

1.1. Supereruptions 1

1.2. The Peach Spring Tuff 4

CHAPTER II: GEOLOGIC BACKGROUND 7

2.1. Southern Black Mountain Volcanic Center, Arizona 7

2.2. Northern Colorado River Extensional Corridor 11

CHAPTER III: METHODS 15

3.1. Elemental Data 15

3.2. Isotopic Data 16

3.3. Modeling 18

3.3.1. Closed system trace element modeling 18

3.3.2. Open system modeling 21

CHAPTER IV: ELEMENTAL AND ISOTOPIC COMPOSITION OF PST 27

4.1. Elemental Geochemistry 27

4.2. Isotope Geochemistry 29

CHAPTER V: PEACH SPRING PETROGENESIS 32
5.1. Isotopic Constraints 32
5.1.1. A single Peach Spring Tuff Magma 32
5.1.2. Isotopic Constraints on Source Materials 33
5.2. Elemental Constraints on Petrogenetic Conditions 41
5.3. Evaluation of Magma-Generating Processes 47
5.3.1. Closed system models 48
5.3.2. Open system models 52
5.3.3. Timing of Hybridization 61
CHAPTER VI: IMPLICATIONS 62
CHAPTER VII: CONCLUSIONS 67
APPENDIX 69
REFERENCES 113

LIST OF TABLES

Page

1. Isotope data for the southern Black Mountain volcanic center....9

2. Estimates of NCREC crustal compositions, Old Woman Mountains....14

3. Felsic partition coefficients used during modeling....20

4. Model mineral assemblages that best reproduce PST composition....21

5. End members used during open system trace element modeling....23

6. Representative AFC modeling parameters....26

7. Isotope data for Peach Spring Tuff....30

8. Average Peach Spring Tuff, NCREC Compositions....34

9. Example of binary mixing results....53

10. Closed system parameters for partial melting of AFC end members....55

LIST OF FIGURES

Page

1. Generalized geologic map showing PST outflow deposit extent 3

2. Generalized stratigraphy, southern Black Mountains 8

3. Map showing extent of northern Colorado River extensional corridor 11

4. εHf vs. εNd for PST and SBMVC 36

5. $^{208}Pb/^{204}Pb$ and $^{207}Pb/^{204}Pb$ vs. $^{206}Pb/^{204}Pb$ for PST, NCREC, and SBMVC 37

6. εNd vs. $^{87}Sr/^{86}Sr_{initial}$ 38

7. Ba and Sr vs. SiO_2 43

8. Zr and Zr/Sr vs. SiO_2 44

9. Chondrite-normalized REE 45

10. Feldspar saturation temperature vs. H_2O; rhyoliteMELTS model results 47

11. Equilibrium partial melting model results 50

12. Perfect fractional crystallization model results 52

13. Bulk mixing model results 54

14. AFC model, enriched basalt + 1.7 Ga bulk crust/melt 57

15. AFC model, enriched basalt/WSWPST1 + 1.4 Ga melt 58

16. Two stage AFC model, enriched basalt + 1.7 Ga melt 59

17. AFC model, enriched basalt + <1.7 Ga melt/>1.7 Ga melt 60

18. Rb vs. Nb+Y 63

19. Spider diagram (Continental crust-normalized extended trace element) 64

CHAPTER I

INTRODUCTION

1.1. Supereruptions

The term supereruption refers to short-term eruptive events that eject over 1000 km^3 of volcanic material (i.e. eruptions of VEI 8 [volcanic explosivity index] and above [Newhall and Self, 1982]), a vastly greater volume than that produced during more frequent small-scale eruptions that typify most volcanism. For comparison, the 1815 eruption of Indonesia's Mt. Tambora, a VEI 7 eruption whose global climatic impacts were so large that they led to what is referred to as "the year without a summer," ejected ~100 km^3 of pyroclastic material (Self et al, 2004). Clearly, if an eruption one-tenth as large as the *smallest* supereruption can have such profound worldwide effects, larger eruptions have the potential to be globe-altering events. The high impact of such events demands further inquiry into how supereruption-forming magma bodies are assembled and evolve.

It has been proposed that sustained, elevated basaltic flux from the mantle is necessary to thermally and mechanically mature the crust to a state that is conducive to generating super-eruptive systems (e.g. de Silva, 2008; de Silva and Gosnold, 2007). Supereruptions can occur in diverse tectonic settings: in active subduction zones, both as part of volcanic arcs (e.g. South America, Indonesia) or in association with back-arc extension (e.g. New Zealand), in rift settings and large igneous provinces (e.g. Parana-Etendeka), and others in intraplate provinces of extension- (e.g. Basin and Range) or hotspot-related magmatism (e.g. Yellowstone-Snake River Plain) (Bryan et al., 2010; Mason

et al., 2004). In arc settings, an elevated basaltic flux may be the result of relatively fast plate convergence involving thickened crust (Hughes and Mahood, 2008). In non-arc settings, elevated mantle output may instead be due to the presence of a plume (Condie, 2001), regional lithospheric extension (Daley and DePaolo, 1992), or delamination of lower crust (Anderson, 2005) that facilitates decompression melting of rising asthenosphere.

Models of silicic magma petrogenesis attempt to evaluate the roles the mantle and crust play in generating evolved compositions. Mantle-derived basalts may induce partial melting by introducing heat and volatiles to the crust while contributing relatively little mass to the resulting melts (e.g. Christiansen and McCurry, 2008), or they may evolve by closed-system fractional crystallization as they ascend through the crustal column (Bowen, 1915, and many subsequent references). Alternatively, both processes may occur, and in many instances they may be coupled, with concurrent assimilation of crustal melt produced by the release of latent heat from the crystallizing basalt (AFC processes; DePaolo, 1981). Whether AFC occurs in the deep crust (MASH or 'hot' zones where partial melting and hybridization occur [Hildreth and Moorbath, 1988; Annen et al., 2006]) or during periods of storage at shallower crustal depths could depend on the thermal conditions of the upper and lower crust (Perry et al., 1993). Whether most silicic magma is generated by closed- or open-system processes and has a larger mass contribution from the mantle or crust remains a topic of great debate.

This paper focuses on the petrogenesis of the magma that erupted to form the Peach Spring Tuff (PST), a supereruption-derived ignimbrite blanketing large areas of northwestern Arizona, southern Nevada, and southeastern California (Figure 1). In this study, I report new elemental data (major and 35 trace elements) for 13 pumice clasts and

a single magmatic enclave as well as isotopic data (Sr, Nd, Pb, and Hf) for 8 pumice clasts and two magmatic enclaves from the PST. I compare these and existing data for the PST with other felsic magmatism of similar age from its source region, the northern Colorado River extensional corridor (NCREC), to demonstrate the compositional uniqueness of the PST and infer distinct petrogenetic processes by which the giant PST magma body was formed. Finally, I discuss the potential role that the conditions leading to the assembly of the PST magma body may have played in generating a super-sized eruption.

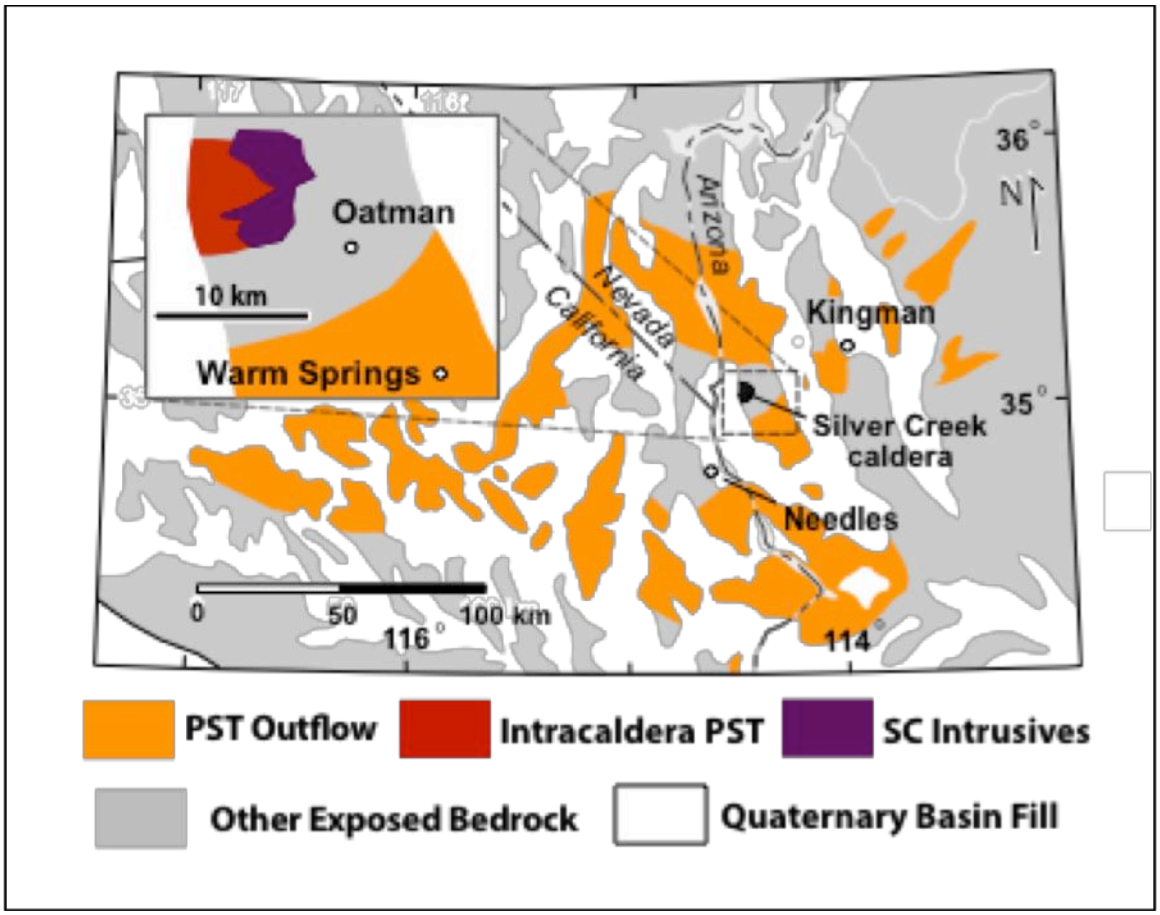

Figure 1. Generalized geologic map showing the source caldera and extent of the PST outflow deposit (adapted from Ferguson et al., 2013). SC denotes Silver Creek caldera.

1.2. The Peach Spring Tuff

Young and Brennan (1974) originally defined the PST in the region between Kingman and Peach Springs, Arizona and used it to study the geomorphological evolution of the boundary between the Colorado Plateau and the Basin and Range. Glazner et al. (1986) used phenocrysts assemblages and field observations to correlate tuff outcrops as far west as Barstow, California with the PST, broadening its known extent to the central Mojave Desert. Buesch (1992) estimated that the PST outflow sheet had a minimum volume of 640 km^3 dense rock equivalent (and thus much greater than the 1000 km^3 minimum volume that defines supereruptions) spread over an areal extent of at least 32,000 km^2. As the only laterally extensive deposit in a highly extended region with difficult-to-correlate stratigraphic sections (Glazner et al. 1986), the PST has been used as a valuable marker horizon in tectonic studies (e.g. Hillhouse and Wells, 1991).

The PST erupted from the southern Black Mountains volcanic center (SBMVC) prior to the initiation of extension within the NCREC during the early Miocene (Faulds et al., 2001; Metcalf, 2004). During the early Miocene, the NCREC was a locus of converging northward- and southward- migrating magmatic fronts (Faulds et al., 2001), each potentially associated with removal of the subducting Farallon slab by inward propagating tears from its edges. These magmatic fronts represent the time-space evolution of a mid-Tertiary ignimbrite flare up, with many large ash flow tuffs having erupted from volcanic fields throughout the Great Basin (NV and Utah) and southern Basin and Range (AZ and NM, Humphreys, 1995). The PST itself, however, was an isolated supereruption within a region otherwise characterized by copious lavas, small explosive eruptions, and large upper crustal plutons. This is somewhat of an oddity, as many supereruptions erupt from

relatively long-lived individual centers that produce multiple large-magnitude eruptive events (e.g. Yellowstone, Wyoming; Toba, Indonesia; Cerro Galan, Argentina; Valles, New Mexico) or during episodes of ignimbrite flare-up characterized by supervolcanism on a regional scale (e.g. Sierra Madre Occidental [Ferrari et al., 2002]; Altiplano Puna volcanic complex, Andes [de Silva 2008]).

The PST was a geologically instantaneous eruptive event and is comprised of one (Glazner et al., 1986), or perhaps two (Varga et al., 2004) cooling units. Nielsen et al. (1990) obtained an age of 18.5 ± 0.2 Ma for PST sanidine phenocrysts using Ar/Ar techniques, but Ferguson et al. (2013) report an updated and more precise age of 18.78 ± 0.02 Ma (using the 28.20 Ma age of the Fish Canyon sanidine standard; [Kuiper et al., 2008]; Nielsen et al.'s less precise age also adjusts to 18.8 Ma using the revised standard). Despite the efforts of many workers, the location of the source caldera of the PST was not recognized until recently. Isopach maps of PST thickness (Young and Brennan, 1974) and paleomagnetic studies (Hillhouse and Wells, 1991) suggested the caldera was near the intersection of Nevada, Calidronia, and Arizona, possibly in the Newberry or southern Black Mountains or beneath the sediment fill of the intervening Colorado River trough. Detailed field studies of the Black Mountains stratigraphy near Oatman, AZ (Pearthtree, 2007) allowed Ferguson et al. (2008) to correlate trachytic ignimbrite within Silver Creek caldera (formerly the Alcyone caldera of Thorson, 1971) with PST outflow. Identical sanidine $^{40}Ar/^{39}Ar$ ages and near-identical phenocrysts assemblages for the intracaldera trachyte and the rhyolitic outflow confirmed Silver Creek caldera as the source of the PST (Ferguson et al., 2013).

The PST is typically strongly welded and ranges in thickness from 10-15m distally (Barstow, CA) up to 130m in more proximal localities (e.g. southern Black Mountains, AZ,

and Piute Mountains, CA) (Ferguson et al., 2013; Glazner et al., 1986). Pamukcu et al. (2013) present geochemical and textural evidence suggesting that the PST magma body was compositionally and thermally zoned, with an outflow comprised of early-erupted phenocryst-poor, high-silica rhyolite and the phenocryst-rich intracaldera trachyte representing a remobilized basal cumulate. Resporption features and Ti-rich rims of zircon indicate that the trachyte was affected by a late-stage heating event, which may have remobilized the cumulate and triggered eruption of the PST (Pamukcu et al., 2013). The outflow's mineral assemblage contains between 4 and 14% phenocrysts (Young and Brennan, 1974) and it is dominated by feldspar (primarily sanidine with subordinate plagioclase) with minor biotite, hornblende, pyroxene, and rare quartz. Sphene is notably abundant, and it is joined by a rich assemblage of other accessory minerals (zircon, allanite, chevkinite, apatite, opaque minerals)(e.g. Glazner et al., 1986; Pamukcu et al., 2013). The trachyte has a similar phenocryst population but is more crystal-rich (~35%; Thorson, 1971; Ferguson et al., 2013) than the outflow, and sphene is less prominent. This accessory mineral assemblage is unusual among NCREC volcanic rocks and unknown among other Miocene-aged ash flow tuffs in the region (Gusa et al., 1987).

CHAPTER II

GEOLOGIC BACKGROUND – POTENTIAL SOURCES FOR PEACH SPRING PETROGENESIS

2.1 The Southern Black Mountain Volcanic Center, Arizona

The Southern Black Mountains, Arizona, experienced intense, protracted magmatism during the early Miocene. Activity began roughly 19.5 Ma and was pervasive until ~17 Ma (e.g. Faulds et al., 2001; Lang et al., 2008; McDowell et al., 2012), but persisted intermittently until ~13.7 Ma (Pearthree et al., 2009). In addition to the PST, magmatism manifested by copious lava flows and domes, abundant dikes and sills, a few small and one larger pyroclastic deposit (Cook Canyon Tuff), and a shallow intrusive complex that was largely confined to the Silver Creek caldera (Ferguson et al., 2013). The stratigraphic section (Figure 2) lies unconformably over crystalline Proterozoic basement and here I divide the units into pre- and post-PST sequences. The pre-PST volcanics erupted ~19.5-18.8 Ma and consist of >1 km of homogeneous, phenocryst-rich trachyte lava flows overlain by basalt-trachyandesite and trachyite lavas and the trachytic Cook Canyon Tuff, the only large (~100 km^3) ignimbrite in the region other than the PST (Faulds et al., 2001). The post-PST volcanics include ~0.5 km of trachyte and rhyolite lava flows, domes, and small pyroclastic deposits, mostly representing block-and-ash flows (~18.5-17 Ma; McDowell et al., 2011), capped by a much younger (~13.7 Ma; Pearthree et al., 2009) olivine basalt unit.

With the exception of this capping basalt, the entire suite of Miocene volcanic and plutonic rocks appears to be broadly cogenetic (Dewitt et al., 1986; McDowell et al., 2011). The SBMVC as a whole shows a diverse range of isotopic characteristics (Table 1, McDowell

in prep.). Isotopic data for these trachytes and the rest of the SBMVC are consistent with significant mixing of enriched mantle lithosphere and Proterozoic crust of the Mojave terrane (McDowell et al., 2012), which has been used to explain the petrogenesis of other Miocene-age NCREC magmas (see below; e.g. Falkner et al., 1995; Metcalf et al., 1995; Bachl et al., 2001).

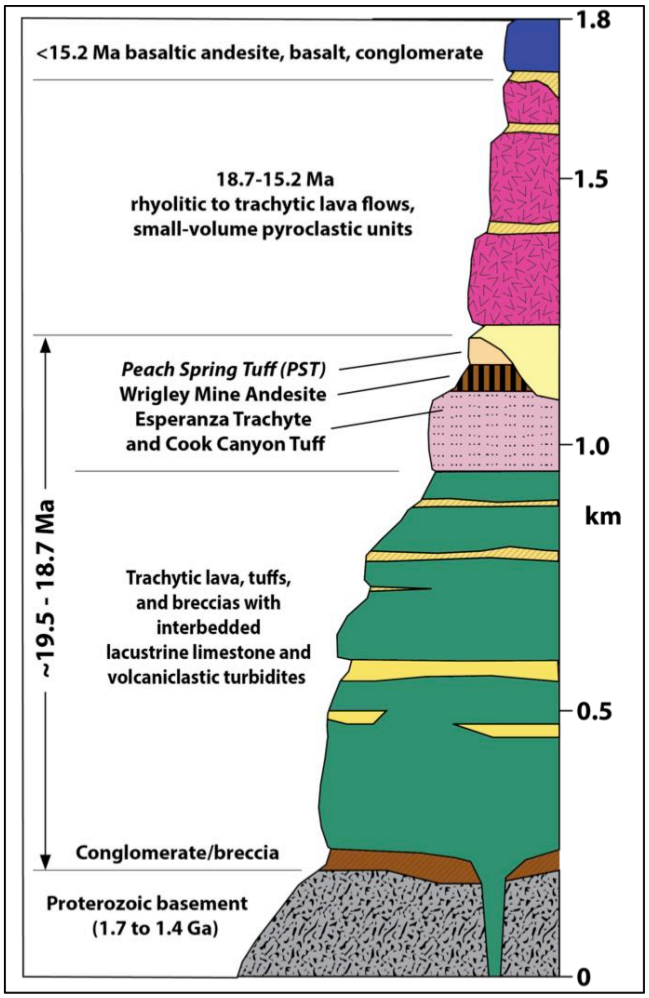

Figure 2. Generalized stratigraphic column for the SBMVC region. The Miocene section lies unconformably on Proterozoic crystalline rocks ranging in age from ~1.7 to 1.4 Ga. Basement in vicinity of Silver Creek Caldera appears to be 1.7 Ga, with increasing amounts of 1.4 Ga granite the northwest toward the Colorado River (Faulds et al., 2001). The Gold Road (SCM-41) and Alcyone (sample SCM-34) formations are part of the large section of pre-PST trachyte lavas.

Table 1. Isotope data for the Southern Black Mountain Volcanic Center, excluding the Peach Spring Tuff (McDowell et al., in prep).

Sample	PSK-14	PSK-7	PST-11	SCM-34	SCM-41	SCM-1	SCM-30	SCM-42	MP-1
Group	Pre-PST	Pre-PST	Pre-PST	Pre-PST	Pre-PST	Post-PST	Post-PST	Post-PST	Post-PST
Formation	Wrigley Mine	Hershey Squirt	Esperanza	Alcyone Trachyte	Gold Road Trachyte	Feldspar Porphyry Dike	Feldspar Porphyry Dike	Felsic Dike	Moss Porphyry
$^{87}Sr/^{86}Sr$	0.70933±10[1]	0.71008±10	0.70944±14	0.71115±8	0.71052±8	0.71046±8	0.70958±10	0.71324±8	0.71054±6
$^{87}Sr/^{86}Sr_{initial}$[2]	0.70925	0.71003	0.70930	0.71098	0.71037	0.71015	0.70946	0.71110	0.71088
$^{143}Nd/^{144}Nd$	0.512212±14	0.512083±14	0.512193±11	0.512041±7	0.512039±7	0.512193±14	0.512194±12	0.512155±13	0.512104±15
εNd[3]	-8.3	-10.8	-8.7	-11.6	-10.0	-9.6	-8.7	-9.4	-10.4
$^{176}Hf/^{177}Hf$	0.282552±4	0.282415±4	0.282502±4	0.282390±2	0.282461±2	0.282487±4	0.282536±3	0.282479±4	0.282446±4
εHf[4]	-8.2	-13.1	-10.0	-14.0	-11.5	-10.5	-8.8	-10.8	-12.0
$^{206}Pb/^{204}Pb$[5]	18.4513±28	18.4072±28	18.3477±21	18.1867±28	18.3758±35	18.2755±27	18.2450±22	18.3135±22	18.2696±36
$^{207}Pb/^{204}Pb$	15.6173±26	15.6157±26	15.6088±20	15.5984±27	15.6151±29	15.6019±26	15.5987±21	15.6105±21	15.6064±30
$^{208}Pb/^{204}Pb$	39.1675±62	39.1719±62	39.0056±50	39.0465±66	39.1831±68	39.0810±61	39.0089±53	39.1217±54	39.1177±69

1. Uncertainties for Sr, Nd, and Hf isotopes are the in-run errors and refer to the sixth decimal place.
2. $^{87}Sr/^{86}Sr_{initial}$ values calculated using concentrations tabulated in the appendix (A.Table 2). All corrections were performed using an age of 18.8 Ma.
3. εNd calculated using the present day CHUR value of 0.512638.
4. εHf calculated using the present day CHUR value of 0.282785.
5. Uncertainties for Pb isotopes are the in-run errors and refer to the third decimal place.

Table 1 (con't.)

MPe-1	WSE-3a	SCM-38	TIP-1	SCM-5a	SCM-26	SCM-27b	SIT-1	SIT-1b	SIT-2
Post-PST	Pre-PST	Post-PST	Post-PST	Post-PST	Post-PST	Post-PST	Post-PST	Post-PST	Post-PST
Enclave in Moss Porphyry	Cook Canyon Tuff	Times Porphyry	Times Porphyry	Felsic Dike	Mafic Dike	Enclave in Times Porphyry		Enclave in Moss Porphyry	
0.71042±6	0.71038±10	0.71593±8	0.71132±8	0.71593±8	0.71019±10	0.71103±8	0.71054±16	0.70918±8	0.70981±8
0.71031	0.71018	0.71214	0.71016	0.71202	0.71012	0.70966	0.71013	0.70913	0.70977
0.512197±7	0.512122±7	0.512126±7	0.512134±7	0.512171±7	0.512050±12	0.512208±7	0.512155±14	0.512157±13	0.512104±7
-8.6	-10.1	-10.0	-9.8	-9.1	-10.4	-8.4	-9.4	-9.4	-10.4
0.282511±3	0.272465±2	0.282450±3	0.282456±2	0.282510±3	0.282450±4	0.282535±2	0.282498±2	0.282501±3	0.282414±2
-9.7	-11.3	-11.8	-11.6	-9.7	-11.8	-8.8	-10.2	-10.0	-13.1
18.2868±36	18.2836±36	18.2845±36	18.2898±35	18.3577±36	18.4917±22	18.3025±35	18.2477±27	18.3178±23	18.4263±35
15.6066±31	15.6053±31	15.6052±30	15.6089±30	15.6067±30	15.6248±21	15.6050±30	15.6033±26	15.6030±21	15.6136±30
39.1199±71	39.0609±75	39.0957±70	39.1205±68	39.2780±70	39.2867±52	39.0611±70	39.1237±61	38.9528±53	39.1490±68

2.2. The Northern Colorado River Extensional Corridor

The SBMVC is part of the northern Colorado River extensional corridor (NCREC), a region of moderately to highly extended crust within the greater Basin and Range province. Comprising a 50-100 km wide area straddling the Arizona, Nevada, and California borders (Figure 3), the NCREC lies at the eastern edge of the Mojave crustal province of Bennett and DePaolo (1987). Proterozoic basement rocks in this region yield Nd model ages between 2.0 and 2.3 Ga and are characterized by higher $^{208}Pb/^{204}Pb$ and $^{207}Pb/^{204}Pb$ values for a given $^{206}Pb/^{204}Pb$ than the younger (1.8 to 2.0 Ga Nd model ages) Arizona crustal province directly to the east (Bennett and DePaolo, 1987; Wooden and Miller, 1990; Feuerbach et al., 1998).

Figure 3. Map showing the extent of the NCREC and the boundary between the Mojave and Arizona crustal provinces (from Bachl et al., 2001). Numbers denote middle Miocene plutons: 1—Boulder City; 2—Nelson; 3—Aztec Wash; 4—Searchlight; 5—Spirit Mountain; 6—Mirage (part of Spirit Mountain Batholith); 7—Sacramento; 8—Mt. Perkins; 9—Wilson Ridge.

Since its formation in the Proterozoic, the Mojave province has experienced numerous periods of major crustal modification (Miller and Wooden, 1994). Multiple events from 1.76 to 1.62 Ga introduced into the crust and subsequently metamorphosed abundant gabbroic to granitic intrusions. Moderate amounts of granitic magma with relatively minor exposed mafic input intruded the eastern Mojave at ca. 1.4 Ga. A diabase dike swarm at 1.1 Ga marked the final Proterozoic modification event, after which magmatism in the region was quiescent until the Mesozoic. Mesozoic magmatism in the Mojave occurred during the Triassic and Jurassic from ~245 to 145 Ma, with subduction–related magmatism continuing during the Cretaceous until ~65 Ma. Much of this Mesozoic magmatism, expressed as exposed intrusive rocks all across the Mojave, may consist of hybrid compositions generated by interaction of enriched-mantle-derived mafic magma and existing Proterozoic crust (Miller and Wooden, 1994).

The most extensive period of crustal modification in the NCREC region during the Cenozoic occurred in the Miocene from ca. 20 to 11 Ma (Faulds et al., 2001; Metcalf, 2004), and is associated with the inception of Basin and Range extension. The onset of volcanism preceded extension by ca. 1-4 Ma (Faulds et al., 2001), and largely consisted of calc-alkaline, mafic to intermediate small-volume lava flows, domes, and pyroclastic eruptions. Syn-extensional volcanics became progressively more bimodal with time, although tholeiitic and alkalic compositions were much more prevalent than silicic magmas after major extension. From 17 to 15 Ma, nine shallow crustal plutons intruded the base of the Miocene section in the NCREC. Isotopic data for Searchlight (Bachl et al. 2001) and Aztec Wash plutons (Falkner et al. 1995) may indicate hybridization processes similar to those proposed for the petrogenesis of Mesozoic magmas were operating in the NCREC during

the Miocene, but cannot rule out the possibility that the bulk of these magmas were derived by partial melting of a previously hybridized Mesozoic crust (Metcalf, 2004). Isotopic data and sparse inherited zircons (both Proterozoic and Mesozoic) suggest that the NCREC magmas were products of mixing between mantle and crustal end materials, but as exposed Mesozoic crustal rocks in the NCREC are isotopically similar to Miocene rocks, it is possible that hybridization occurred earlier and that the Miocene magmas were direct partial melts of Mesozoic crust (Falkner et al., 1995).

Because erosion and tectonic denudation have been relatively limited since the early Miocene, only the shallowest part of the crust beneath the volcanic sequence can be directly inspected, and evaluating the nature of the crustal column requires extrapolation from the limited local basement exposures and more extensive exposures elsewhere in the NCREC. Exposed basement in the vicinity of Silver Creek caldera appears mostly to correlate with the older (>/~1.7 Ga) Mojave complex of metamorphosed granitic and supracrustal rock, with lesser ~1.4 Ga granite. The proportion of 1.4 Ga granite increases to the northwest along and across the Colorado River (Faulds et al., 2001). The mean compositions of Proterozoic and Mesozoic rock units in the vicinity of the Old Woman Mountains (CA) along the westernmost edge of the NCREC are given in Table 2 (from Miller and Wooden, 1994). Although this area is ~60 km west of Silver Creek caldera, it exposes a range of initial crustal depths and the lithologies are similar to those exposed throughout the eastern Mojave province, and thus they provide a useful crustal model that constrains what may have underlain the SBMVC while it was active. Given the obvious evidence elsewhere in the NCREC for hybridization involving crustal contributions, which I will show

is also required for the PST, this model proves useful for evaluation of the genesis of this "super" magma body.

Table 2. Estimates of igneous crustal compositions in the vicinity of the Old Woman Mountains, CA, eastern edge of the NCREC. From Miller and Wooden (1994).

Crustal Type	Mean Jurassic	Mean Cretaceous	Mean Mesozoic	Mean 1.7 Ga	1.4 Ga Granite
SiO_2	63.58	67.12	66.65	68.33	67.67
TiO_2	0.76	0.47	0.51	0.70	0.59
Al_2O_3	15.65	15.61	15.62	13.70	13.59
Fe_2O_3	5.15	3.13	3.40	6.00	5.61
MnO	0.09	0.04	0.05	0.09	0.07
MgO	2.20	1.04	1.19	1.51	2.85
CaO	3.55	2.78	2.89	2.31	2.72
Na_2O	3.85	4.02	4.00	2.63	3.04
K_2O	4.14	3.71	3.77	3.84	6.48
P_2O_5	0.25	0.12	0.14	0.25	0.40
Rb	108	97	118	123	121
Th	9.5	10.9	10.6	12.2	11.4
U	1.60	1.70	1.40	1.60	1.50
Nb	17.2	22.0	19.4	21.3	20.3
Ba	1229	1188	1066	954	1011
Y	41	23	22	54	38
Sr	358	108	500	216	361
La	75	52	47	61	54
Ce	145	102	90	116	103
Pr	16.1	12.0	10.2	13.1	11.6
Nd	58	47	38	48	43
Sm	10.2	7.8	7.0	8.6	7.8
Eu	2.53	1.79	1.54	1.88	1.71
Gd	7.6	5.4	4.97	6.3	5.66
Tb	1.17	0.84	0.83	1.11	7.20
Dy	7.48	4.94	5.0	7.2	6.1
Ho	1.56	0.95	0.99	1.52	1.26
Er	4.25	2.37	2.56	4.21	3.38
Tm	0.61	0.31	0.34	0.61	0.47
Yb	3.69	1.74	1.99	3.75	2.85
Lu	0.54	0.25	0.28	0.54	0.41
$^{87}Sr/^{86}Sr$	0.7119	0.7109	0.7110	0.7400	0.7308
$^{143}Nd/^{144}Nd$	-11.4	-11.8	-11.7	-18	-14.9

CHAPTER III

METHODS

My primary goals in this study are to compare the elemental and isotopic composition of the PST relative to that of other felsic magmas within the NCREC region as well as to determine the materials and processes involved in the petrogenesis of the giant magma body. Herein, I combine new and existing data for the PST and NCREC with trace element and isotopic models describing partial melting and/or fractional crystallization of potential parental materials. In this effort, I include estimates of regional crust described above (Miller and Wooden, 1994) and new analyses of units from the SMBVC (McDowell et al., in prep). I also compare the compositions of the PST with regional volcanics (Metcalf, 2004, and personal commun., 2012) and shallow, chilled granites representative of similarly felsic melts in the NCREC (Harper et al., 2004; Bachl et al., 2001; Walker et al., 2007).

3.1. Elemental Data

Pumice and fiamme samples were coarsely crushed using agate mortar and pestle and treated to three successive ultrasonic baths (deionized water, 0.1 M HCl with 2% H_2O_2, deionized water) to reduce the effects of weathering and surface alteration. Samples were then finely ground into powder using a steel shatterbox. Samples were sent to Activation Laboratories (Ancaster, Ontario, Canada) for whole rock geochemical analysis. Actlabs

measured major and trace elements using a combination of fusion inductively coupled plasma mass spectrometry (ICP-MS) and instrumental neutron activation analysis (INAA).

3.2. Isotopic Data

Samples dissolution, chemical separations, and analyses for Nd, Hf, and Pb isotope systems followed the methods outlined in Patchett and Ruiz (1987), Vervoort and Patchett (1996), and Prytulak et al., (2006). Briefly, samples were dissolved in steel jacketed Teflon bombs at 160°C for 5 days using a 10:1 HF/HNO_3 mixture. The initial separation of Hf, Sr, and Nd from these solutions was performed using cation exchange columns containing AG50W-X8 (200-400 mesh) resin. Subsequent purification of each element is as follows, and is further described in the references above. Hafnium aliquots were further purified using Ln spec resin and followed the methods of Munker et al. (2001). Neodymium aliquots were purified from the LREE aliquot using Ln spec resin. Strontium aliquots were purified using micro-columns (0.18 mL resin volume) with Sr-spec resin and HNO_3.

All isotopic compositions were measured using a ThermoFinnigan Neptune™ multi-collector inductively coupled mass spectrometer (MC-ICP-MS) at Washington State University (see Vervoort et al., 2004). During these analyses, the following isotopic values were measured for the Nd and Hf standards: Ames Nd: $^{143}Nd/^{144}Nd = 0.512119\pm13$ and $^{145}Nd/^{144}Nd = 0.348422\pm14$ (2σ SD, n=15), JMC 475 Hf: $^{176}Hf/^{177}Hf = 0.282144\pm5$ and $^{178}Hf/^{177}Hf = 1.467224\pm35$ (2σ SD, n=23). Both Nd and Hf measurements were normalized to the accepted values for these standards: Ames Nd: $^{143}Nd/^{144}Nd = 0.512138$ and $^{145}Nd/^{144}Nd = 0.348420$; JMC 475 Hf: $^{176}Hf/^{177}Hf = 0.282160$ and $^{178}Hf/^{177}Hf = 1.467170$ (Vervoort and Blichert-Toft, 1999). Values of $^{143}Nd/^{144}Nd_{CHUR(0)} = 0.512638$ and

$^{147}Sm/^{144}Nd_{CHUR(0)}$ = 0.1966 (Jacobsen and Wasserburg, 1980) and $^{176}Hf/^{177}Hf_{CHUR(0)}$ = 0.282785 and $^{176}Lu/^{177}Hf_{CHUR(0)}$ = 0.0336 (Bouvier et al., 2008) were used to calculate εNd and εHf.

Solutions for Pb isotopic analyses were dissolved and prepared separately to minimize Pb blanks. Roughly 150 mg of powder was dissolved in ~10 mL of HF/HNO_3 in sealed 15 mL Savillex® beakers at ~140°C on a hot plate for ~24 hours. Pb separation was performed using Biorad® AG 1-X8 anion resin in 0.45 mL volume shrink Teflon columns. Solutions were loaded onto columns using 0.5 M HBr and Pb was eluted using 6.0 M HCl. Samples were then dried down, and separation was performed a second time on the same columns. Following the second pass through the columns, samples were evaporated, treated with concentrated HNO_3 to destroy organics, then re-dissolved in 2% HNO_3. Samples were doped with Tl following the procedure of White et al. (2000). The NBS 981 Pb standard with a target concentration of 150 ppb Pb and 150 ppb Tl was run after every third sample. Mass bias in the Pb isotopic analyses was corrected using a $^{205}Tl/^{203}Tl$ value of 2.3885. To compensate for the difference in mass bias between Tl and Pb, we followed the procedure of White et al. (2000) and Albarede et al. (2004) and normalized the mass bias corrected values with the following accepted values for the NBS 981 Pb standard: $^{206}Pb/^{204}Pb$ = 16.9405, $^{207}Pb/^{204}Pb$ = 15.4963, $^{208}Pb/^{204}Pb$ = 36.7219 (Galer, 1999). During these analyses, the following mass bias corrected values were measured for the NBS 981 Pb standard, also doped with Tl: $^{206}Pb/^{204}Pb$ = 16.9358±0.0028, $^{207}Pb/^{204}Pb$ = 15.4918±0.0025, $^{208}Pb/^{204}Pb$ = 36.7001±0.0059 (2 SD). Accordingly, the average normalization factors for Pb on the days of analyses were: 1.000276 for $^{206}Pb/^{204}Pb$, 1.000294 for $^{207}Pb/^{204}Pb$, and 1.000593 for $^{208}Pb/^{204}Pb$.

Sr analyses were corrected for mass fractionation using $^{88}Sr/^{86}Sr = 0.1194$ and normalized using the NBS-987 Sr standard, for which a mean value of $^{87}Sr/^{86}Sr = 0.710207$ was measured over three days of analyses. The uncertainties in the Sr isotopic compositions are better assessed from the reproducibility of the standard rather than the in-run error. The average reproducibility (2 SD) for the $^{87}Sr/^{86}Sr$ value of NBS-987 was ±0.00026.

3.3. Modeling

3.3.1. Closed System Trace Element Modeling

Isotopic similarity between the Mesozoic basement (Table 2), the pre-PST trachytes of the Alcyone and Gold Road formations (Table 1), and the PST (Table 8; see Section 4.2) allow for the possibility that these materials may be related by petrogenetic processes that approximate a closed system. I evaluate the plausibility of the Mesozoic crust and the trachytes as sources for the PST magma with equilibrium batch partial melting and perfect (Rayleigh) fractional crystallization models, respectively. Partial melting models were calculated using the equation:

$$C_l = \frac{C_0}{(F + D - FD)} \quad (1)$$

where C_l is the concentration of a trace element in the resulting liquid, C_0 is the initial concentration of the trace element in the parent solid, F is the melt fraction, and D is the bulk partition coeffecient of the trace element calculated from a set of mineral/melt

partition coefficients and the mineral modes (mass proportion) of the residual assemblage. Fractional crystallization models were calculated in a similar manner using the equation:

$$C_l = C_0 F^{(D-1)} \quad (2)$$

where the parameters are the same as above. These simple models require that equilibrium is penetrative (all phases are in full equilibrium, no zoning) for the partial melting scenario and surface-only (internal zoning of crystals is preserved) for crystallization. While this cannot be entirely correct, it is reasonable to assume that equilibrium is more closely approached during deep, probably slower melting, than for shallower, presumably faster, crystallization processes.

As the potential source materials (parent magmas and source rocks) range in silica content from ~63 to 67 wt.% SiO_2 and the melt phase must have equal or higher SiO_2, I adopt partition coefficients (Table 3) obtained from glass and phenocryst analyses of natural rhyolite (Bachmann et al., 1995; Colombini et al., 2011; Sisson 1991; Sisson and Bacon, 1992) and experimental work on granite and dacite (Watson, 1979 and Fujimaki, 1986, respectively). The partition coefficients for a rhyolitic liquid may slightly overestimate the compatibility of trace elements in phenocrysts in both crystallizing trachytic liquids and melting granodioritic source rocks. Therefore, the melt fractions necessary to reproduce the PST composition from fractional crystallization of the trachytes should be regarded as maxima. I selected a suite of large ion lithophile, high field strength, and rare-earth elements (REE) for the modeling. Model outputs are normalized to average continental crust (Rudnick and Gao, 2003) and plotted on extended trace element diagrams.

Table 3. Felsic melt partition coefficients used for trace element modeling; from Bachmann et al. (1995), Colombini et al. (2011), Sisson (1991), Sisson and Bacon (1992), Watson (1979) and Fujikami (1986).

	Qtz	Biot	Plag	Kspar	Cpx	Opx	Hbl	Apat	Zirc	Titan	Gar.
Rb	0.00	2.00	0.00	0.70	0.03	0.01	0.00		0.06	0.02	0.01
Th	0.00	0.00	0.00	0.00	0.20	0.14	0.01		7.30	9.10	
U	0.00	0.00	0.02	0.00	0.90	0.10	0.01		22.10	3.65	
Nb	0.00	2.90	0.00	0.00	0.60	0.31	2.00		0.27	61.10	
Ba	0.00	4.40	0.61	17.10	0.10	0.10	0.08		0.20	0.00	0.02
Y	0.00	0.02	0.02	0.10	3.00	1.10	13.50		79.80	344.00	130
Sr	0.00	0.10	12.50	7.40	0.50	0.17	0.40	2.30	0.24	0.90	0.02
La	0.00	0.00	0.40	0.06	0.65	0.00	1.40	28.20	0.08	79.00	0.001
Ce	0.00	0.01	0.30	0.02	1.30	0.01	3.20	37.40	0.70	161.00	0.01
Pr	0.00	0.01	0.24	0.00	2.00	0.01	5.57	47.84	0.49	280.00	0.06
Nd	0.00	0.01	0.20	0.00	3.06	0.02	9.70	61.20	0.34	412.00	0.4
Sm											
Eu	0.00	0.00	0.10	0.00	4.70	0.03	15.50	98.50	3.26	614.00	6.4
Gd	0.00	0.30	3.10	2.90	4.82	0.06	10.80	17.10	8.75	553.00	11.2
Tb	0.00	0.20	0.08	0.10	4.94	0.12	14.90	95.60	11.10	648.00	24.4
Dy	0.00	0.04	0.04	0.00	5.07	0.25	16.19	76.36	29.37	619.00	53.2
Ho	0.00	0.01	0.02	0.00	5.20	0.52	17.60	61.00	59.48	480.00	116
Er	0.00	0.01	0.00	0.00	4.39	0.66	15.24	50.37	79.83	404.00	140
Tm	0.00	0.02	0.00	0.01	3.70	0.85	13.20	41.60	122.15	352.00	170
Yb	0.00	0.02	0.00	0.02	2.58	0.64	11.26	33.88	127.77	256.00	154
Lu	0.00	0.03	0.01	0.03	1.80	0.48	9.60	27.60	166.34	166.00	140

Elemental (see Section 5.2) and Ti-in-zircon (Pamukcu et al, 2013) data indicate that the PST was a relatively hot and dry magma. Assuming that these conditions can be traced back to its petrogenesis, I utilized residual and fractionating assemblages poor in hydrous minerals such as amphibole and biotite in the modeling. While they do not list mineral modes, Dewitt et al. (1986) observed between 30% and 40% phenocrysts of plagioclase, clinopyroxene, and orthopyroxene with minor quartz, biotite, and alkali feldspar within the Gold Road formation. They note ~35% phenocrysts of alkali feldspar, plagioclase, biotite, and minor pyroxene and quartz in lava flows of the Alcyone formation. As such, I performed the fractional crystallization models using feldspar-dominated assemblages containing variable amounts of pyroxene and biotite. These mineral assemblages were

modified in numerous ways (e.g. adding small amounts of hornblende or accessory minerals such as zircon and apatite to the mineral assemblage, decreasing the amount of feldspar and/or increasing the amount of pyroxene) to determine the range of possible evolutionary paths. In each model, melt compositions were calculated for melt fractions between 0.1 and 1.0 at 0.1 increments in order to explore the degrees of partial melting and fractional crystallization required to roughly reproduce the PST composition. Roughly fifteen mineral assemblages for each parent were modeled; the modes of the assemblages that appear to best reproduce the PST composition as well as plausible ranges for the melt fraction are given in Table 4.

Table 4. Representative modes of mineral assemblages and melt fractions that best reproduce the Peach Spring Tuff trace element composition during closed-system partial melting and/or fractional crystallization.

Parent	Gold Road Trachyte	Alcyone Trachyte	Mean Jurassic	Mean Cretaceous	Mean Mesozoic
Process	Fractional Crystallization	Fractional Crystallization	Partial Melting	Partial Melting	Partial Melting
Quartz	5	4.7	5	10	10
Biotite	5	15	0	5	0
Plagioclase	65	40	55	40	45
Alkali Feldspar	5	30	20	25	25
Clinopyroxene	10	10	10	10	10
Orthopyroxene	10	0	9	10	10
Hornblende	0	0	0	0	0
Apatite	0	0.25	0.45	0	0
Zircon	0	0.5	0.05	0	0
Sphene	0	0	0	0	0
Garnet	0	0	0.5	0	0
F	0.65-0.75	0.7-0.8	0.3-0.4	0.35-0.45	0.45-0.55

3.3.2 Open System Modeling – Bulk Mixing, Assimilation and Fractional Crystallization

Isotopic evidence for mixing of ancient Proterozoic crustal and enriched-mantle materials is preserved in igneous rocks across the NCREC (Metcalf, 2004; Faulds et al., 2001), including the PST (see Section 5.1). I created simple (bulk) mixing and AFC models to assess the plausibility of such an origin for the PST, using estimates of enriched mantle (Miller and Wooden, 1994; Farmer et al., 1989) and various Proterozoic lithologies (Miller and Wooden, 1994) as end members (see Table 5 for examples). Bulk mixing models track the changes in the concentrations of Sr and Nd, $^{87}Sr/^{86}Sr$, and $^{143}Nd/^{144}Nd$ as a function of melt fraction, *F*, using the equations:

$$\varepsilon_{mix} = \frac{\varepsilon_1[a]_1 F}{[a]_1 F + [a]_2(1-F)} + \frac{\varepsilon_2[a]_2(1-F)}{[a]_1 F + [a]_2(1-F)} \quad (3)$$

and

$$[a]_{mix} = [a]_1 F + [a]_2(1-F) \quad (4)$$

where ε is an isotope ratio, a refers to an element, brackets signify a concentration, and subscripts *1* and *2* refer to the end members involved in the mixing. We also considered a class of energy-constrained AFC models (e.g. Spera and Bohrson, 2001) that may be more realistic in terms of how such open-system processes work in reality. However, due to lack of constraints on some important variables (e.g. the enthalpies, heat capacities, and parameters describing the relationships between melt fractions and temperature within the subsystems [magma, wallrock] of the model) we did not pursue this approach beyond preliminary efforts.

Table 5. End members used in open-system (binary mixing and AFC) modeling. Crustal melts were produced by closed system partial melting of bulk crustal end members (see Section 5.3.2 for a discussion of the basis for and parameters used in the partial melting models).

	Enriched Basalt[1]	Enriched Mantle[2]	Depleted Mantle[1]	WSWPST1	1.7 Ga bulk crust[1]
[Sr]	900	1100	100	1514	200
[Nd]	50	60	40	104	50
$^{87}Sr/^{86}Sr$	0.7065	0.707	0.7025	0.7091	0.74
$^{143}Nd/^{144}Nd$	0.51233	0.51218	0.51315	0.51222	0.51172
εNd	-6	-8.9	+10	-8.2	-18

1. Wooden and Miller (1994)
2. Farmer et al. (1989)

Table 5 (con't.)

1.7 Ga crustal melt	<1.7 Ga bulk crust[1]	<1.7 Ga crustal melt	>1.7 Ga bulk crust[1]	1.4 granitic crust[1]	1.4 Ga crustal melt
63	400	127	100	245	100
61	80	97	35	149	69
0.74	0.72	0.72	0.78	0.7308	0.7308
0.51172	0.51172	0.51172	0.51172	0.51187	0.51197
-18	-18	-18	-18	-14.9	-14.9

The AFC models were performed using a spreadsheet program (Keskin, 2012) that utilizes the equations of DePaolo (1981). The main parameters involved in the modeling are the r- and F-values and the bulk partition coefficients of the evolving magma body. The r-value is the ratio of the rate at which mass is assimilated to the rate at which mass is fractionated. The F-value is the non-dimensional mass of the magma body relative to its original mass at any given point during its evolution, tracking both the mass lost due to fractional crystallization and added due to assimilation. The partition coefficients apply to phenocryst/melt fractionation of trace elements (Sr, Nd) during crystallization, while assimilation occurs by bulk mixing with the contaminant composition (wallrock in the treatment of DePaolo, 1981; I also used estimated compositions of melt derived from wallrock as contaminants [cf. Hildreth and Moorbath, 1988, "MASH"]). As the partitioning behavior of trace elements within an evolving magma body will vary as a function of both evolving melt composition (Brophy, 2008) and changes in crystallizing assemblage, I performed two types of AFC models attempting to simulate this behavior. These were a one-stage model in which the partition coefficients were held at intermediate values in an attempt to approximate the average behavior of Sr (estimated to be slightly incompatible early, highly compatible later) and Nd (highly incompatible early, ~neutral later) over the course of the magma's evolution, and a two-stage model in which the partition coefficients were changed after an arbitrary period of AFC had occurred (Table 6). The two-stage model was performed for only one set of end members, while two types of mafic, mantle-derived end member and roughly 25 different crustal end member compositions (see Section 5.3.2) were utilized during one-stage modeling. During the latter, the effects of highly incompatible and highly compatible behavior for both Sr and Nd were also explored.

Table 6. Representative parameters used during AFC modeling. Variable bulk D intends to simulate increasing partition coefficients with increasing silica content in the magma; each set approximates the partitioning behavior of a feldspar dominated mineral assemblage with minor pyroxene and only trace amounts of other minerals. The given ranges of r and F are those that best reproduce the PST isotopic and elemental composition.

Bulk Partition Coefficients, D	Sr	Nd
Mafic	0.75	0.1
Intermediate	3	1
Felsic	8	1.75
Assimilation and Fractional Crystallization Parameters		
r	0.3 – 0.7	
F	0.5 – 0.7	

CHAPTER IV

ELEMENTAL AND ISOTOPIC COMPOSITION OF THE PEACH SPRING TUFF

4.1. Elemental Geochemistry

Elemental data for Peach Spring Tuff pumice, fiamme, and magmatic enclaves are given in the Appendix (A.Table 1). Pumice and fiamme samples range from 66 to 76 wt.% SiO_2 (major element oxides normalized to 100%). Following Pamukcu et al. (2013), I divide them into three groups: high-silica rhyolite (SiO_2 > 74 wt.%), low-silica rhyolite (74 wt.% > SiO_2 > 70 wt.%), and trachyte (SiO_2 < 70 wt%) groups. Two samples are placed in the trachyte group despite silica contents above 70 wt.% on the basis of high Ba and Sr (28556-P1) and REE (WSWPST4B) concentrations (see below). Samples analyzed for this study (marked with asterisks in A.Table 1) include nine high-silica rhyolites, one low-silica rhyolite, and three trachytes, all of which fall broadly within the range of PST compositions analyzed by Pamukcu et al. (2013; also included in A.Table 1 and in figures and discussions that follow).

For the most part, major elements vary regularly with SiO_2 (see Appendix, Figure 1), with Al_2O_3, CaO, TiO_2, Fe_2O_3, and P_2O_5 decreasing monotonically with increasing silica content. All samples have high alkali oxide concentrations, especially K_2O; samples from the high-silica rhyolite group have slightly lower Na_2O and K_2O contents than the low-silica rhyolites and trachytes. The high- and low- silica rhyolite groups show relatively minor trace element distinctions, but are markedly different from the trachytes. Almost all high-silica rhyolite samples exhibit low [Ba](<70 ppm; brackets indicate concentration), [Sr]

(<40 ppm), and [Zr] (<250 ppm), but relatively high [Nb] (>30 ppm), [Rb] (>190 ppm), and [Th] (>30 ppm). Low-silica rhyolites share similar [Ba], [Sr], and [Nb], but are characterized by lower [Rb] (between 120-180 ppm), higher [Zr] (between 270-510 ppm), and higher concentrations for light- and middle-REEs than the high-silica rhyolites. Trachyte samples are marked by much higher [Ba] (500-3000 ppm), [Sr] (>200 ppm), [Zr] (>500 ppm), and LREEs and MREEs than both rhyolite groups. Concentrations of HREEs are similar across the groups.

Eight samples exhibit anomalously high MgO contents for their silica-content; subsequent investigation by scanning electron microscope reveals the presence of subtle, secondary Mg-rich smectite in the petrographic thin sections of these samples that apparently survived acid bath treatments of the powdered material that was analyzed. Likewise, post-emplacement alkali exchange (e.g. Fisher and Schmincke, 1984), indicated by relatively low Na_2O and high K_2O contents, apparently affected thirteen samples, all but one of which fall in the high-silica rhyolite group. Detailed analysis of PST pumice glass suggests that Na_2O <3.2 wt.% demonstrates alkali exchange (McCracken, 2012). This alkali exchange does not appear to have altered the other major and trace element concentrations in these samples, and the values of MgO, Na_2O, and K_2O for affected samples have, been excluded from the calculation of average PST compositions (see Section 5.1.1., Table 8).

The magmatic enclaves *WSWPST1* and *PSTNY01A* are quite different. Sample *WSWPST1* is trachyandesitic with SiO_2 = 57.6 wt.%. Despite its more mafic major element geochemistry, *WSWPST1* exhibits trace element concentrations similar to the trachyte group. Sample *PSTNY01A* has 70 wt.% SiO_2, but otherwise has a very unusual composition

with high Na_2O contents, extremely low CaO, and a combination of trachyte-like (e.g. [Zr] = 635 ppm, high REE concentrations) and HSR-like (e.g. [Ba] = 30 ppm, [Sr] = 11 ppm).

4.2. Isotope Geochemistry

The PST demonstrates remarkably uniform isotope characteristics, with similar Sr, Nd, Hf, and Pb ratios across the HSR, LSR, and trachyte groups (Table 7). With the exception of a lone sample, all PST samples show $^{207}Pb/^{204}Pb$ between 15.602 and 15.615, and $^{206}Pb/^{204}Pb$ between 39.084 and 39.205 (WSWPST-4D is very unusual among rocks of the entire NCREC and is possibly a suspect analysis: =15.673 and 39.327, respectively [currently being reanalyzed]). All pumice and fiamme have $^{208}Pb/^{204}Pb$ ranging from 18.204 to 18.286. Data for εNd (-11.5 to -11.7) and εHf (-13.8 to -14.2) are similarly highly restricted. Initial $^{87}Sr/^{86}Sr$ ratios for PST are also tightly clustered from 0.7112 to 0.7121 except for a sample *PST01-D* (0.7228); this analysis is likely valid (see discussion in Section 5.3.2).

The two magmatic enclaves exhibit isotopic characteristics that are distinct from and much less evolved than PST pumice and fiamme. While Pb isotopic ratios for samples *WSWPST-1* and *PST-NY01A* ($^{208}Pb/^{204}Pb$: 39.022 and 39.226, respectively; $^{207}Pb/^{204}Pb$: 15.886 and 15.605; $^{206}Pb/^{204}Pb$: 18.261 and 18.372) are not significantly displaced from PST values, εNd (-7.5 and-8.3), εHf (-8.7 and -7.4), and initial $^{87}Sr/^{86}Sr$ (0.7091 and 0.7162) are markedly different.

Table 7. Isotopic Composition of the Peach Spring Tuff.

Sample	WSWPST2A*	PST01D*	WSWPST4D*	GJPST1A*
Group	HSR	HSR	LSR	LSR
$^{87}Sr/^{86}Sr$	0.72002±6[1]	0.73159±10	0.71576±22	0.71566±12
$^{87}Sr/^{86}Sr_{initial}$[2]	0.71185	0.72282	0.71124	0.71080
$^{143}Nd/^{144}Nd$	0.512045±7	0.512039±6	0.512042±13	0.512050±13
εNd[3]	-11.6	-11.7	-11.6	-11.5
$^{176}Hf/^{177}Hf$	0.282392±3	0.282396±2	0.282390±4	0.282388±4
εHf[4]	-13.9	-13.8	-14.0	-14.0
$^{206}Pb/^{204}Pb$[5]	18.2863±35	18.2604±36	18.2592±22	18.2035±22
$^{207}Pb/^{204}Pb$	15.6153±29	15.6094±31	15.6726±21 [6]	15.6013±21
$^{208}Pb/^{204}Pb$	39.2033±67	39.2056±70	39.3269±51	39.0845±51

*Samples marked with an asterisk were analyzed using powders prepared from different pieces of pumice than were used for elemental analyses for those same samples.

1. Uncertainties for Sr, Nd, and Hf isotopes are the in-run errors (2σ) and refer to the sixth decimal place.
2. $^{87}Sr/^{86}Sr_{initial}$ values calculated using concentrations tabulated in the appendix (A.Table 1). All corrections were performed using an age of 18.8 Ma.
3. εNd calculated using the present day CHUR value of 0.512638.
4. εHf calculated using the present day CHUR value of 0.282785.
5. Uncertainties for Pb isotopes are the in-run errors (2σ) and refer to the third decimal place.
6. Value in red is highly suspect and in the process of being re-analyzed; the $^{207}Pb/^{204}Pb$ is unrealistically high for the NCREC region.

Table 7 (con't.)

PSTSWA01A Trachyte	PSTG1c* Trachyte	MLPT5D Trachyte	28856P1* Trachyte	WSWPST1* Enclave	PST-NY01A Enclave
0.71145±6	0.71259±6	0.71236±10	0.71180±10	0.70912±8	0.72623±18
0.71125	0.71206	0.71162	0.71122	0.70906	0.71622
0.512037±7	0.512047±7	0.512047±12	0.512053±8	0.512215±7	0.512256±7
-11.7	-11.5	-11.5	-11.4	-8.3	-7.5
0.282380±2	0.282385±2	0.282395±5	0.282388±5	0.282539±2	0.282576±2
-14.3	-14.2	-13.8	-14.0	-8.7	-7.4
18.2048±36	18.2587±36	18.2319±23	18.2183±28	18.2610±27	18.3727±36
15.6025±30	15.6086±30	15.6041±21	15.6039±21	15.5886±26	15.6037±30
39.0989±69	39.1034±69	39.1168±53	39.1403±52	39.0224±62	39.2265±70

CHAPTER V

PEACH SPRING PETROGENESIS

5.1. Isotopic Constraints

5.1.1. A Single Peach Spring Tuff Magma

Pamukcu et al. (2013) suggested that closed-system fractional crystallization of the PST magma body created a zoned magma chamber exhibiting the elemental diversity spanning trachyte and rhyolite compositions. This suggestion assumes that the PST was as single, stratified magma. The remarkable homogeneity of the PST isotope data strongly bolsters the notion that the tuff was formed from a single magma body with an initially uniform composition, with its variability being a result of internal differentiation as implied by Pamukcu et al. (2013). Based on the isotopic uniformity as well as on the elemental and petrographic evidence suggesting a single fractionated magma, I treat the PST as a single magma, I estimate its average elemental composition, and I seek a petrogenetic model consistent with its geochemical characteristics.

To estimate the main composition of the PST, I first calculated the mean compositions of the analyzed HSR, LSR, and trachytes (Table 8). Assuming that the caldera fill was entirely trachyte and the outflow contained minimal trachyte, a modest fraction of LSR, and was dominated by HSR, I calculated estimated mean PST compositions using a range of proportions of caldera fill and outflow. These proportions were consistent with the general assumption that caldera fill is a very substantial proportion, roughly on the

order of 50%, of ignimbrite products of caldera-forming eruptions (cf. Lipman, 1984). Using this estimated bulk composition (or range of possible compositions), it is possible to use elemental constraints to model petrogenesis of the large magma volume that filled the putative PST chamber. This approach assumes that the observed elemental variability is the product of internal differentiation of that chamber and can therefore be ignored. We can also use this mean composition as a basis for comparison with other magmas from the NCREC (averages also given in Table 8) to make inferences about similarities and differences in regional petrogenetic processes (see Section 5.2).

5.1.2. Isotopic Constraints on Source Materials

Because magmatic processes do not appreciably fractionate the isotope ratios of heavy elements, isotope data provide direct information about the materials from which the PST magma body was ultimately derived. Previous studies have demonstrated that isotopes of Pb, Sr, and Nd in rocks of the Mojave province range widely and document contributions of very different materials to Mesozoic and Cenozoic magmas. The PST's isotopic values sit broadly within the array of NCREC compositions (see Appendix, A.Table 3), but are distinct in both their uniformity and more crustal character (Figures 4, 5, and 6). The PST data cluster between εNd = -11.5 and -11.7, and plot further toward the crustal end of the terrestrial εNd-εHf array (Patchett et al., 1981; Vervoort et al., 1999) than pre- and post-PST magmas within the SBMVC (McDowell et al., in prep.) (Figure 4). NCREC $^{208}Pb/^{204}Pb$, $^{207}Pb/^{204}Pb$, and $^{206}Pb/^{204}Pb$ range from roughly 38.5 to 39.3, 15.5 to 15.6, and 17.8 to 18.5, respectively, whereas the PST data show much more restricted ranges (Figure

5). The $^{87}Sr/^{86}Sr_i$ data show a similarly limited range for the PST and plot closer to Proterozoic crustal values compared to the majority of NCREC magmas (Figure 6).

Table 8. Averages of PST compositional groups and NCREC data, estimates of the bulk PST composition. Estimates based on potential outflow to intracaldera ratios and the averages of the high-silica rhyolite, low-silica rhyolite, and trachyte PST composition groups. Isotopic composition is the simple average of all PST isotope data.

	PST High-silica rhyolite	PST Low-silica rhyolite	PST Trachyte	75%HSR 10%LSR 15%Trachyte	60%HSR 10%LSR 30%Trachyte
SiO_2	74.85	72.17	67.66	73.29	72.25
Al_2O_3	13.21	14.84	16.44	13.86	14.34
Fe_2O_3(T)	1.40	1.80	2.97	1.68	1.91
MnO	0.07	0.06	0.07	0.07	0.07
MgO	0.24	0.24	0.69	0.30	0.37
CaO	0.82	0.76	1.48	0.92	1.01
Na_2O	3.46	3.88	3.86	3.56	3.62
K_2O	6.05	6.27	6.21	6.09	6.12
TiO_2	0.22	0.34	0.50	0.28	0.32
$P2O_5$	0.02	0.04	0.12	0.04	0.05
Rb	207	149	132	190	178
Ba	51	93	1448	265	474
Th	31	23.4	17.7	28.4	26.4
U	5.5	2.88	2.61	4.77	4.34
Ta	2.49	2.41	1.26	2.30	2.11
Nb	34	32	20.7	32	29.9
Sr	30	28	260	64	99
Zr	229	437	611	307	365
Hf	7.5	10.9	12.9	8.6	9.5
Y	32	47	30	33	33
La	64	94	157	81	95
Ce	118	190	290	151	177
Pr	12.8	23.8	33	16.9	19.9
Nd	40	87	109	55	66
Sm	7.2	18.0	16.3	9.6	11.0
Eu	0.55	1.34	3.18	1.02	1.42
Gd	5.8	13.0	10.5	7.3	8.0
Tb	0.94	2.05	1.31	1.10	1.16
Dy	5.4	10.8	6.6	6.1	6.3
Ho	1.07	1.95	1.20	1.18	1.20
Er	3.18	4.99	3.34	3.39	3.41
Tm	0.50	0.71	0.47	0.52	0.51
T_{zircon}	823	886	908	842	859

Table 8 (con't.)

45%HSR 10%LSR 45%Trachyte	25%HSR 10%LSR 65%Trachyte	SBMVC[1]	NCREC Volcanics[2]	Chilled Granites[3]
71.20	69.82	68.82	71.57	72.80
14.80	15.47	14.60	14.18	14.35
2.14	2.46	3.62	2.39	1.87
0.07	0.07	0.06	0.08	0.04
0.44	0.53	1.29	0.87	0.54
1.11	1.25	2.40	1.71	1.55
3.67	3.76	3.46	3.31	3.63
6.13	6.17	4.96	5.35	4.85
0.36	0.42	0.59	0.40	0.28
0.07	0.08	0.20	0.15	0.08
167	152	146	161	144
684	963	1088	849	1041
24.4	21.7	21.3	19.9	17.9
3.92	3.35	3.31	2.81	2.74
1.93	1.68	1.46	1.53	1.27
27.9	25.2	22.2	21.9	16.1
133	180	437	502	294
422	498	308	204	173
10.3	11.3	8.1	6.2	4.99
33	32	24.5	19.9	16.5
109	128	77	59	52
203	237	147	102	92
22.9	26.8	15.9	10.5	8.7
76	90	53	36	29.6
12.4	14.2	8.6	6.0	4.80
1.81	2.34	1.60	1.28	0.89
8.7	9.6	6.4	4.33	3.46
1.22	1.29	0.87	0.60	0.55
6.5	6.7	4.55	3.31	2.92
1.22	1.25	0.89	0.64	0.55
3.43	3.46	2.55	1.78	1.73
0.51	0.50	0.38	0.27	0.27
866	890	831	791	798

1. Southern Black Mountain volcanic center magmas; McDowell et al. (in prep)
2. Regional volcanics 65-80 wt.% SiO_2; Metcalf (2004) and Metcalf (personal commun., 2012)
3. Fine-grained granite sills, dikes, and chilled margins of plutons in southern Nevada inferred to represent magmatic input to the upper crust; Bachl et al. (2001), Harper et al. (2004), and Walker et al. (2007)

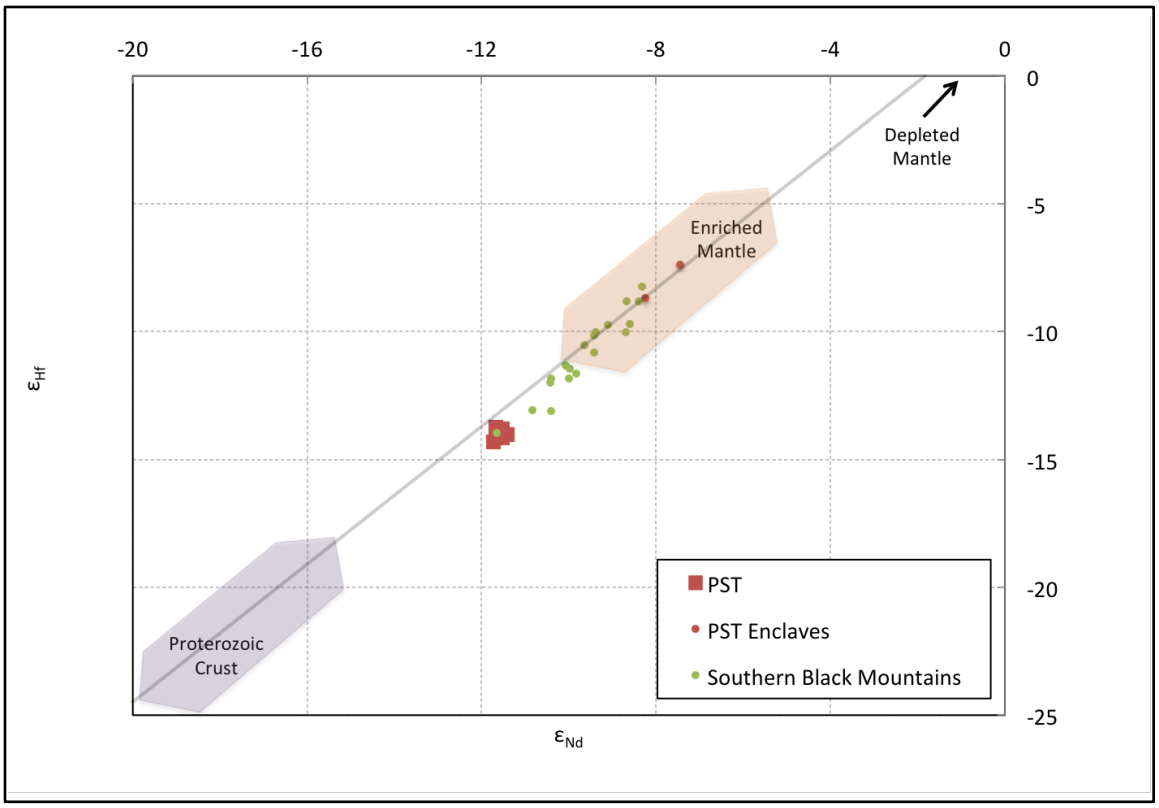

Figure 4. εNd vs. εHf for the PST and other SBMVC magmas. (McDowell et al., in prep). Isotope compositions fall along the terrestrial array (Patchett et al., 1981; Vervoort et al., 1999). The PST's isotopic compositions are more "crustal" than other SMBVC samples, with the exception of SCM-34 (pre-PST Alcyone trachyte) and plot within a more restricted range. Hafnium isotope data are unavailable for enriched Mojave province mantle and Proterozoic crust; therefor, I have estimated likely εHf values of Proterozoic crust and mantle based upon the known range of Mojave province εNd and the known global correlation between εHf and εNd.

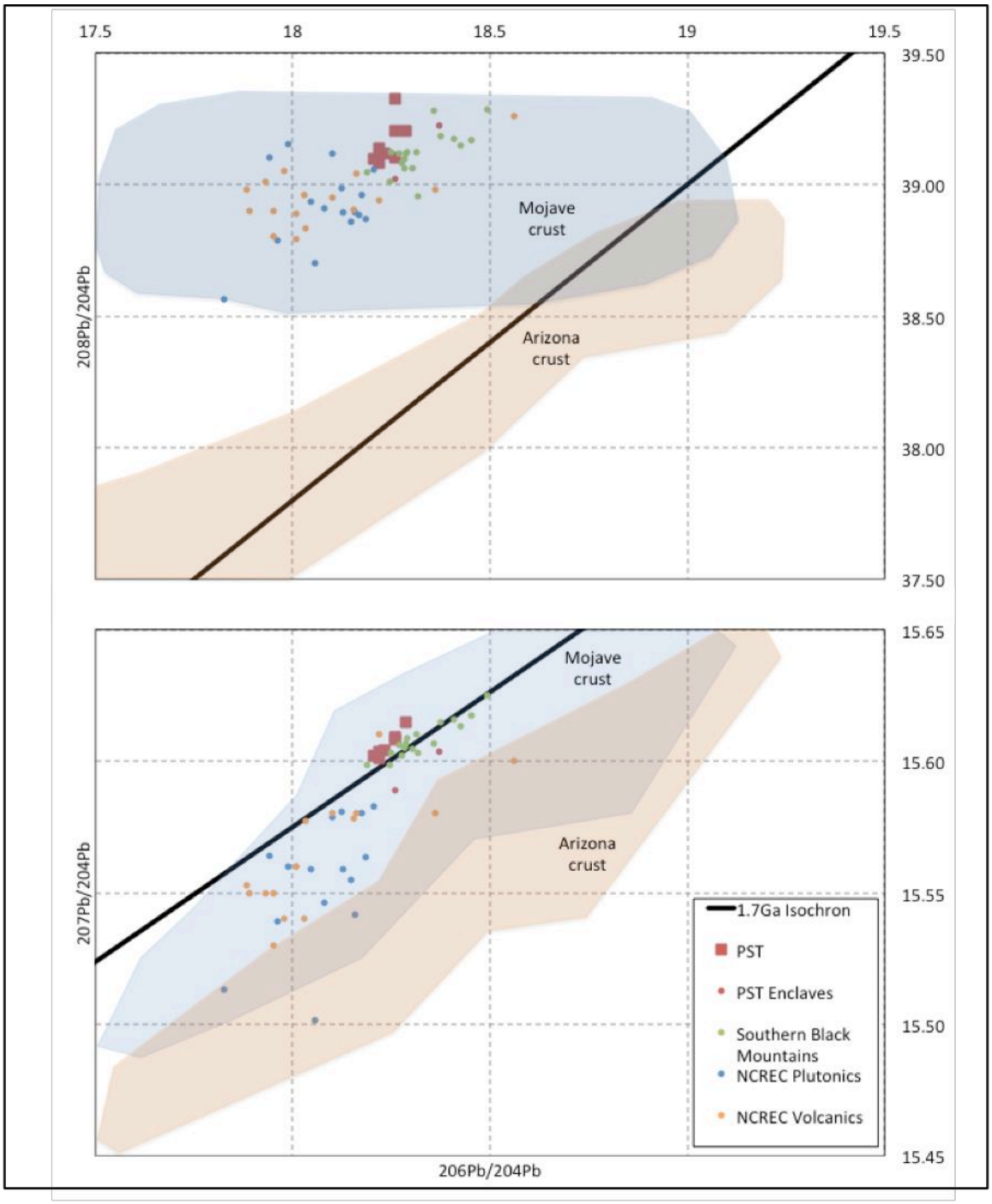

Figure 5. Pb isotope data for the PST and other, similarly felsic NCREC magmas. The regional data are consistent with the ranges of Cenozoic felsic lavas interpreted as having originated in and erupted from the Mojave crustal province ($^{208}Pb/^{204}Pb$ fields modified from Feuerbach et al., 1998; $^{207}Pb/^{204}Pb$ encompasses data from Wooden and Miller, 1990; Wenrich et al., 1995; Kempton et al., 1991; and Feuerbach et al., 1998). The PST data possess a restricted range of Pb isotope values relative to other NCREC magmas.

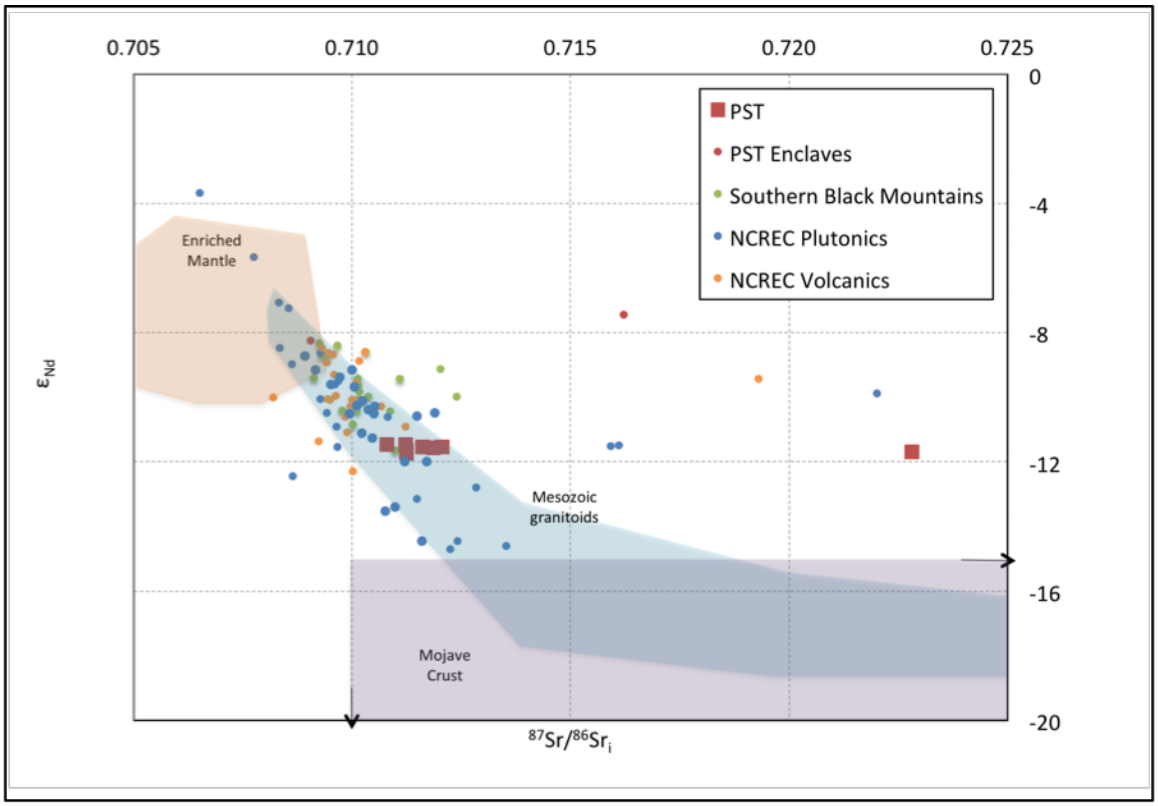

Figure 6. εNd vs. initial $^{87}Sr/^{86}Sr$ for the PST and other, similarly felsic NCREC magmas. The PST's isotopic compositions are more restricted (εNd in particular) than the remainder of NCREC magmas. Regional data is consistent with magma derivation from mixing of enriched mantle and Mojave crustal materials. The lone PST sample with high $^{87}Sr/^{86}Sr$ can be explained by late-stage contamination of >1.7 Ga Proterozoic crust (see Section 5.3.2). Miocene magmas from the NCREC, including the PST, share isotopic characteristics with Mesozoic granitoids. The enriched mantle, Mesozoic granitoid and Mojave crust fields are modified from Bachl et al. (2001) and Falkner et al. (1989). The Mojave crustal composition extends to much, much more radiogenic values of $^{87}Sr/^{86}Sr$ and εNd than shown (see for example, the $^{87}Sr/^{86}Sr$ of >1.7 Ga Proterozoic crust [Table 5]).

Pb isotopic ratios of Mojave rocks are especially distinctive (Wooden and Miller, 1990). These ratios are thought to be especially sensitive tracers of crustal contributions to magmas because the [Pb] in the crust is several times higher than in mantle-derived basalts. Feuerbach et al. (1998) took advantage of this sensitivity to distinguish contributions from rocks of the Mojave province crust from those of the Arizona province crust in weakly contaminated basalts of the NCREC. This distinction is important for the PST and other SBMVC rocks: while the surface exposure of the boundary between the

Mojave and Arizona provinces lies east of the Black Mountains, the geometry of this division at depth is poorly understood and may be gradational (Feuerbach et al., 1998; Kapp et al., 2002; Miller and Glazner, 1995). The Mojave crustal province is characterized by distinctively high values of $^{208}Pb/^{204}Pb$ and $^{207}Pb/^{204}Pb$ for a given $^{206}Pb/^{204}Pb$, which distinguishes it from the Arizona crustal province (Wooden and Miller, 1990). PST pumice samples consistently plot within the Mojave crustal range rather than that of Arizona crust (Figure 5). However, the high $^{208}Pb/^{204}Pb$ and $^{207}Pb/^{204}Pb$ signature appears by itself to identify Mojave lithosphere and not necessarily demonstrate crustal origin: Miocene-aged basalts from southern Nevada and the central Mojave, for which crustal contamination is inferred to be negligible, also have these Pb characteristics. These basalts have been interpreted as derived from enriched Mojave lithospheric mantle rather than depleted, asthenospheric mantle (Glazner et al., 1991 and Farmer et al., 1989). The range of Mojave crustal Pb ratios is far greater than that of the basalts, but the PST data are close to the more restricted range for the basalts. Thus, PST Pb documents Mojave lithosphere sources, but it does not uniquely indicate either crust or mantle.

The Nd and Sr isotopic data complement the Pb in constraining PST genesis. They cannot distinguish between Mojave and Arizona origin, but they clearly reveal an origin involving both ancient crust and mantle. The ancient crust in this region (both Mojave and Arizona) has very low εNd and high to very high $^{87}Sr/^{86}Sr_i$. The PST samples have far lower εNd and higher $^{87}Sr/^{86}Sr_i$ than depleted asthenospheric-mantle and are also distinct from estimated Nd and Sr isotopic compositions of Mojave enriched mantle (e.g. Farmer et al., 1989). However, they also have more radiogenic Nd and less radiogenic Sr than Proterozoic crust (Figure 6).

Derivation of PST magma from both Mojave province Proterozoic crust and enriched-mantle lithosphere is consistent with proposed hybrid origins of both Mesozoic and Miocene NCREC magmas (e.g. Miller and Wooden, 1994; Metcalf et al., 1995; Falkner et al., 1995; Bachl et al., 2001). Most pre- and syn-extensional Miocene magmas in the region have isotopic characteristics intermediate between those of the Mojave crustal province and the underlying enriched lithospheric mantle. It was not until later that syn- and post-extensional magmas in the region began to exhibit isotopic compositions reflecting input from the younger Arizona crustal province to the east (Feuerbach et al., 1998) and depleted, asthenospheric mantle upwelling in response to lithospheric thinning (e.g. Kempton et al., 1991; Farmer et al., 1989).

While the isotopic data strongly suggest that the PST magma was ultimately derived from a mixture of enriched-mantle and ancient Proterozoic crustal materials, it cannot distinguish between hybridization of these sources during the Miocene as the magma body was assembled (e.g. by assimilation and fractional crystallization or magma mixing) or during an earlier period of crustal modification (e.g. Mesozoic arc-related magmatism, with the PST derived from rocks produced during this episode). Abundant magmatism during the Jurassic and Cretaceous added substantially to the Mojave crust, perhaps even doubling the volume of the mid to upper crust in places (e.g. Old Woman Mountains area, western edge of NCREC; Miller and Wooden, 1994). Miller and Wooden (1994) estimate a mean isotopic composition of Mesozoic rocks in the Old Woman Mountains area of $^{87}Sr/^{86}Sr_i$ = 0.711 and εNd = -11.7, a close match with the PST isotopic data ($^{87}Sr/^{86}Sr_i$ = 0.7117 and εNd = -11.6). Bachl et al. (2001) and Metcalf (2004) noted that, although it was impossible to identify the source of NCREC magmas with certainty, a largely or entirely Mesozoic

source was plausible, pointing to abundant inherited zircons of both Proterozoic and Mesozoic age in a 65 Ma pluton in the southern Eldorado Mountains, NV, 65 km NNW of Silver Creek Caldera (Kapp et al., 2002). Subsequent SHRIMP zircon studies have documented very sparse inherited grains of Proterozoic and Mesozoic age in Miocene igneous rocks of the NCREC (e.g. Walker et al., 2007). The PST itself contains very few pre-Miocene zircons, and most or all of those that are present lack Miocene rims and are probably locally derived xenocrysts rather than grains inherited from the source (Lidzbarski et al., 2012).

5.2. Elemental Constraints on Petrogenetic Conditions

While the isotope data suggest that the materials comprising the PST are similar to those from which other regional magmas were derived, there are marked distinctions in elemental geochemistry between the PST and other NCREC magmas. In this section, I compare the PST with a compilation of Miocene felsic volcanics (Metcalf, 2004, and personal commun., 2012), pre- and post-PST magmas from the SBMVC in the vicinity of Silver Creek caldera (McDowell et al., in prep), and fine-grained granite sills, dikes, and chilled margins of plutons in southern Nevada inferred to represent magmatic input to the upper crust (Bachl et al., 2001; Harper et al., 2004; Walker et al., 2007; see A.Table 2).

The PST magma shows extreme depletion in Ba and Sr compared to other NCREC magmas (Figure 7, Table 8). The most Ba- and Sr- rich estimate of the average PST composition has [Ba]~965 ppm and [Sr]~180 ppm at 69.8 wt.% SiO_2, which are much lower than the bulk of other NCREC magmas at similar SiO_2. If the PST magma is dominantly rhyolitic (73.3 wt.% SiO_2), these values drop to ~265 and ~65 ppm,

respectively, concentrations drastically lower than any other comparably silicic magma in the region. Depletion of Ba and Sr must involve extensive fractionation of alkali feldspar ± plagioclase, as the only other mineral with appreciably high partition coefficients for Ba is biotite, which does not occur in sufficient enough abundance in the PST to drastically affect [Ba]. These data suggest that the PST underwent more extensive feldspar fractionation than other, similarly felsic NCREC magmas.

Conversely, the PST exhibits enrichment in Zr and REE relative to other NCREC magmas (Figures 8 and 9, Table 8). It shows higher concentrations of all REEs than comparable NCREC magmas (with the exception of Eu in the case of the PST average composition calculated with maximum HSR fraction). The estimated range of PST compositions are also far richer in Zr than comparable NCREC magmas. These elevated concentrations indicate that the PST underwent less accessory mineral fractionation than otherwise similar NCREC magmas. Extremely high Zr/Sr attest to the far greater influence of feldspar fractionation than accessory mineral fractionation in the evolution of the PST magma (Figure 8).

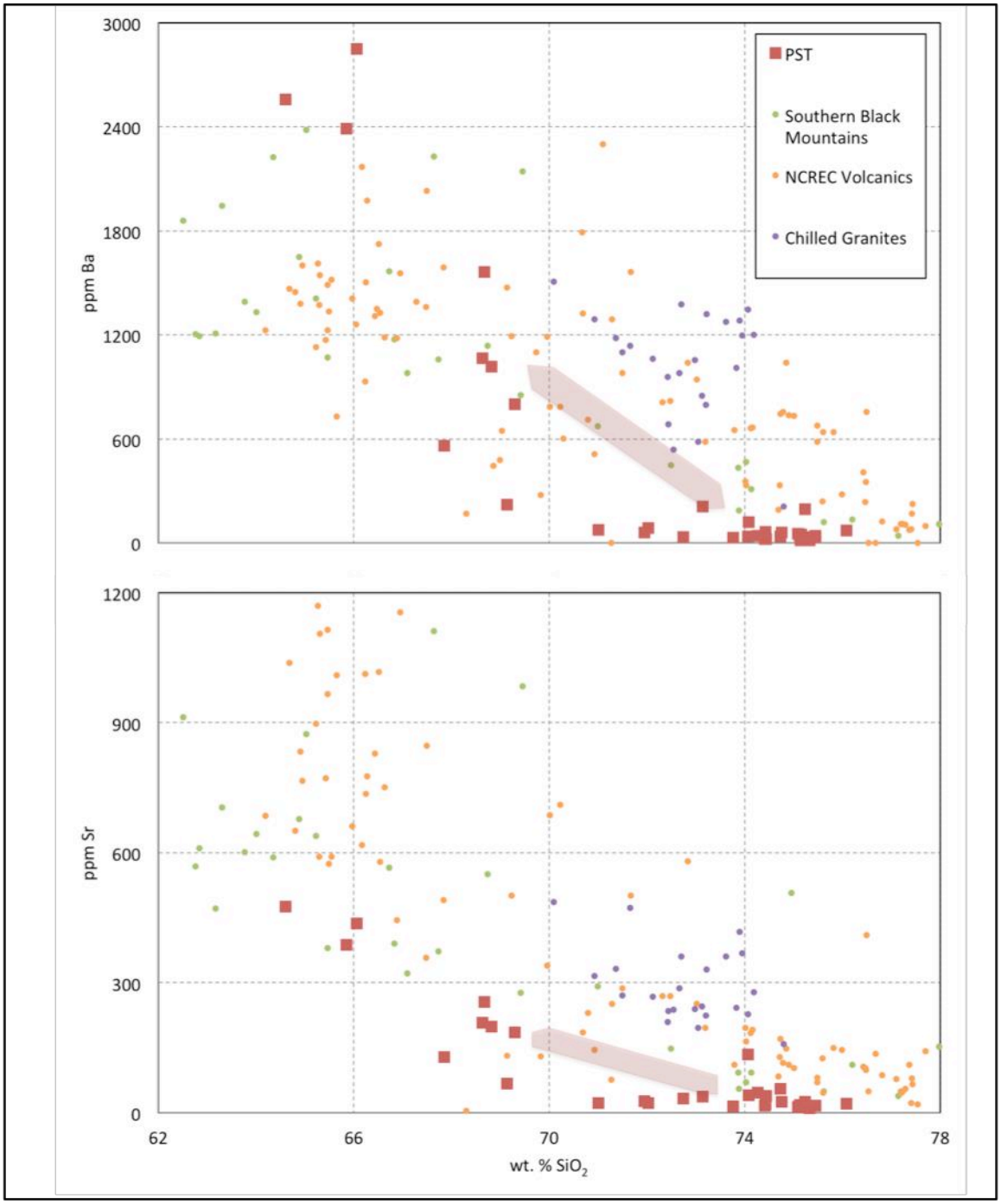

Figure 7. [Ba] and [Sr] vs. SiO_2 of the PST and other, similarly felsic NCREC magmas. The red shaded field showing the range of estimated bulk PST compositions confirms that, for a given silica content, the PST has [Ba] and [Sr] lower than almost all other NCREC compositions. Data sources are as stated in Table 8.

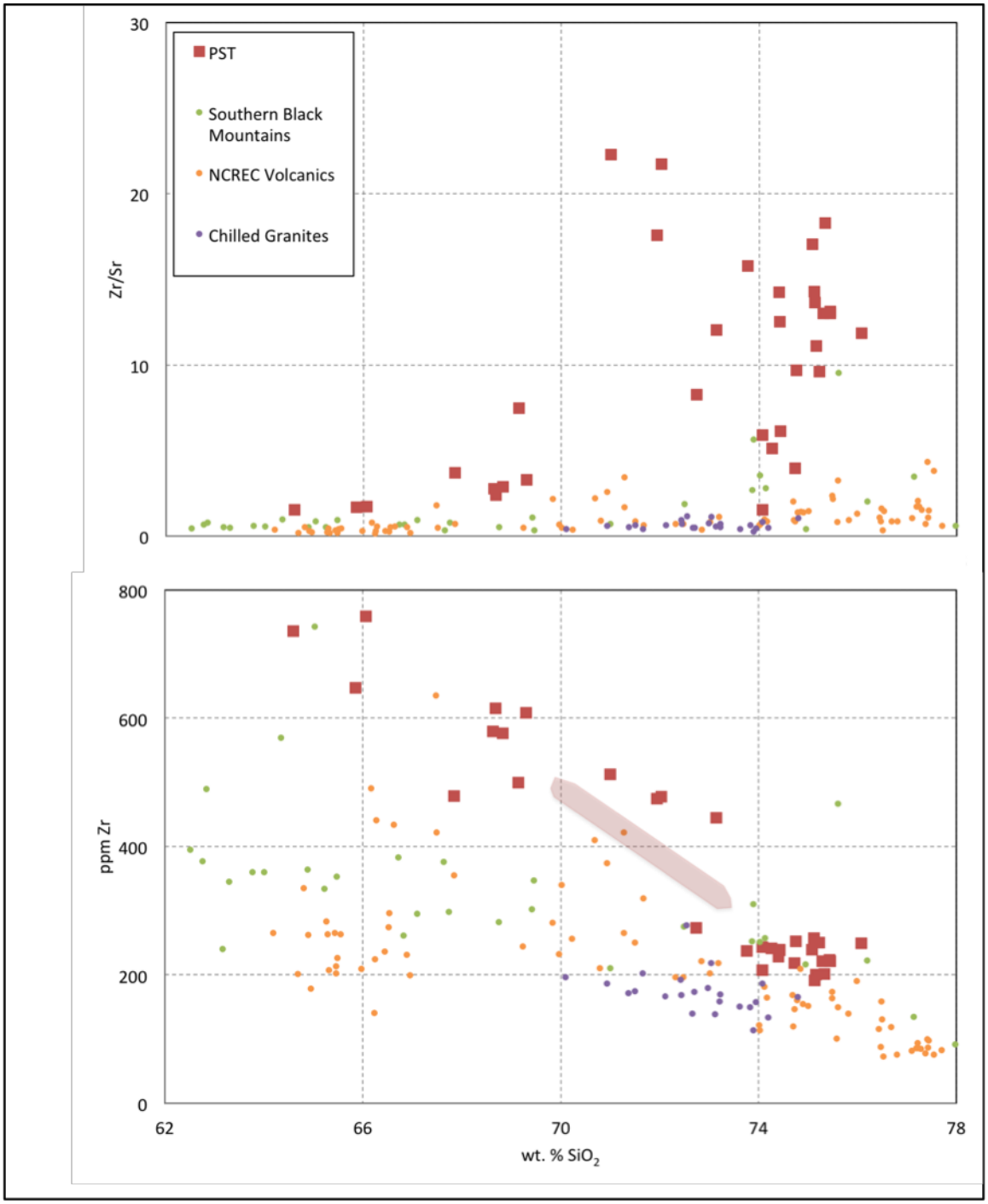

Figure 8. Zr/Sr and [Zr] vs. SiO_2 of the PST and other, similarly felsic NCREC magmas. The average PST [Zr] are enriched relative to the rest of the NCREC (including the SBMVC) data. The PST samples also have much higher Zr/Sr, consistent with the inference that the PST magma underwent more extensive feldspar fractionation compared to zircon fractionation. Source are as stated in Table 8.

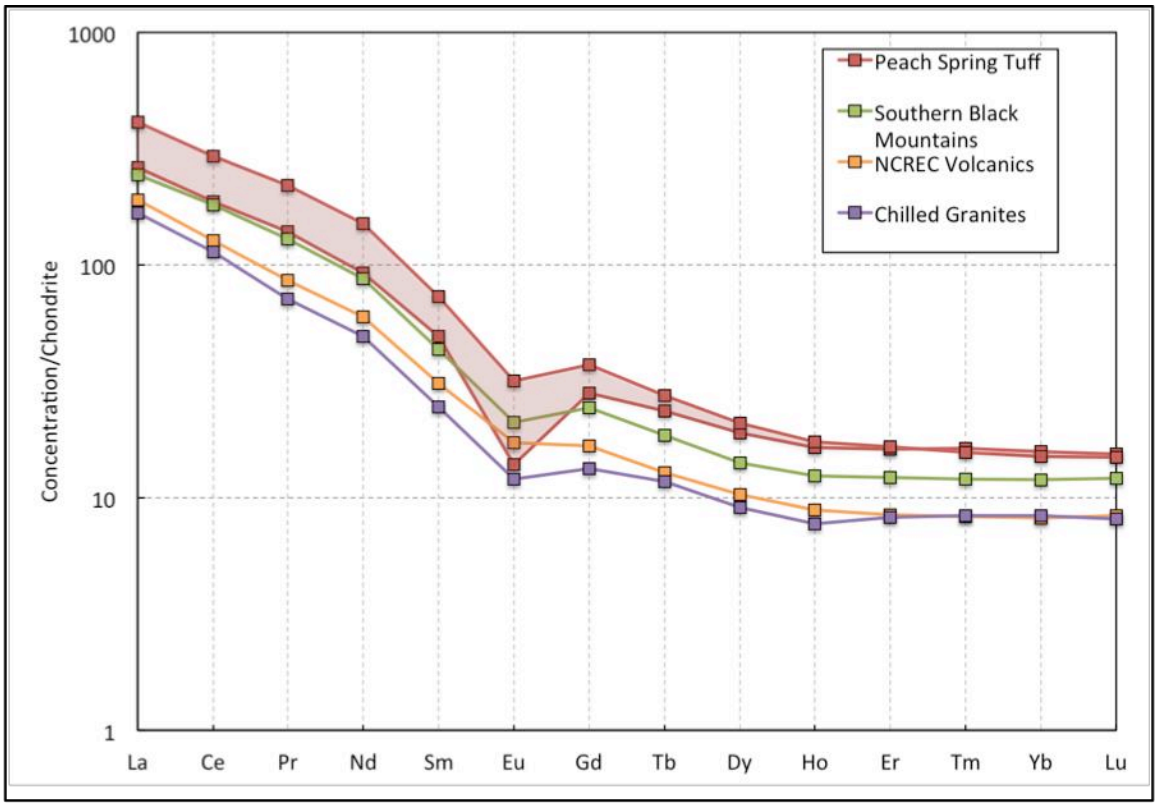

Figure 9. Chondrite-normalized (normalization values from Sun and McDonough, 1995) REE patterns for the PST and other, similarly felsic NCREC magmas. The red shaded region shows the range from dominantly trachytic (top) to dominantly rhyolitic (bottom) PST estimated bulk compositions. The other NCREC magmas have little to no Eu anomaly, while the PST has a relatively deep anomaly. With the exception of this Eu anomaly, the PST's REE contents are higher than those of other regional felsic magmas, although magmas from the SMBVC also show elevated concentrations.

The solubility of feldspars is very sensitive to the water content of magma (e.g. Tuttle and Bowen, 1958; Johannes and Holtz, 1996); with rising water contents at constant temperature, feldspar solubility increases. In contrast, the solubility of zircon and other accessory minerals is relatively insensitive to water content (e.g. Watson and Harrison, 1984). Simulations utilizing rhyolite-MELTS (Gualda et al., 2012) combined with zircon saturation thermometry (Watson and Harrison, 1983; Hanchar and Watson, 2003) illustrate these relationships and they can be used to constrain the temperature and water contents of the PST magma body and other NCREC magmas (Figure 10). These models

illustrate that for the PST and the NCREC granitic melts, both feldspars have higher saturation temperatures at 2 wt.% H_2O than zircon, but as water content increases, the feldspars appear on the liquidus at lower temperatures as expected. Eventually, feldspar saturation is achieved concurrent with or after zircon saturation. For the PST, alkali feldspar and zircon have similar saturation temperatures at ~4 wt.% H_2O, while plagioclase and zircon saturate at the same temperature at ~2.5 wt.% H_2O. For the NCREC, these water contents are ~4 wt.% and 6 wt.% H_2O, respectively.

Based on the lines of evidence cited above, we estimate that the parental PST magma formed at a temperature greater than ~850°C, above its zircon saturation temperature, with an H_2O concentration low enough to permit feldspar saturation (<~3 wt.%). In contrast, using similar reasoning, other NCREC magmas were substantially cooler and wetter (perhaps 800-850°C, >~4 wt.% H_2O). That is, PST magma and its parentage were substantially hotter and drier than typical NCREC magmas. This higher temperature we infer for the PST, along with its vast volume, may have facilitated vigorous convection that effectively homogenized the magma and eliminated isotopic heterogeneity that characterizes NCREC magmas, which formed and ascended as smaller, cooler magma batches.

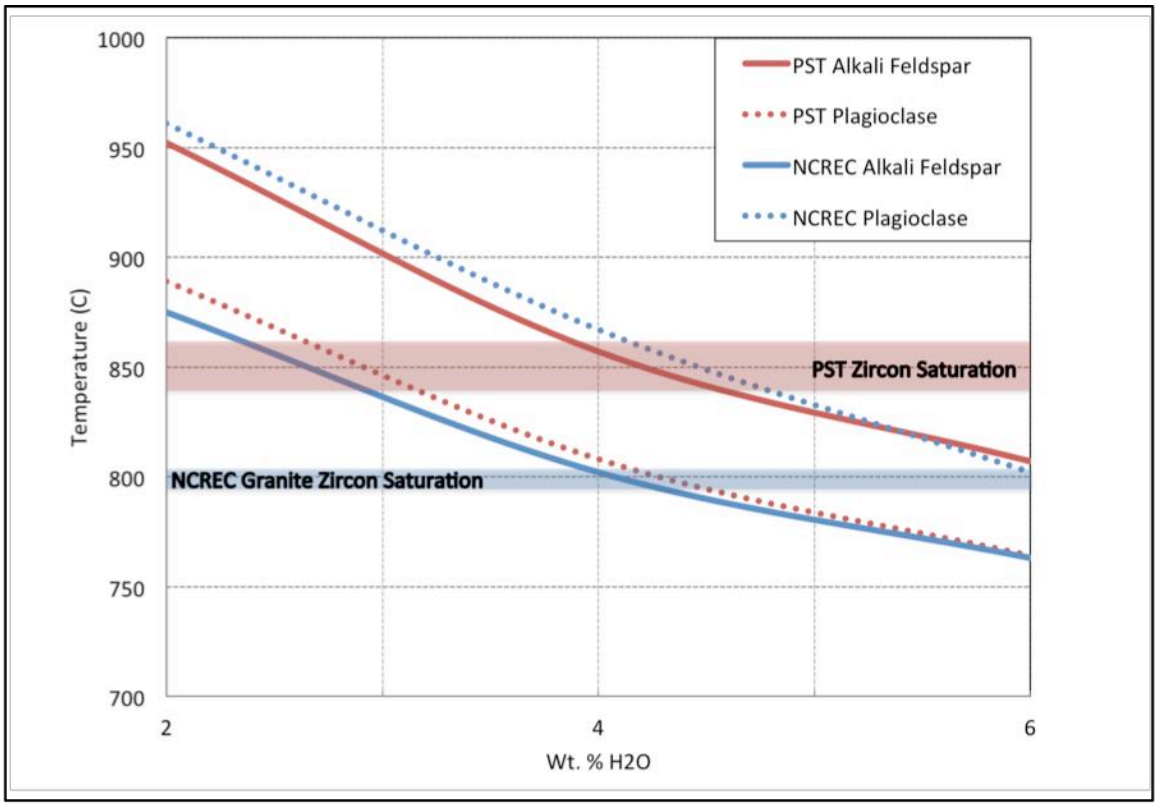

Figure 10. Results of rhyolite-MELTS (Gualda et al., 2012) simulations using the average PST (45% HSR) and chilled granite compositions. The curves track the temperature at which plagioclase and alkali feldspar saturate as a function of the water content of the magma. For comparison, zircon saturation temperatures for melts with average PST (45% HSR) and chilled granite compositions are also shown. The rhyolite-MELTS results are consistent with experimental work (e.g. Tuttle and Bowen, 1958; Holtz and Johannes, 1994) demonstrating the effect of water on the solubility of feldspar. These phase relations combined with the PST'S depleted [Ba] and [Sr] and enriched [Zr] and [REE] suggest that the PST evolved under relatively hot and dry conditions compared to other NCREC magmas.

5.3. Evaluation of Magma-Generation Processes: Open vs. Closed System

The PST isotope data require an open system at some time to create a hybrid composition that includes both Proterozoic Mojave crust and enriched lithospheric mantle components. A central question is when did hybridization occur: during Miocene PST generation or during the Mesozoic? If the former, then two possibilities arise; hybridization processes may have directly generated the PST magma, or instead produced a less-evolved magma (e.g. akin to pre-PST trachytes in the SBMVC) that subsequently underwent closed-system fractional crystallization to form the PST magma. If the latter, Mesozoic crust acted

as parental material during closed-system partial melting. Below, I briefly provide rationale for end members and conditions that we used during modeling.

5.3.1. Closed System Models: Partial Melting and Fractional Crystallization

Isotopic data (estimates for the NCREC crust [Miller and Wooden, 1994]; see Table 2) indicate that Mesozoic igneous rocks are the only potential parents that may produce the PST magma by closed-system partial melting. The Proterozoic basement possesses much too evolved $^{87}Sr/^{86}Sr$ and εNd to act alone as a parent. Mesozoic igneous rocks as estimated from the Old Woman Mountains region, however, have mean isotopic compositions ($^{87}Sr/^{86}Sr \sim 0.710$ to 0.712, εNd ~ -11.4 to -11.8; Table 2) that are almost identical to the PST ($^{87}Sr/^{86}Sr \sim 0.7107$ to 0.712 with the exception of a lone sample, εNd ~ -11.5 to -11.7). As discussed in section 5.2, the elemental composition of the PST suggests that the magma was hot and relatively dry. Therefore, if it was the product of closed-system partial melting, it would have left behind residue dominated by feldspar + anhydrous mafic minerals with little or no amphibole or biotite.

Trace element modeling indicates two potential partial melting pathways to produce the PST magma from Mesozoic crust, one in which garnet is a residual phase, consistent with deeper generation, and the other in which garnet is absent (see Section 3.3.1). Partial melting (F~0.4) of Jurassic crust with a small amount of garnet in the residue can reproduce the PST trace element pattern (Figure 11). The amount of garnet remaining in the residuum is quite small (~0.5 wt.%); larger amounts of garnet drastically deplete the melt in HREE except at high (F~0.9) melt fractions. Above F=0.5, the melt becomes low in

Rb, Th, and U, so while adding more garnet to the residue may improve the REE fit, it does not correct the deficiency in LIL elements.

Alternatively, garnet-absent partial melting of Cretaceous and mean Mesozoic crust (F~0.4-0.5) can generate the PST magma's trace element pattern (Figure 11). The average Mesozoic crust provides a better fit due to initially higher [Sr] and lower [Nb] than the Cretaceous crust. The latter requires a small amount of biotite (~5 wt.%) to properly reproduce the PST's [Nb] and leads to too low a [Sr]. Removing some feldspar from the residue results in higher [Sr], but requires the addition of hornblende, pyroxene, or quartz. Residual hornblende or pyroxene draws down the MREE and HREE (the MREE in particular) patterns down too much, while enough feldspar would have to be removed that replacing it all with quartz would be unlikely. The fit between the Cretaceous melt and the PST trace element pattern, however, is quite good. In these partial melting scenarios, the assemblage is dominated by feldspar with minor pyroxene and quartz. Hornblende and biotite are either sparse or absent. No accessory minerals were included in the assemblage. Small amounts of zircon and apatite will affect the HREE and LREE patterns, respectively, but not enough to alter the overall REE fit to fall outside of the PST range. Sphene, however, drastically draws down the MREE, even in tiny amounts, and cannot be present in the residue.

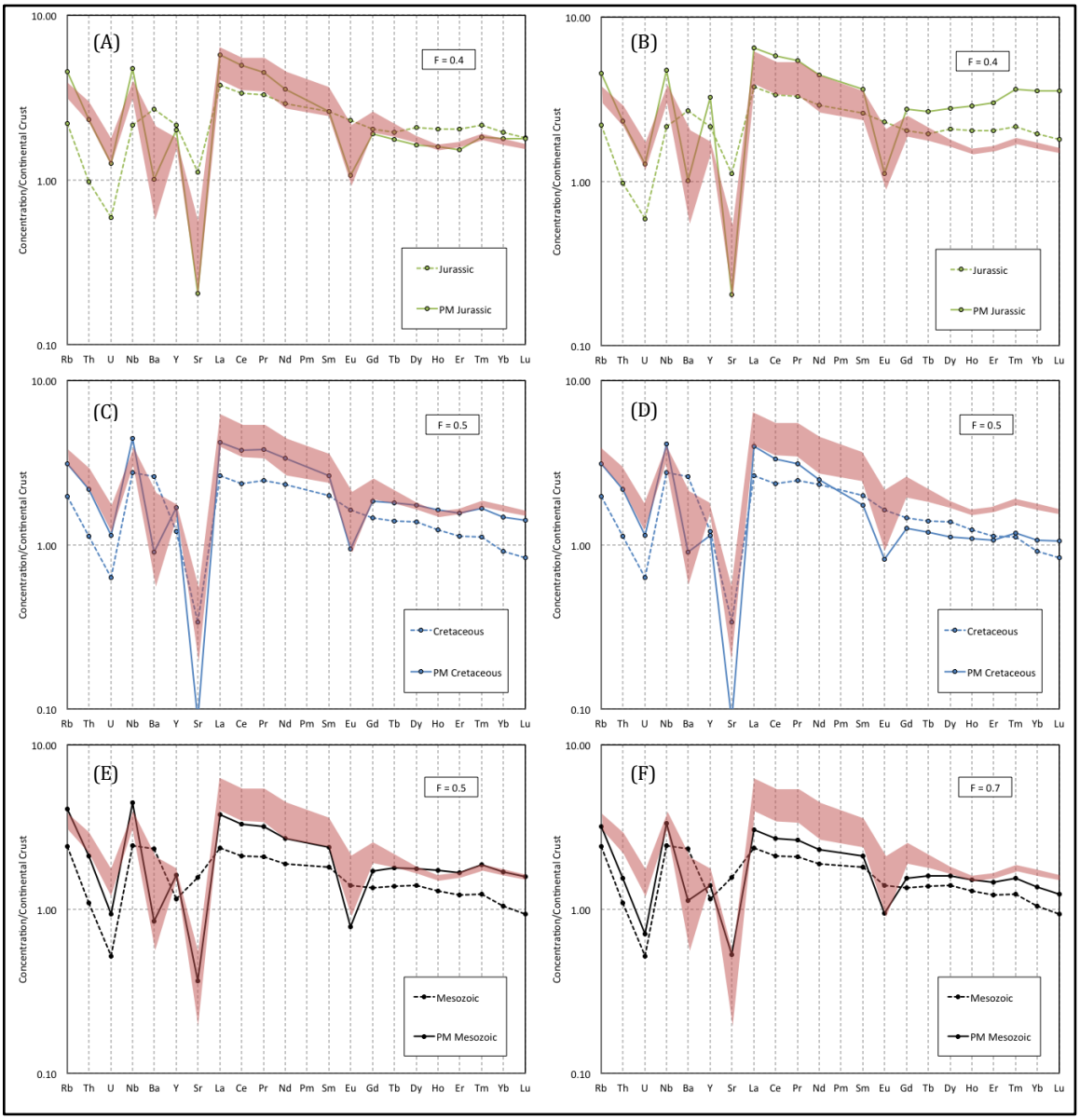

Figure 11. Equilibrium partial melting (PM) models (solid lines) of Mesozoic crustal compositions (mean 'Mojave Mesozoic', 'Jurassic', 'Cretaceous' plutonic rocks; dashed lines). Compositions from Miller and Wooden (1994). Mineral assemblages for (A), (C), and (E) shown in Table 4. Red shaded fields show range of PST compositions, between the 25% and 75% HSR estimated averages (see Table 8). **(A)** Partial melting of mean Jurassic crust with a small amount of residual garnet can generate the PST's trace element pattern. **(B)** Garnet-absent partial melting of Jurassic crust (all other parameters equal to those in (A) cannot produce [HREE] as low as those seen in the PST. **(C)** Garnet- and hornblende-absent partial melting of mean Cretaceous rocks can produce the PST magma's trace element characteristics. **(D)** Hornblende (5%) in the residual assemblage, partial melting of mean Cretaceous rocks: partial melt is too depleted in MREE. **(E)** Partial melting of mean Mesozoic crust at a melt fraction of 0.5 can reproduce the PST's trace element concentrations. **(F)** More complete partial melting (F=0.7) of mean Mesozoic igneous rocks; resulting melt is too low in REE.

Another closed-system process that may have been important in petrogenesis of the PST is fractional crystallization from a less silicic parent. The most obvious candidate is magma similar to the trachyte magmas that erupted in great abundance from the SBMVC shortly before the supereruption. The Gold Road (SCM-41) is not quite as isotopically evolved as the PST ($^{87}Sr/^{86}Sr_i$=0.7103, εNd=-10.0, εHf=-11.5), but would require only minor crustal contamination to reach the PST's composition, while the Alcyone has virtually indistinguishable isotopic characteristics from the PST ($^{87}Sr/^{86}Sr_i$=0.7110, εNd=11.6, εHf=-14.0). Both compositions can produce the PST magma (Figure 12) using fractionating assemblages and melt fractions similar to those that we observe in the trachytes: 25%-40% phenocrysts dominated by plagioclase with lesser clinopyroxene and biotite and minor apatite (cf. Dewitt et al., 1986; Lang et al., 2008). The REE in the models tightly constrain possible scenarios: they yield best fits at melt fractions on the order of 0.7, with zero to small amounts of apatite in the assemblage.

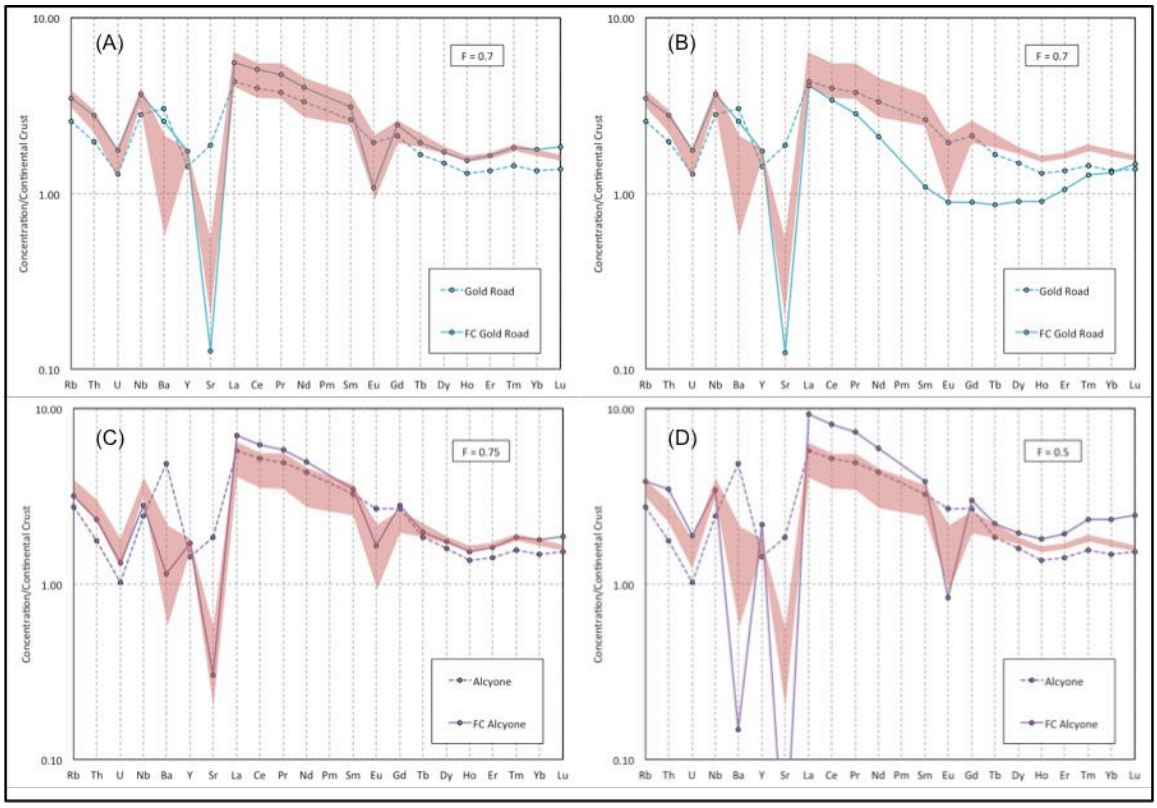

Figure 12. Perfect fractional crystallization (FC) models (solid lines) of pre-PST trachyte lava (using SCM-34 [Alcyone] and SCM-41 [Gold Road] samples as parents; dashed lines). **(A)** Roughly 30% fractional crystallization of a feldspar-dominated mineral assemblage containing minor pyroxene and biotite and no hornblende (see Section 3.1.1) using the Gold Road trachyte (SCM-41) as a parent can produce the PST magma composition. **(B)** An equal amount of fractionation of a similar assemblage but with apatite (3 wt.%) leads to an overly depleted REE pattern. **(C)** Roughly 25% fractional crystallization of a mineral assemblage that has similar feldspar contents but is more biotite-rich and pyroxene-poor from the Alcyone trachyte (SCM-34) can generate the PST magma. **(D)** Larger amounts of fractionation (F=0.5) of the same mineral as in (C) assemblage leads to over depletion of Sr and Ba and enrichment of LREE (despite the presence of 0.25% apatite, the partition coefficients for the LREEs are still below 1).

5.3.2. Open System Models: Bulk Mixing, Assimilation and Fractional Crystallization

Bulk mixing models support the possibility that open system processes may have either generated the PST magma directly or the pre-PST trachytes during the Miocene. Bulk mixing (Table 9 and Figure 13) models indicate that mean 1.7 Ga, >1.7 Ga Mojave crust, or the 1.4 Ga granitic component of the crust (see Tables 2 and 5) could have mixed in sub-equal proportions (~0.4) with enriched basalt to generate trachytic compositions similar to the Gold Road and Alcyone formations ($^{76}Sr/^{86}Sr \sim 0.7107$, εNd=-10.8, [Sr]~580 ppm,

[Nd]~80 ppm). While mixtures of WSWPST1, the trachyandesitic magmatic enclave in the PST, with <1.7 Ga Mojave crust can generate similar isotopic compositions, the relatively enriched [Sr] (1514 ppm) and [Nd] (104 ppm) of the enclave lead to concentrations above those found in the trachytes. Depleted mantle-like compositions mixed with <1.7 Ga Mojave crust can also produce trachyte-like magmas (somewhat poorer in Sr), but considering the paucity of pre- and syn-extensional basalts in the NCREC that exhibit depleted mantle-like isotopic characteristics (e.g. Daley and DePaolo, 1992, although see Metcalf et al., 1995 for an exception), we consider enriched mantle to be a more likely major contributor to the PST magma. Bulk mixing cannot directly account for the low [Sr] of the PST in any of the models. Fractional crystallization, either after mixing created the trachytes (as discussed above) or concurrent with assimilation of crustal material (AFC), must be responsible this depletion.

Table 9. Example of binary mixing results. End members are enriched basalt and 1.7 Ga bulk crust, whose compositions are listed in Table 5. In this case, an F=0 corresponds to a composition that is 100% 1.7 Ga crust, whereas an F=1 represents 100% enriched basalt.

F	εNd	$^{87}Sr/^{86}Sr_{initial}$	[Nd]	[Sr]
0	-6	0.7065	50	200
0.1	-7.2	0.7073	50	270
0.2	-8.4	0.7082	50	340
0.3	-9.6	0.7094	50	410
0.4	-10.8	0.7108	50	480
0.5	-12.0	0.7125	50	550
0.6	-13.2	0.7148	50	620
0.7	-14.4	0.7179	50	690
0.8	-15.6	0.7222	50	760
0.9	-16.8	0.7288	50	830
1	-18.0	0.7400	50	900

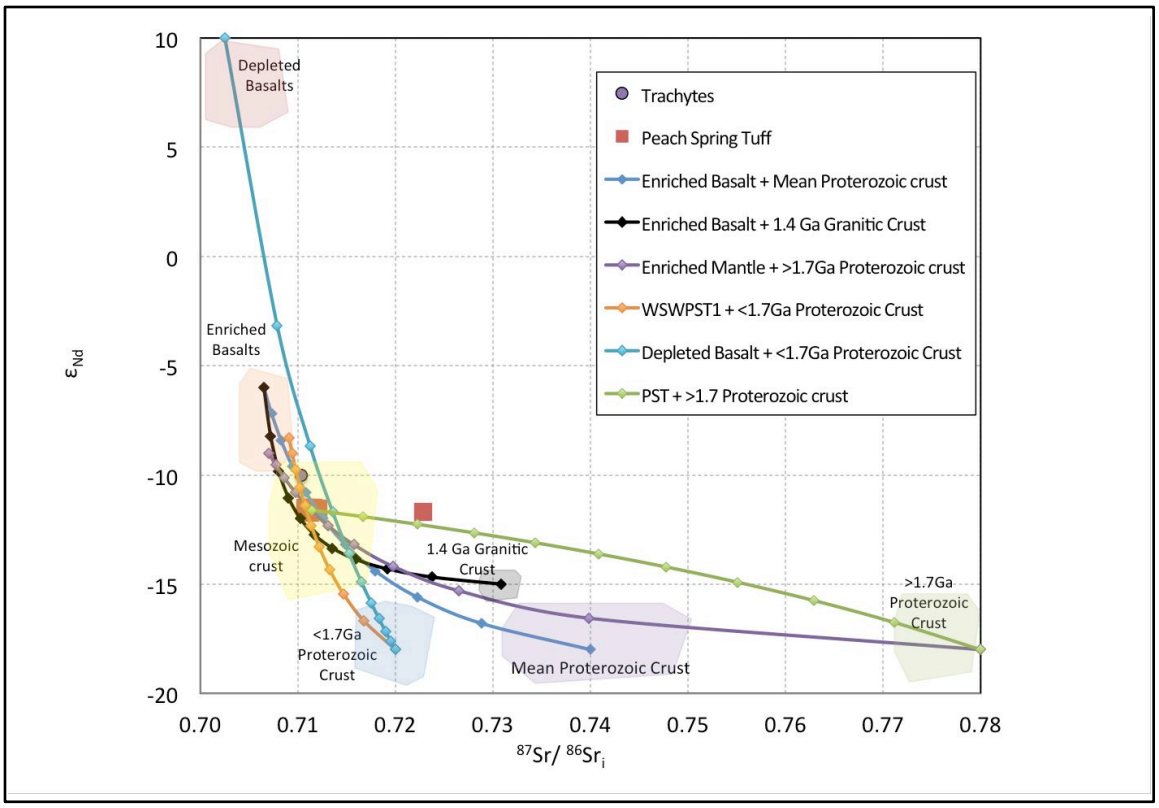

Figure 13. Bulk mixing models showing mathematically plausible mixtures of crustal and mantle end members (see Tables 5 and 9) that could produce isotopic compositions similar to those seen in the PST and pre-PST trachytes. Bulk mixing cannot, however, reproduce the low [Sr] and [Nd] of the PST; concurrent or subsequent fractional crystallization would be required to do so. Models mixing subequal proportions of enriched basalt and the various Proterozoic crustal types (~60% crust) can generate [Sr] and [Nd] similar to those seen in the trachytes. While the depleted mantle can produce PST- or trachyte-like isotopic compositions by bulk assimilation of >1.7 Ga crust, the paucity of basaltic magmas that display primitive, depleted isotopic characteristics make this an unlikely scenario. Simple bulk mixing between an already formed PST and >1.7 Ga crust can approximate the isotopic and elemental composition of the lone PST sample with high $^{87}Sr/^{86}Sr$.

AFC modeling (DePaolo, 1981; Keskin, 2021) suggests that concurrent assimilation of crust and crystallization of an initial juvenile magma represents a viable possibility for PST petrogenesis. Latent heat considerations seem to preclude pure, bulk assimilation, as DePaolo (1981) originally pointed out, thus providing support of his approach. However, my initial AFC models using crustal end members discussed above resulted in evolving melt that reached the correct $^{87}Sr/^{86}Sr$ while $^{143}Nd/^{144}Nd$ was still to high. This was a consequence of the high $^{87}Sr/^{86}Sr$ of the crust and its domination of the mixture as

relatively Sr-rich crust was added to fractionated, Sr-depleted melt. Relatively Sr-poor partial melts (see Section 3.3.1), rather than bulk crust, are probably more reasonable approximations of contaminants and in any case are required for AFC models to reproduce PST isotopic values (Figure 14). I carried out closed system partial melting models with a feldspar- and pyroxene- dominated residual mineral assemblage to estimate [Sr] and [Nd] of the crustal melt (Table 10; using partition coefficients in Table 3). These models result in melts that are relatively enriched in Nd compared to bulk crust, but they do not significantly affect the leverage that the crustal end member has on $^{143}Nd/^{144}Nd$.

Table 10. Parameters used in closed-system partial melting models of bulk crust to create Sr-poor crustal melts used as end members during AFC modeling.

Mineral	Mode
Quartz	5
Biotite	0
Plagioclase	50
Alkali Feldspar	25
Clinopyroxene	10
Orthopyroxene	10
Hornblende	0
Apatite	0
Zircon	0
Sphene	0
Garnet	0
D_{Nd}	0.408
D_{Sr}	8.167
F	0.7

The PST isotopic and elemental composition can be modeled by AFC involving a typical enriched mantle basalt composition and mean 1.7 Ga Mojave or 1.4 granitic crust (see Table 5) using bulk partition coefficients that approximate partitioning behavior for intermediate, dacitic melts (D_{Sr} =3, D_{Nd}=1), r-values between ~0.3 and 0.7, and values of F

between ~0.5 and 0.7 (Figure 14 and 15, A.Table 4). A two-stage model simulating the increasingly compatible behavior of trace elements with increasing SiO_2 content in the melt (Figure 16) is similar to these one-stage models, as at intermediate values of F during the stage of AFC when the trace elements are behaving most incompatibly, the isotopic trajectories do not vary widely with the r-value. Models involving a >1.7 Ga Mojave melt and using similar parameters never approach the PST isotopic composition, while a <1.7 Ga Mojave melt becomes too depleted in Sr at these isotopic values (Figure 17).

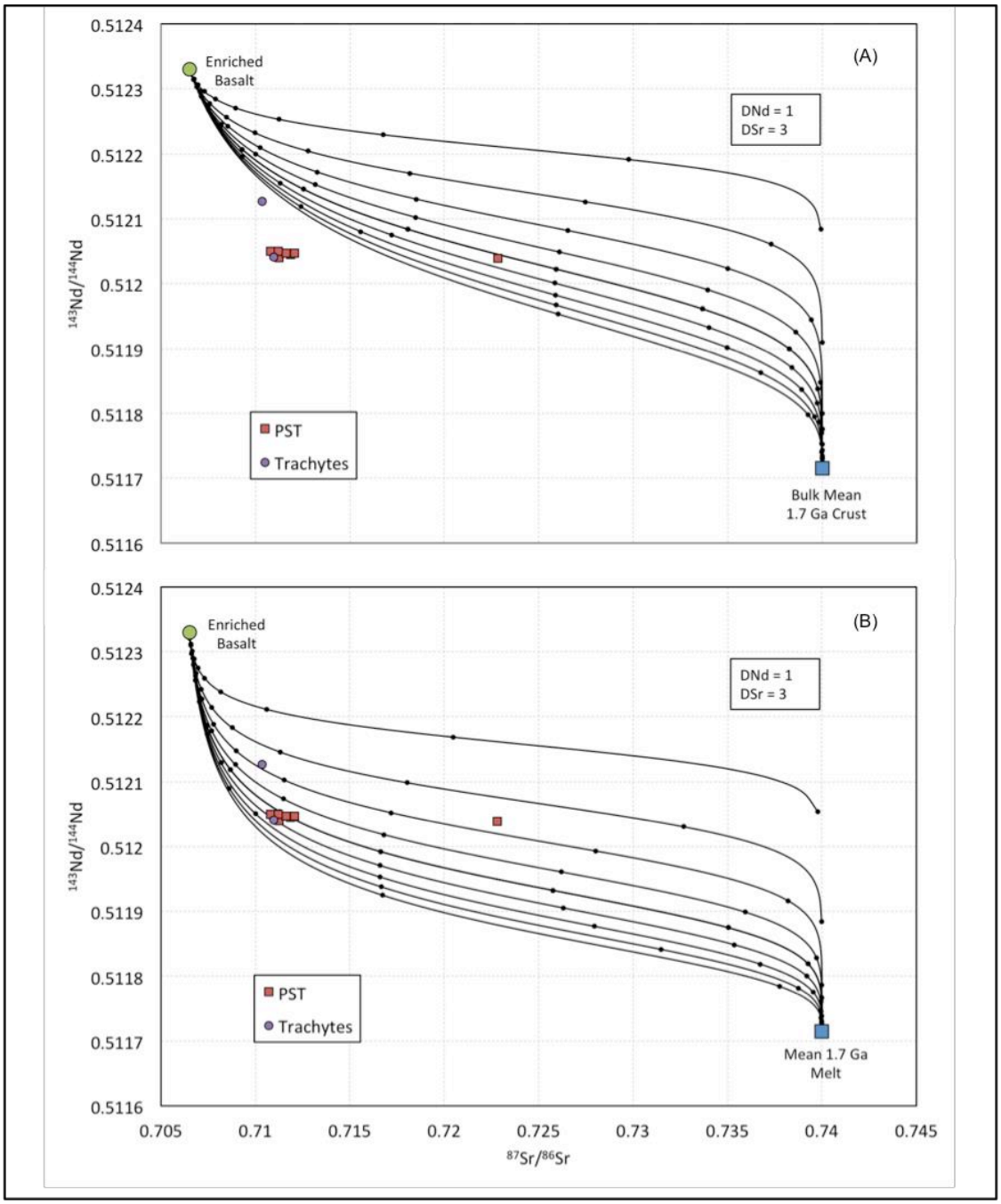

Figure 14. AFC models mixing enriched basalt and the mean 1.7 Ga crustal materials using intermediate partition coefficients. Trajectories trace out models for r-values between 0.1 (top) and 0.9 (bottom). Each tick mark on a given curve represents a 0.1 increment of F, which is the ratio of the magma's mass relative to its original mass (includes both remaining intial melt and added mass of melt derived from crust). **(A)** Assimilation of bulk 1.7 Ga crust: while Sr-poor compared to the enriched basalt, the crust has a sufficiently high [Sr] to give it more leverage on the $^{87}Sr/^{86}Sr$ of the mixture. As a result, the $^{87}Sr/^{86}Sr$ of the evolving magma changes more rapidly than the $^{143}Nd/^{144}Nd$, reaching the PST's composition at elevated $^{143}Nd/^{144}Nd$. **(B)** Assimilation of melt derived from crust: partial melt of the 1.7 Ga crust (see Section 3.1.2), is depleted in Sr as a consequence of residual feldspar, and therefore, is a more suitable end member composition for modeling the PST composition. An r-value between 0.4 and 0.5 and F-value between 0.5 and 0.6 can produce the PST isotopic and elemental composition. Both of these models result in lower [Sr] than the trachyte compositions.

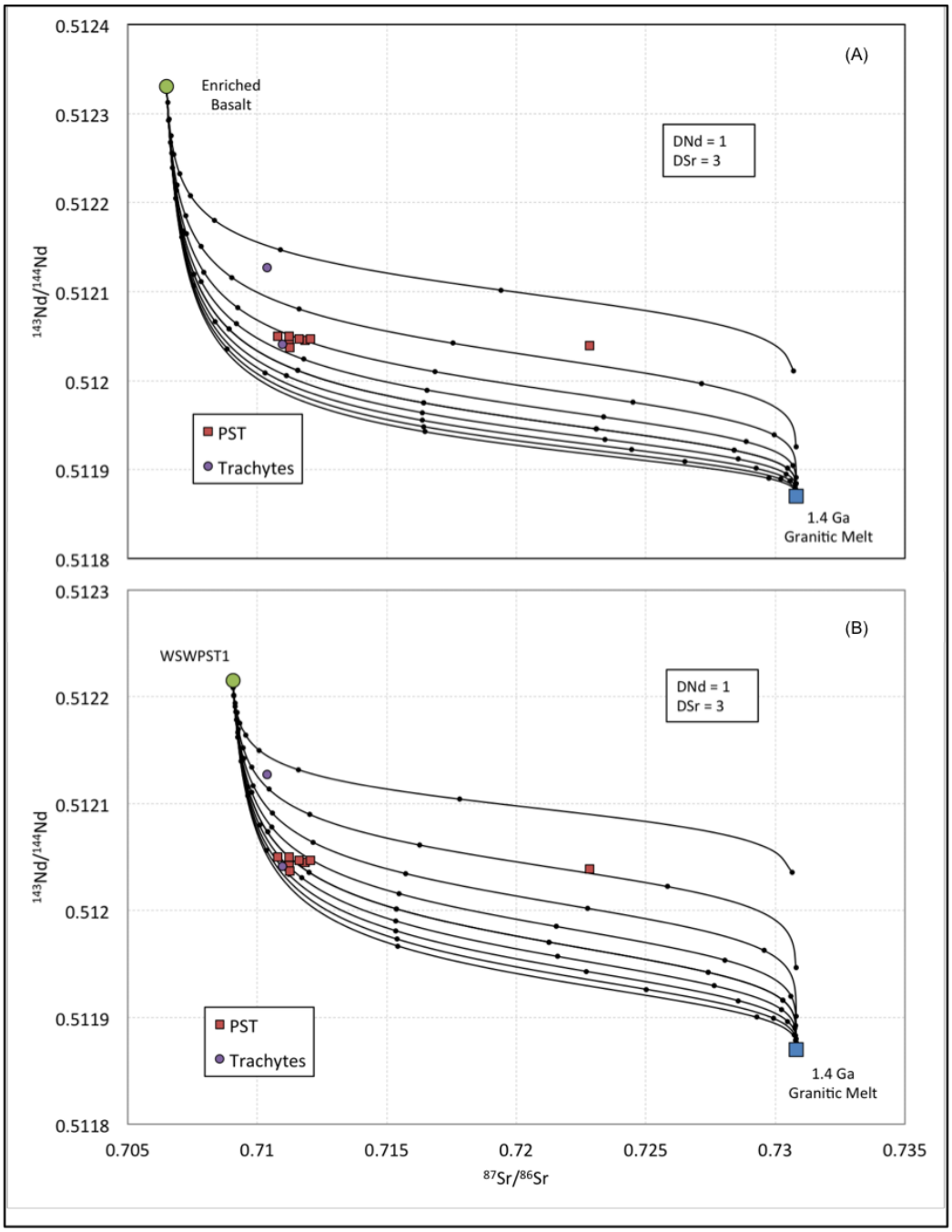

Figure 15. AFC mixing models involving melt derived from 1.4 Ga granitic rocks and either enriched basalt or trachyandesitic enclave WSWPST1. Trajectories and tick marks are same as given in Figure 14. **(A)** Assimilation of 1.4 Ga crustal melt by enriched basalt leads to a PST-like composition for r-values between 0.4 and 0.5 and F-values between 0.6 and 0.5. **(B)** Enclave WSWPST1 can assimilate 1.4 Ga crustal melt to produce PST- and trachyte-like isotopic compositions, and leads to [Sr] and [Nd] intermediate between the two.

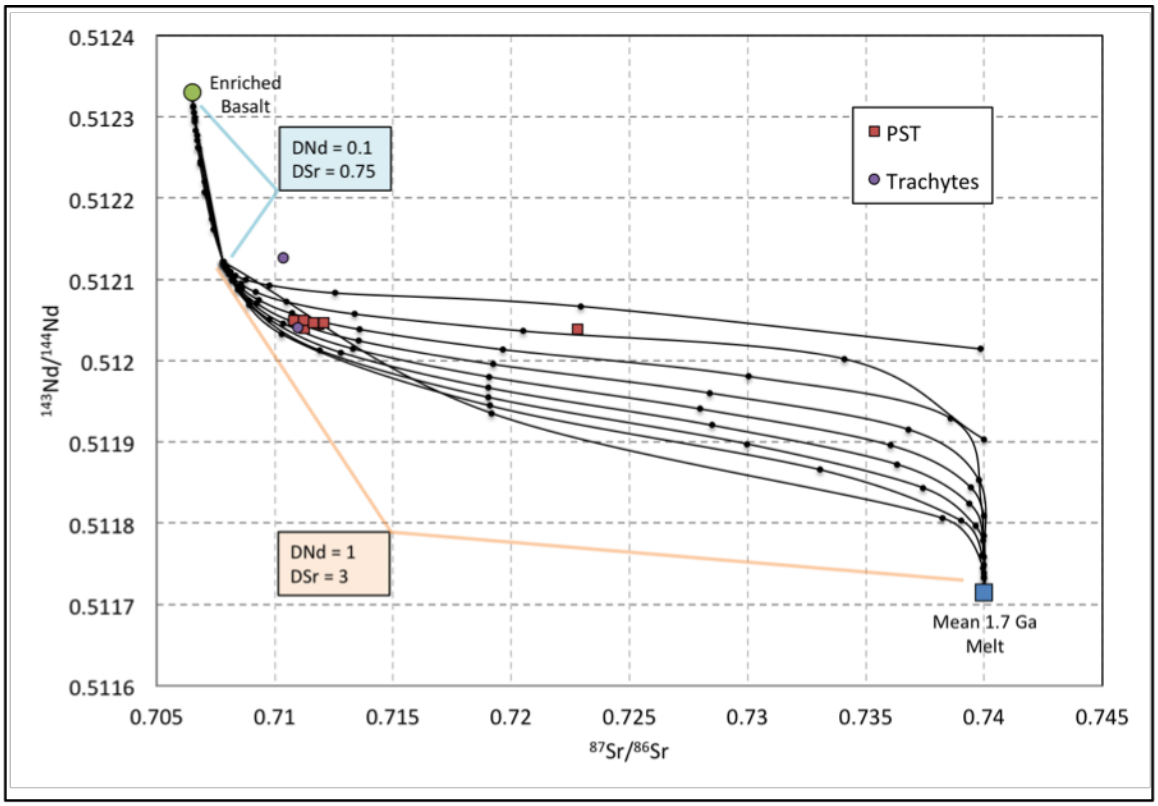

Figure 16. Two-stage AFC model simulating variable partitioning behavior of trace elements within an evolving magma body. Trajectories and tick marks are as described in Figure 14. The first stage is characterized by highly incompatible behavior and slightly incompatible behavior by Nd and Sr, respectively. For F < 0.5, the isotopic trajectories for different values of r do not vary much, leading to a fairly small range of isotopic compositions regardless of the ratio of assimilation to fractional crystallization, although the elemental compositions that result vary more widely. The first stage was performed with an r-value of 0.5 (although r-values from 0.1 to 0.6 are shown for stage 1) and ended when F=0.6 (twice as much fractional crystallization as assimilation had occurred; mass lost to fractionation was 80% of original magma's mass, which was then "replaced" by a mass of assimilant equal to 40% of the original magma's mass). The resulting isotope and elemental compositions were then used as the mafic end member for the second stage of the model, in which the partition coefficients reflect neutral partitioning behavior of Nd ($D_{Nd} = 1$) and moderately compatible behavior by Sr. This second stage reproduces the PST composition with an r-value of 0.4 and an F-value between 0.6 and 0.5.

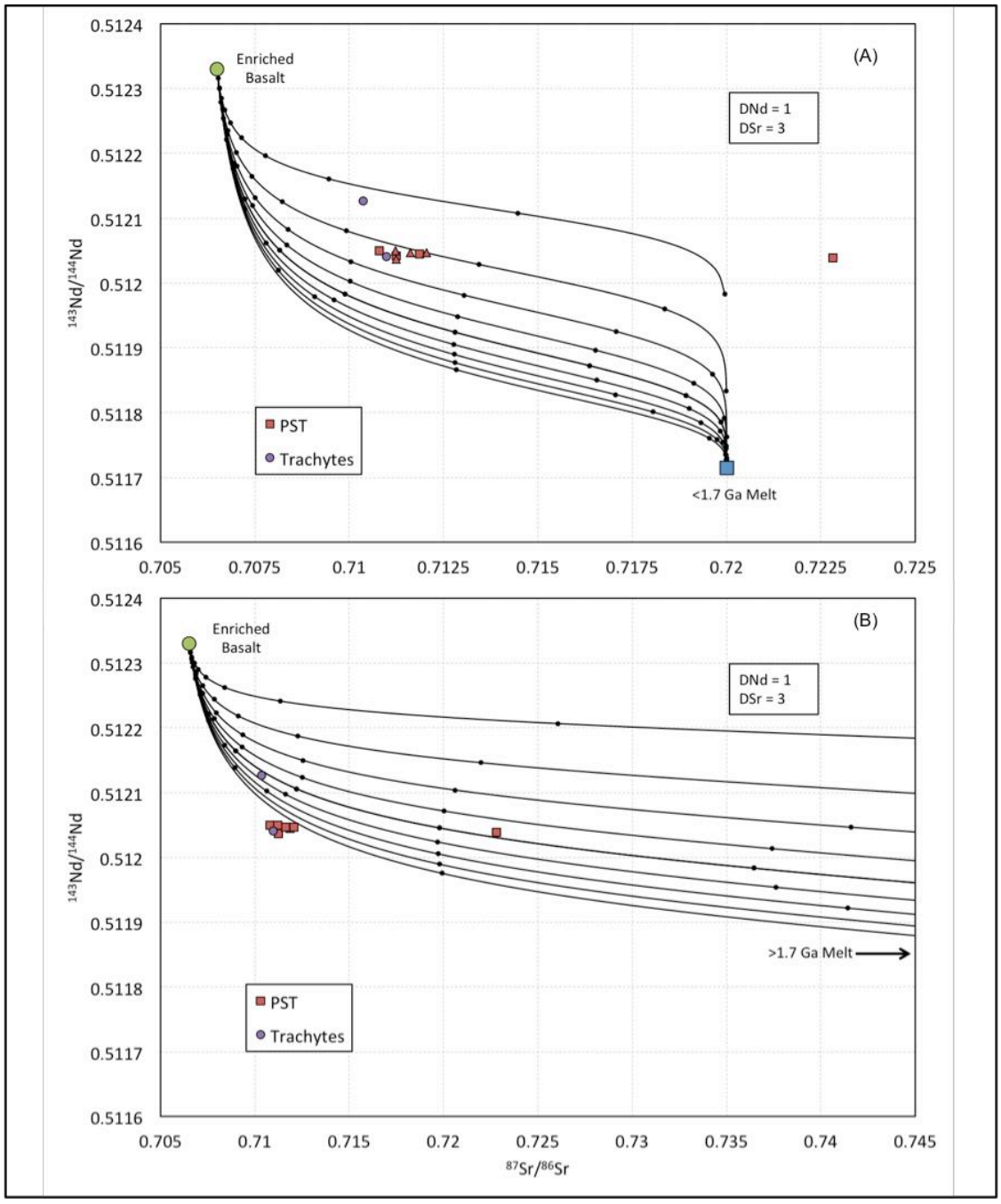

Figure 17. AFC models mixing enriched basalt with <1.7 Ga and >1.7 Ga Proterozoic melt. Trajectories and tick marks are the same as described in Figure 14. **(A)** While the >1.7 Ga crustal end member can produce the PST's isotopic composition using r-values between 0.2 and 0.3 and F values ~0.25, [Nd] (38 ppm) is more depleted than either the trachytes or the most Nd-poor (55 ppm) estimate of the PST bulk composition (see Section 5.1.1, Table 10). **(B)** The >1.7 Ga crust's Sr dominates the mixture because of its highly evolved $^{87}Sr/^{86}Sr$, causing the trajectories to pass by the PST's $^{87}Sr/^{86}Sr$ at elevated $^{143}Nd/^{144}Nd$.

5.3.3. Timing of Hybridization

The models described in the preceding sections cannot effectively constrain the when the hybridization that is required by the PST isotopic composition took place. Either "pre-hybridization" (anatexis of hybrid crustal rocks, presumably produced in the Mesozoic) or "syn-hybridization" (hybridization during generation of the PST by AFC of bulk mixing) can explain the elemental and isotopic composition of the PST. No Mesozoic rocks are exposed in the Black Mountains, or elsewhere within ~60 km of Silver Creek caldera. However, inheritance of Mesozoic zircon in latest Cretaceous and Miocene intrusions in the NCREC (Kapp et al., 2002 suggests that such rocks underlie at least part of the region and that a Mesozoic source is plausible. The PST itself contains very rare Proterozoic zircon, and to date it has yielded no Mesozoic grains (Lidzbarski et al., 2012). Proterozoic zircon with εHf~-30 may indicate contributions from 1.4 Ga sources (J. Miller, personal comm.), but further work must be done to determine whether these zircons represent inherited grains or are instead locally derived xenocrysts. While the exposed basement in the vicinity of Silver Creek Caldera is ~1.7 Ga, 1.4 Ga granitic compositions can be found increasingly to the NW toward the Colorado River (Faulds et al., 2001).

CHAPTER VI

IMPLICATIONS

The PST shows distinct similarities to silicic volcanic rocks at Yellowstone and along the Snake River Plain (Y-SRP), while other NCREC magmas are more akin to dacites and rhyolites of the Great Basin (Figure 18). Christiansen and McCurry (2008) demonstrate that rhyolites in the former region are hot and dry, exhibiting trace element characteristics indicative of early feldspar precipitation and delayed Fe-Ti oxide crystallization, while the latter group has a subduction heritage that imposed cool, wet conditions that led to delayed feldspar saturation at the expense of amphibole and oxides. They propose that the Y-SRP rhyolites were largely the products of partial melting of variably fractionated, underplated basalt, while the Great Basin volcanics were generated within an open-system with a large degree of crustal assimilation. PST data overlap the Y-SRP data in the within-plate granite field of the tectonic discrimination diagram of Pearce et al. (1984), while other NCREC magmas plot similarly to the Great Basin dacites and rhyolites in the volcanic-arc field. Amphibole and Fe-Ti oxides are the main minerals that sequester appreciable amounts of Nb and Y, and early precipitation of these phases is interpreted to have prevented enrichment in these elements while the concentration of the incompatible element Rb rose. Thus, compositions of silicic Great Basin magmas remained within the volcanic arc granite field, evolving roughly parallel to the boundary between the volcanic-arc and within-plate granite fields of the tectonic discrimination diagram of Pearce et al. (1984). By implication, similar NCREC magmas may have had a similar history. In Christiansen and McCurry's

(2008) interpretation, the Y-SRP volcanics underwent feldspar-dominated fractionation without early saturation of amphibole and oxides (or other accessories), and therefore Nb and Y behaved incompatibly. The magmas thus evolved to higher Nb and Y as Rb rose, traversing the boundary into the within-plate granite field. A similar interpretation is consistent with the PST, wherein the PST magma attained its composition through fractionation under hot and dry conditions.

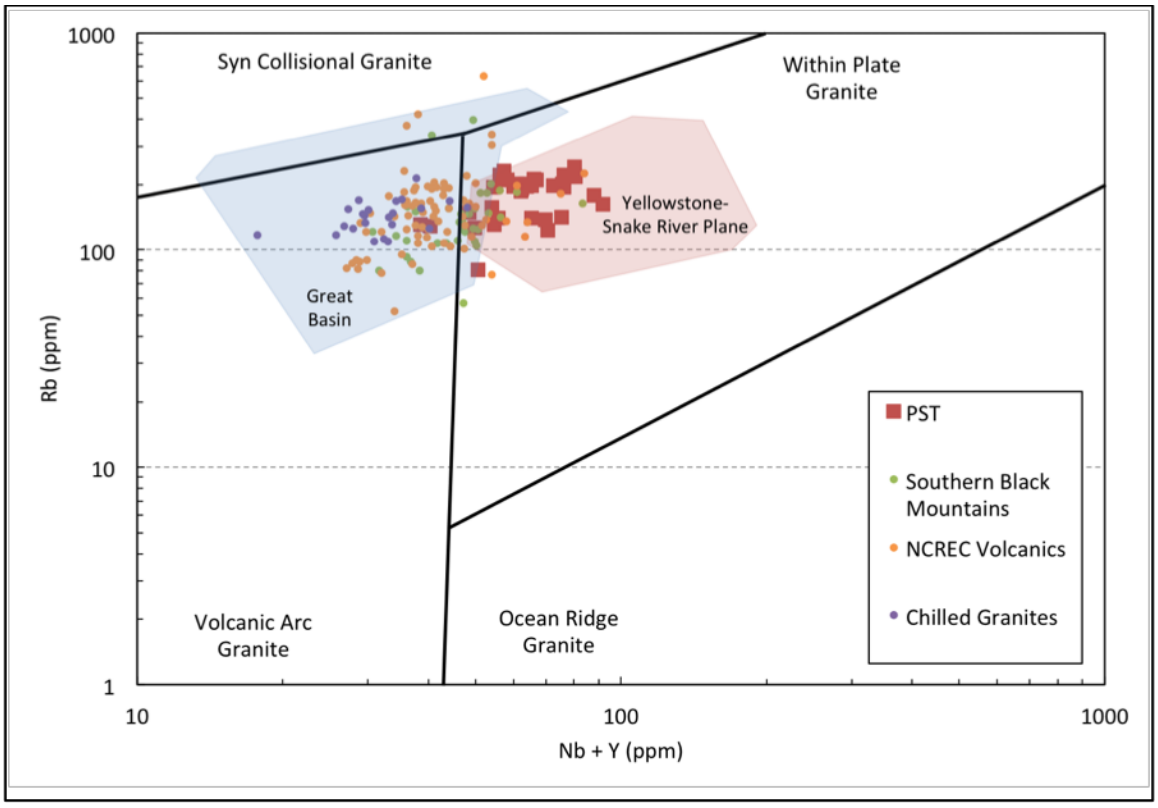

Figure 18. Tectonic discrimination diagram for silicic rocks (Pearce et al., 1984) comparing the PST and other, similarly felsic NCREC magmas. A few magmas from the SBMVC and NCREC show similar characteristics to the PST, but the vast majority exhibit much lower Nb+Y concentrations for a given [Rb]. The PST samples appear similar to magmas erupted from the Yellowstone-Snake River Plain, while other NCREC compositions share characteristics with Oligocene and younger volcanics from the Great Basin, NV and UT (fields from Christiansen and McCurry, 2008). Christiansen and McCurry (2008) interpret the former group to plot in the within-plate granite field of the diagram due to extensive feldspar fractionation under relatively hot and dry conditions (hydrous minerals absent), while the latter plot in the volcanic-arc granite field due to amphibole fractionation under cooler, wetter conditions.

It is perhaps surprising that the PST would have such markedly different characteristics from magmas of the same age within the same region. Christiansen and McCurry (2008) attribute the geochemical distinctions between the Great Basin and Y-SRP volcanics to differences in intensive parameters that were imparted on the magmas by their differing tectonic settings. The same cannot be said for the differences between the PST and the remainder of early Miocene NCREC magmas, which ostensibly are all related to the onset of crustal extension. Broadly similar patterns on a primitive mantle normalized extended trace element diagram (Figure 19) are consistent with similar tectonic origins for the two groups. The large negative Nb-Ta anomaly in the PST and NCREC data are typical of subduction zone rhyolites (Ionov and Hofmann, 1995) and probably reflect prior modification of the region's lithosphere during magmatism in the Proterozoic and/or Mesozoic. The PST's enrichment in many trace elements relative to other NCREC magmas reflects contrasting petrologic evolutions caused by dissimilar thermal conditions and water contents that cannot simply be attributed to tectonic setting.

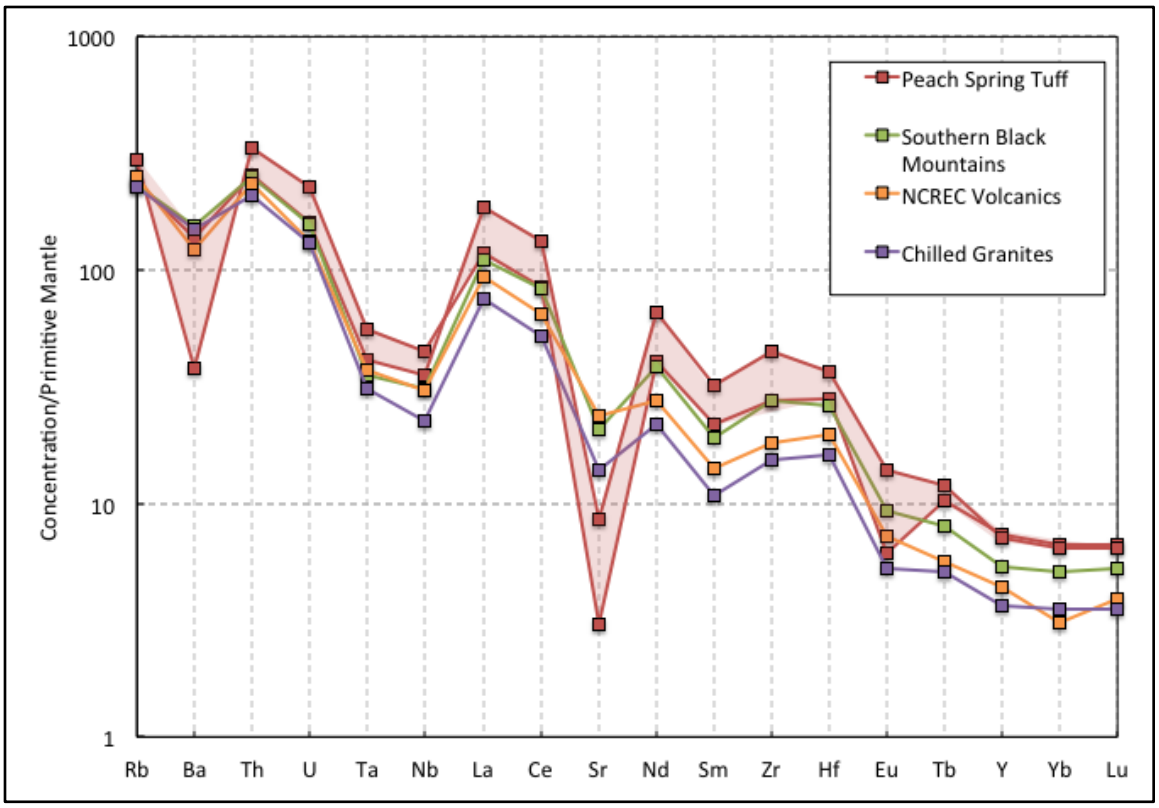

Figure 19. Extended trace element ("spider") diagram for the PST and other, similarly felsic NCREC magmas. The PST compositions (from 25% HSR to 75% HSR; shaded red region), with the exception of deep Ba and Sr anomalies, exhibit elevated trace element concentrations, consistent with lesser degrees of accessory mineral fractionation. Despite the intra-plate, extensional tectonic regime under which these magmas were generated, the PST exhibits the deep Nb-Ta anomaly that is usually interpreted to reflect subduction zone processes. This is probably a consequence of derivation from or extensive contamination by lithosphere that was formed or modified by arc processes (Mesozoic and/or Proterozoic).

So the question remains, why was the PST hotter and dryer than its NCREC counterparts? Intuitively, the relatively high temperature is most simply explained by elevated magma flux, and therefore heat flux, from the mantle. The relative dryness may simply be a consequence of higher temperatures that produce more melt and thus dilute the available water. The SBMVC magmas exhibit trace element characteristics that suggest they may have evolved under thermal conditions intermediate between the PST and the rest of the NCREC. The SBMVC may represent an intense, but relatively short-lived and localized progression of waxing (pre-PST trachyte lavas and Cook Canyon Tuff),

culmination (PST), and waning (Silver Creek intrusive complex and diverse, post-PST volcanics) stages of a magmatism—a very brief ignimbrite "flare-up" (e.g. Lipman, 2007). The remainder of NCREC magmatism reflected less focused and intense thermal flux from the mantle. In any case, as a large body of crystal-poor magma, the PST was probably able to convect vigorously and homogenize itself isotopically and perhaps assimilate relatively large amounts of host crust. This contrasts with the remainder of the NCREC, where other smaller batches of cooler magma were less able to convect, homogenize, and assimilate, resulting in a wider and less evolved range of isotopic compositions.

CHAPTER VII

CONCLUSIONS

The PST outflow reflects the local accumulation of a vast quantity of magma on a relatively short timescale. New isotope data presented here strongly suggest that the PST represents a single and unusually well mixed, homogenous magma prior to the crystal segregation that produced zonation within the magma chamber. Isotopic and elemental data as well as the results of trace element and AFC modeling support the following conclusions:

- The PST exhibits isotopic evidence for hybridization of Proterozoic crust and enriched lithospheric mantle. Lead isotopes verify involvement of crust of the Mojave, rather than Arizona, crustal province, while Nd, Hf, and Sr isotopes require mantle as well as regional crustal components. Taken together, the isotopic data support a hybrid origin within the Mojave lithosphere (enriched mantle and Proterozoic crust), similar to the origin that has been proposed for both Mesozoic and Miocene magmas across the NCREC.
- The PST's depletion in Sr and Ba, enrichment in REE, and elevated zircon saturation temperatures relative to similarly felsic magmas from throughout the NCREC suggest early precipitation of alkali feldspar ± plagioclase in the absence of accessories. This can be explained by a higher temperature and drier heritage for the PST.

- Plausible high temperature petrogenetic scenarios that can explain the origin of the PST include:
    - Partial melting of "pre-hybridized" Mesozoic igneous crust, potentially in response to intense heating by influx of mantle-derived mafic magmas may have directly created the PST.
    - Open-system processes (AFC or MASH-like) mixing enriched mantle-derived mafic magma with Proterozoic Mojave crust may have directly generated the PST or instead produced voluminous trachyte magmas (the Gold Road and Alcyone formations) that subsequently fractionated in a mostly closed system, forming the PST.
- Comparison of the PST and other NCREC compositions with magmas erupted from the Y-SRP and in the Great Basin suggest that the PST, and to a lesser degree the SBMVC, was the response to intense heat flux from the mantle to Mojave crust. The petrogenetic situation appears to have been very similar, though much more spatially and temporally restricted, to that which has produced the Y-SRP magmas, and in contrast with Cenozoic magmatism in the rest of the NCREC and Great Basin.

APPENDIX

A.Table 1. Elemental Composition of PST pumice, fiamme, and enclaves. Data for samples marked with asterisks are from this study.

Sample	PST14001B*	PSTLW01B*	PSTPMCA02B*	PSTSWA-01E*	PSPSTC*
Group	HSR	HSR	HSR	HSR	HSR
SiO_2	74.07	73.77	74.73	74.26	74.07
Al_2O_3	14.39	14.31	13.58	14.62	12.78
Fe_2O_3(T)	1.33	1.67	1.85	1.60	1.78
MnO	0.06	0.07	0.08	0.05	0.08
MgO	0.72	0.85	0.98	1.68	0.72
CaO	0.65	0.64	0.80	0.95	1.49
Na_2O	2.38	2.19	3.18	2.33	3.21
K_2O	6.07	6.21	4.56	4.25	5.63
TiO_2	0.29	0.25	0.24	0.25	0.21
P_2O_5	0.03	0.03	<0.01	<0.01	0.03
Ba	16	22	15	22	32
Be	5	5	5	5	5
Cs	3.1	3.4	3.3	3.1	3.5
Cu	8	6	3	13	1
Ga	17	19	19	18	19
Ge	2.0	2.2	2.1	1.9	1.3
Hf	5.8	6.8	6.4	6.8	8.6
Nb	29.1	32.2	32.7	30.3	37.8
Pb	25	25	31	33	30
Rb	211	187	202	199	201
S	60	60	80	260	60
Sc	3.54	4.14	3.73	4.20	3.63
Sr	14	16	11	39	17
Ta	2.28	2.58	2.46	2.54	2.50
Th	29.3	31.5	30.8	31.4	32.2
U	5.50	4.98	5.69	5.74	6.06
V	8	9	9	8	6
Y	29	30	31	35	38
Zn	62	63	59	66	50
Zr	191	228	201	239	221
La	53.1	58.4	54.2	67.9	70.1
Ce	95	111	102	129	127
Pr	10.0	11.5	10.8	13.7	14.7
Nd	33.2	38.1	35.2	46.0	42.2
Sm	5.78	6.99	6.59	8.46	7.82
Eu	0.42	0.49	0.50	0.62	0.58
Gd	4.78	5.70	5.66	6.68	6.51
Tb	0.79	0.92	0.92	1.05	1.06
Dy	4.70	5.25	5.31	6.16	6.07
Ho	0.94	1.05	1.06	1.19	1.17
Er	2.77	3.22	3.15	3.48	3.4
Tm	0.45	0.50	0.48	0.51	0.53
Yb	3.09	3.28	3.28	3.40	3.37
Lu	0.49	0.53	0.51	0.59	0.47
Tl	0.95	0.99	1.29	0.92	1.41

A.Table 1 (con't.)

PST01B	PST01C	PST01D	PST01E	PT1B4	WSWPST2A
HSR	HSR	HSR	HSR	HSR	HSR
75.08	75.44	75.45	75.16	75.23	75.12
12.80	12.24	13.14	12.90	12.76	12.84
1.17	1.09	1.06	1.18	1.19	1.40
0.07	0.07	0.07	0.07	0.06	0.08
0.26	0.35	0.20	0.24	0.43	0.20
0.61	1.15	0.75	1.02	1.05	0.61
2.63	2.61	2.72	2.29	2.12	3.63
7.15	6.82	6.39	6.91	6.93	5.86
0.21	0.19	0.20	0.22	0.21	0.23
0.02	0.03	0.03	0.02	0.02	0.02
51	34	40	48	193	40
4	5	4	4	5	4
3.8	3.9	3.3	3.3	4.0	1.5
1	3	2	2	8	10
22	21	20	18	19	18
1.5	1.4	1.3	1.3	1.7	1.8
9.1	8.7	8.8	7.9	9.2	8.1
44.5	43.4	39.4	38.4	49.3	21.5
34	23	24	26	26	24
217	221	198	194	242	195
180	430	100	2830	220	60
3.42	3.43	3.48	3.59	3.32	3.63
14	17	17	18	26	18
2.80	2.80	2.50	2.50	2.55	2.43
34.4	35.3	32.9	30.2	37.1	24.5
6.30	6.69	6.18	5.69	6.99	4.10
6	7	<5	9	7	<5
36	33	33	38	31	33
58	52	50	37	20	46
239	223	221	200	250	257
72.1	68.8	69.7	69.0	59.0	78.3
131	124	124	121	118	141
15.2	13.9	13.9	14.5	11.9	15.6
43.4	38.6	38.7	41.7	36.5	48.2
7.93	6.81	6.72	7.52	6.70	8.50
0.64	0.51	0.57	0.58	0.42	0.63
6.62	5.66	5.51	6.48	5.33	6.48
1.08	0.91	0.89	1.02	0.87	1.03
6.17	5.44	5.20	5.71	5.26	5.85
1.19	1.07	1.03	1.10	1.06	1.19
3.50	3.29	3.17	3.36	3.24	3.47
0.56	0.52	0.51	0.52	0.54	0.55
3.51	3.37	3.18	3.24	3.68	3.46
0.50	0.48	0.47	0.45	0.57	0.47
1.32	1.40	1.14	2.27	0.90	0.20

A.Table 1 (con't.)

WSWPST2D	WSWPST2F	WSWPST2G	WSWPST2B	GJPST1A	WSWPST4D
HSR	HSR	HSR	LSR	LSR	LSR
76.08	74.76	74.43	71.00	72.03	71.94
12.69	13.35	13.57	14.70	14.74	14.80
1.09	1.27	1.32	1.96	1.83	1.69
0.05	0.04	0.05	0.08	0.04	0.05
0.09	0.13	0.12	0.23	0.17	0.35
0.51	0.60	0.65	0.85	0.55	0.92
3.29	3.45	3.56	4.04	3.89	3.86
5.99	6.17	6.06	6.77	6.32	6.03
0.19	0.21	0.22	0.35	0.36	0.34
0.02	0.02	0.02	0.02	0.06	0.03
70	60	65	75	87	59
4	4	4	3	3	3
1.4	1.4	1.7	1.0	0.9	2.1
5	7	4	4	3	2
17	18	18	19	20	20
1.7	2.0	1.7	2.1	1.9	1.8
7.6	7.5	7.6	12.2	11.4	11.8
30.9	34.0	33.9	31.0	28.3	30.8
20	16	18	25	25	25
196	213	211	178	142	162
120	150	70	40	10	20
2.71	3.15	3.31	3.58	3.22	3.28
21	26	19	23	22	27
2.23	2.33	2.53	2.18	2.22	2.29
27.6	28.4	29.0	20.0	22.2	20.8
4.89	4.07	4.62	2.77	2.82	2.91
6	<5	<5	8	19	9
33	32	33	57	47	61
27	36	39	55	46	49
249	252	238	513	478	475
75.3	69.1	78.2	115.0	108.0	88.2
127	117	136	231	202	185
14.4	13.2	15.1	30.0	26.7	24.7
43.9	41.8	45.1	107.0	98.6	96.3
8.01	7.35	8.01	22.30	20.30	20.80
0.60	0.59	0.63	1.55	1.54	1.53
6.08	5.45	6.53	15.9	14.10	15.70
0.99	0.91	1.01	2.63	2.18	2.50
5.66	5.21	5.62	14.00	11.10	13.20
1.12	1.08	1.15	2.49	1.96	2.45
3.18	3.14	3.37	6.32	4.88	6.16
0.54	0.52	0.55	0.88	0.73	0.85
3.17	3.31	3.47	4.86	3.83	4.79
0.44	0.46	0.48	0.62	0.51	0.60
0.33	0.38	0.41	0.14	0.32	0.24

A.Table 1 (con't.)

GJPST1C LSR	PSTLW01C* LSR	PSTG1C Trachyte	PSTG1A Trachyte	PSTSWA01A* Trachyte	PSTSWA01H* Trachyte
73.15	72.74	68.82	68.63	64.60	65.85
14.08	15.87	16.16	16.06	17.28	16.96
1.80	1.71	2.24	2.32	4.16	3.74
0.08	0.07	0.07	0.07	0.08	0.08
0.19	2.24	0.42	0.48	0.78	0.83
0.61	0.89	1.29	1.39	2.37	2.23
3.74	2.01	4.00	4.15	3.92	3.64
5.96	4.12	6.41	6.29	6.07	6.02
0.33	0.32	0.47	0.49	0.59	0.54
0.06	0.02	0.10	0.11	0.14	0.12
209	33	1016	1066	2559	2391
3	4	3	3	2	2
1.0	2.4	2.0	1.0	2.0	2.0
4	16	10	5	15	13
18	21	21	20	19	19
1.7	1.7	1.9	2.2	2.2	2.0
11.0	8.1	13.3	13.1	13.3	12.3
31.8	36.7	21.8	21.7	14.3	13.5
20	29	39	30	29	21
138	123	140	131	129	131
180	80	80	20	370	350
3.31	4.97	6.05	6.55	8.64	8.40
37	33	199	208	475	388
2.48	2.88	1.40	1.40	1.08	1.06
20.6	33.3	19.8	19.4	13.3	13.9
2.50	3.41	4.11	3.83	1.85	1.92
12	19	16	21	28	26
38	34	34	33	26	25
40	88	70	65	75	66
445	273	576	579	736	647
97.1	59.8	173.0	173.0	133.0	135.0
191	139	338	336	236	242
24.6	13.2	35.6	38.7	26.9	26.9
90.4	45.1	106.0	109.0	98.1	96.0
18.00	8.44	18.10	17.60	13.70	13.60
1.42	0.67	3.14	3.23	3.52	3.45
12.60	6.90	10.90	11.10	8.96	8.30
1.84	1.09	1.45	1.45	1.07	1.01
9.09	6.36	7.60	7.44	5.51	5.29
1.62	1.24	1.41	1.39	0.98	0.98
4.06	3.51	3.93	3.89	2.82	2.74
0.58	0.52	0.57	0.55	0.40	0.38
3.42	3.46	3.49	3.32	2.55	2.49
0.45	0.56	0.50	0.50	0.43	0.42
0.33	0.98	0.78	0.65	0.76	0.71

A.Table 1 (con't.)

MLPT5D*	CRW2A	28556P1	CRWPST	WSWPST4B	PSTNY01A	WSWPST1
Trachyte	Trachyte	Trachyte	Trachyte	Trachyte	Enclave	Enclave
67.85	68.68	69.30	66.07	69.14	69.95	57.61
16.62	16.30	15.39	17.00	16.18	15.53	16.96
3.04	3.33	2.65	3.26	1.98	2.62	7.48
0.07	0.05	0.08	0.06	0.05	0.08	0.07
0.53	0.66	1.11	0.81	0.60	0.32	2.50
1.28	0.74	1.65	1.21	1.19	0.20	5.41
3.29	5.82	2.69	3.49	3.75	4.95	3.50
6.72	3.80	6.56	7.33	6.67	5.82	4.59
0.53	0.49	0.46	0.57	0.39	0.48	1.32
0.07	0.13	0.13	0.20	0.04	0.05	0.55
560	1565	802	2950	222	30	1943
2	3	3	2	2	3	3
1.0	1.0	2.0	2.0	2.0	2.9	0.1
10	7	6	10	7	6	33
20	19	19	19	17	29	22
2.1	1.3	1.4	1.7	2.0	2.3	1.9
10.2	13.5	14.4	14.9	11.0	13.7	9
16.9	23.7	31.4	18.5	24.1	35.1	21.5
31	16	15	28	25	21	46
127	81	141	149	157	146	96
180	60	60	20	160	90	350
8.64	6.84	6.80	7.36	5.30	7.34	12.2
129	256	185	437	67	11	1514
1.31	0.95	1.38	1.18	1.61	2.05	1.27
18.9	16.5	22.0	16.7	19.0	19.2	20.3
2.00	2.03	2.80	2.39	2.53	3.24	4.15
20	21	18	32	12	17	109
33	27	34	30	30	52	31
65	49	49	62	54	97	87
479	615	608	759	500	635	400
174.0	154.0	147.0	172.0	154.0	159	151
320	295	298	294	254	236	238
35.8	32.8	32.3	34.2	31.0	37.6	30.8
129.0	114.0	112.0	113.0	108.0	136	104
18.80	15.90	16.80	16.00	16.50	23.9	15.8
2.84	3.46	2.66	3.77	2.52	1.41	3.38
12.00	9.93	11.40	12.00	10.30	14.8	11
1.39	1.21	1.52	1.29	1.39	2.15	1.2
7.11	5.85	7.58	6.13	6.8	11.5	5.64
1.27	1.07	1.38	1.10	1.26	2.06	1.01
3.43	2.89	3.81	3.08	3.43	5.78	2.74
0.48	0.37	0.54	0.42	0.50	0.87	0.365
2.98	2.65	3.46	2.72	3.02	5.49	2.35
0.49	0.42	0.54	0.40	0.45	0.855	0.328
1.90	0.37	4.14	0.45	0.12	0.57	0.54

A.Table 2. Elemental composition non-PST NCREC magmas, including similarly felsic Miocene volcanics (Metcalf, 2004 and personal communication, 2012), SBMVC units (McDowell et al., in prep.), granitic chilled margins (Harper et al., 2004; Bachl et al., 2001; Walker et al., 2007).

Sample	MP1	SCM-6	SCM-17a	PSM1	TIP-1
Group	SBMVC	SBMVC	SBMVC	SBMVC	SBMVC
Description	Moss Porphyry	Moss Porphyry	Moss Porphyry	Moss Porphyry	Times Porphyry Granite
SiO_2	66.83	62.77	65.47	62.84	74.13
Al_2O_3	14.92	15.29	15.25	16.12	13.14
Fe_2O_3(T)	4.27	6.12	4.74	5.15	2.13
MnO	0.06	0.09	0.04	0.10	0.04
MgO	1.49	2.42	2.00	2.41	0.26
CaO	2.64	3.92	2.81	3.84	0.80
Na_2O	3.97	3.26	3.96	4.39	3.80
K_2O	4.92	4.90	4.75	3.92	5.38
TiO_2	0.69	0.93	0.77	0.90	0.29
P_2O_5	0.21	0.31	0.22	0.33	0.02
Ba	1175	1206	1068	1193	309
Be	3	3	4	3	3
Cs	1.8	1.7	1.8	1	2.3
Cu	14	22	26	11	4
Ga	20	21	22	22	20
Ge	1.7	1.8	1.6	2.2	1.9
Hf	6.3	8.7	8.4	12.1	7.7
Nb	17.2	20.6	22.7	19.5	27.5
Pb	19	46	15	33	24
Rb	158	147	147	108	142
S	0.004	0.016	0.008	0.043	0.003
Sc	7.61	11.8	8.75	10.7	3.83
Sr	391	569	380	611	92
Ta	1.1	1.32	1.53	1.3	1.97
Th	16.7	18.6	21	20.1	26.1
U	2.64	2.73	2.81	4.11	3.52
V	62	99	69	94	14
Y	19	28	24	24	29
Zn	57	47	56	86	55
Zr	261	377	353	490	257
La	75.8	89.3	91.8	80.7	84.9
Ce	146	176	178	160	157
Pr	15.6	19	18.9	18.7	15.8
Nd	53.4	66.3	64.9	55.5	49.4
Sm	8.39	10.8	10.5	9.63	8.06
Eu	1.57	2.06	1.89	2.31	0.885
Gd	5.8	7.76	7.22	6.84	5.94
Tb	0.77	1.08	0.97	0.98	0.9
Dy	4.03	5.6	5.05	5.27	5.1
Ho	0.78	1.04	0.97	1.03	1.05
Er	2.14	2.82	2.66	2.96	3.07
Tm	0.309	0.404	0.374	0.428	0.466
Yb	2.01	2.6	2.32	2.63	3.13
Lu	0.313	0.411	0.355	0.387	0.501
Tl	1.31	3.3	0.24	0.87	0.72

A.Table 2 (con't.)

SCM-37 SBMVC Time Porphyry Granite	PSTG2 SBMVC Times Porphyry Granite	SCM-20 SBMVC Times Porphyry Leucogranite	SCM-38 SBMVC Times Porphyry Leucogranite	SCM-26 SBMVC Mafic Dike	SCM-1 SBMVC Feldspar Porphyry Dike
72.49	73.89	76.20	77.14	55.28	67.74
13.81	13.41	12.49	12.21	14.97	14.94
2.26	1.36	2.61	1.48	8.70	3.87
0.07	0.07	0.02	0.04	0.12	0.07
0.45	0.25	0.24	0.14	6.11	1.21
1.24	0.90	0.47	0.35	6.32	2.78
3.94	4.57	2.34	3.39	3.61	3.16
5.30	5.23	5.38	5.08	3.29	5.40
0.36	0.28	0.24	0.17	1.13	0.63
0.08	0.05	0.02	0.01	0.47	0.19
448	188	133	42	1167	1059
3	4	2	3	2	3
2.1	2.3	4	1.1	1.3	1.7
6	2	10	4	46	6
19	20	14	17	20	20
2	2.2	1.2	1.7	1.9	1
7	9.6	6.9	5	5.9	7.4
26.3	30.9	31.2	31.8	14.4	23.9
19	29	57	27	13	30
148	185	184	183	80	156
0.014	0.03	0.013	0.006	0.078	0.003
3.73	3.55	1.93	2.08	19.8	7.16
148	55	110	39	827	372
1.66	2.1	2.08	1.97	0.82	1.63
26	28.6	34.7	33.7	11.5	19.3
3.21	4.84	3.6	4.78	1.99	3.35
21	14	10	8	150	51
27	30	20	21	24	26
51	49	39	37	76	74
275	310	222	135	248	298
72.7	82	53.9	48	73.5	79.3
144	158	106	87.8	149	153
14.4	17.1	10.3	7.64	17	16.1
48	47.2	33.1	22.1	63.2	53.4
7.78	8.02	5.52	3.49	10.6	8.63
1.01	0.884	0.384	0.22	2.38	1.45
6.55	5.87	4.55	3.25	7.65	6.42
0.88	0.99	0.63	0.51	1.04	0.96
4.81	5.69	3.51	2.97	5.3	5.18
1	1.17	0.76	0.7	1	1.04
2.88	3.64	2.28	2.27	2.69	2.89
0.436	0.569	0.368	0.381	0.376	0.432
2.89	3.68	2.53	2.67	2.32	2.88
0.47	0.529	0.43	0.442	0.359	0.451
1.03	1.09	0.98	1.09	0.47	0.26

A.Table 2 (con't.)

SCM-13	SCM-30	SCM-31	SCM-35	SCM-40	SCM-42
SBMVC Feldspar Porphyry Dike	SBMVC Feldspar Porphyry Dike	SBMVC Feldspar Porphyry Dike	SBMVC Feldspar Porphyry Dike	SBMVC Felsic Dike	SBMVC Felsic Dike
67.09	61.01	69.41	63.16	73.86	74.02
15.27	14.85	14.42	16.24	13.80	14.08
3.88	5.88	3.26	5.20	1.84	1.66
0.08	0.09	0.07	0.08	0.04	0.02
1.29	5.18	1.22	1.89	0.36	0.73
3.13	5.40	2.16	3.35	0.84	0.58
3.92	3.01	4.21	4.19	2.95	1.95
4.56	3.45	4.56	4.63	5.93	6.58
0.63	0.85	0.51	0.91	0.32	0.33
0.16	0.28	0.17	0.33	0.05	0.04
980	823	854	1208	435	469
3	2	2	2	4	4
2.3	1.7	0.5	0.9	2.5	1.9
5	71	46	17	4	7
20	18	18	20	18	17
0.9	1.8	1.5	1.4	1.7	2
7.4	4.7	7.5	5.8	7.2	7
23.6	14.6	22.8	16.6	28.2	28.9
22	16	22	15	33	26
125	80	126	150	188	202
0.006	0.031	0.024	0.027	0.063	0.005
7.01	13.9	5.72	9	3.35	3.13
321	504	276	471	93	71
1.57	0.81	1.47	0.94	1.85	1.99
19.1	11.9	23.5	15.1	35.4	29.1
3.19	1.86	3.41	2.46	5.5	4.13
55	108	41	102	14	15
27	17	24	21	28	25
64	70	58	64	36	39
295	200	302	240	252	251
78	55.3	76.7	60.5	78.3	74.4
150	110	149	121	153	144
15.6	11.5	14.9	12.7	15.5	14.7
53.1	42.1	50.6	46.3	51.4	49
8.53	6.94	8.27	7.83	8.15	7.77
1.49	1.55	1.38	1.73	1.03	0.974
6.41	5.54	6.62	6.32	6.45	5.64
0.92	0.68	0.89	0.81	0.9	0.8
4.96	3.45	4.65	3.99	4.87	4.68
0.99	0.65	0.93	0.78	0.98	0.95
2.82	1.86	2.67	2.2	2.84	2.78
0.421	0.267	0.408	0.326	0.434	0.461
2.85	1.7	2.66	2.05	2.98	3
0.457	0.265	0.439	0.336	0.496	0.496
0.16	0.4	0.9	1.04	0.88	1.124

A.Table 2 (con't.)

BCD	SCM-5a	SCM-34	SCM-41	SIT-1	SIT-1b
SBMVC Quartz Porphyry Dike	SBMVC Quartz Porphyry Dike	SBMVC Alcyone Pre-PST Trachyte	SBMVC Gold Road Pre-PST Trachyte	SBMVC Post-PST glassy lava	SBMVC Enclave in glassy lava
77.98	79.93	64.35	63.77	71.00	56.57
11.01	10.03	16.10	16.44	14.41	17.14
1.25	1.11	4.53	4.70	2.63	7.12
0.03	0.02	0.07	0.09	0.05	0.09
0.12	0.21	1.51	1.20	0.82	3.91
0.10	0.21	3.08	4.19	2.28	6.98
0.36	0.33	3.61	3.60	3.54	3.59
9.03	8.07	5.63	4.76	4.70	2.95
0.11	0.09	0.80	0.91	0.45	1.14
0.01	0.01	0.32	0.34	0.12	0.49
108	423	2226	1391	674	1511
2	2	3	3	3	2
5.7	2.4	1.4	1.4	2.5	1.4
23	6	12	25	6	35
13	10	21	21	18	23
1.4	1.3	1.9	1.9	1.7	1.8
3.7	3	11.1	8.4	5.6	6.2
30.5	27.7	19.4	22.5	22.1	15.2
22	13	29	24	25	10
397	337	135	126	156	74
0.008	0.004	0.022	0.029	0.012	0.043
1.67	1.58	8.47	8.39	4.68	15.4
152	65	590	602	291	1106
2.28	2.04	1.13	1.42	1.57	0.82
40.3	32.7	17.1	19.2	28.5	18.8
5.38	5.72	2.75	3.47	4.64	2.11
10	8	60	81	36	154
19	13	27	27	22	25
32	11	91	72	40	84
92	67	570	360	210	273
38.4	29.3	115	87.1	66.1	117
74.6	50.9	223	172	126	184
6.66	4.23	24.1	18.5	12.5	24.1
19.7	11.6	86.7	66.2	42.3	86.9
3.33	1.73	12.7	10.3	6.67	13.5
0.213	0.157	2.95	2.14	1.18	2.66
3.17	1.64	9.29	7.86	5.49	9.65
0.5	0.26	1.1	1	0.74	1.17
2.97	1.63	5.75	5.36	3.84	5.43
0.68	0.38	1.05	1	0.78	0.94
2.15	1.36	2.95	2.84	2.27	2.71
0.377	0.269	0.437	0.402	0.353	0.359
2.62	2	2.81	2.57	2.4	2.18
0.442	0.358	0.459	0.412	0.399	0.338
4.86	4.13	1.144	1.412	0.97	0.76

A.Table 2 (con't.)

MPe1	SCM-27b	5/11-#2	5/14-#3	5/29-2B	BML26Z
SBMVC Enclave in Moss Porphyry	SBMVC Enclave in Times Porphyry	SBMVC DP plug	SBMVC Rhyolite flow	SBMVC Rhyolite breccia	SBMVC Rhyolite breccia
59.07	68.08	65.03	80.14	69.45	67.64
16.29	15.37	17.43	11.16	16.71	17.07
7.02	3.94	3.46	0.77	2.41	2.46
0.08	0.07	0.03	0.02	0.04	0.05
3.24	1.01	1.12	0.10	0.62	0.60
4.93	1.63	2.61	0.62	0.72	2.08
4.15	4.72	4.70	3.07	4.79	4.55
3.67	4.37	4.69	3.99	4.81	5.10
1.12	0.61	0.64	0.09	0.32	0.35
0.43	0.19	0.29	0.02	0.12	0.11
1287	1324	2384	108	2142	2229
3	3				
1.4	1.1	0.86	1.80	1.26	1.50
14	4				
20	20	23.2	16.8	20.0	23.0
1.8	1.5				
6.4	9.5	20.6	5.7	11.7	9.8
21.4	21.1	16.8	17.7	16.1	18.1
15	28	32.4	39.9	52.0	30.0
107	142	108	122	110	93
0.021	0.01				
12.5	5.26				3.06
712	286	873	41	985	1112
1.3	1.7	1.0	1.2	1.1	1.1
13	15.2	16.0	16.4	22.5	22.4
2.38	2.24	2.50	2.43	2.47	2.37
121	35	20.2	<5	20.5	14.0
21	21	25	13	20	18
48	71	102.0	54.0	73.6	65.0
279	431	84	19	101	133
74.1	73.9	161.3	43.2	189.0	245.0
146	132	19	5	20	27
15.9	13.2	67.4	20.6	69.2	81.1
56.6	43.7	67.4	20.6	69.2	81.1
9.27	6.6	10.25	4.30	10.19	11.30
2.17	1.37	2.46	0.68	2.07	2.30
6.69	4.82	7.92	3.37	7.49	5.65
0.94	0.69	0.86	0.49	0.75	0.76
4.79	3.79	4.31	2.51	3.39	3.44
0.89	0.75	0.82	0.48	0.61	0.60
2.43	2.19	2.44	1.53	1.72	1.64
0.347	0.333	0.35	0.23	0.26	0.24
2.2	2.26	2.25	1.54	1.62	1.57
0.343	0.37	0.33	0.22	0.23	0.22
0.56	0.78	0.39	0.45	0.80	0.80

A.Table 2 (con't.)

BML 37Z	5/11/01-#2	5/9-#5	1/4-#4	BML22Z	BML 65Z
SBMVC Rhyolite breccia	SBMVC Ignimbrite	SBMVC Trachydacite	SBMVC Trachydacite	SBMVC Trachytdacite	SBMVC Trachydacite
74.96	75.61	64.01	66.72	63.30	64.88
13.87	12.61	16.23	15.63	16.19	16.16
1.33	1.80	5.30	4.68	5.33	4.85
0.03	0.05	0.07	0.06	0.09	0.06
0.18	0.14	1.54	1.36	1.85	0.76
0.88	0.36	3.55	2.61	3.78	4.29
4.05	3.98	3.89	3.28	3.84	3.22
4.49	5.14	4.11	4.43	4.23	4.40
0.19	0.25	0.94	0.90	0.99	0.96
0.04	0.05	0.36	0.34	0.40	0.41
2618	121	1332	1566	1944	1648
3.00	4.29	1.29		2.20	2.10
12.0	22.6	20.2	19.9	20.0	23.0
6.4	12.5	10.3	9.1	8.7	9.1
17.7	36.2	21.0	19.0	21.3	18.7
23.0	32.0	30.4	31.0	17.0	17.0
88	164	109	110	105	121
3.34	3.8			10.4	10.8
507	49	644	565	704	678
1.4	2.6	1.3	1.2	1.2	1.3
19.5	20.9	16.4	13.9	14.3	15.8
3.17	3.55	2.98	3.17	2.28	2.68
< 5	15.0	88.4	87.0	80.0	81.0
19	47	29	27	29	29
60.0	85.9	80.9	75.0	73.0	79.0
90	53	70	91	92	89
173.0	113.9	138.2	170.3	179.0	177.0
19	13	16	19	20	20
54.6	47.4	56.0	65.8	66.9	64.5
54.6	47.4	56.0	65.8	66.9	64.5
7.88	10.31	9.30	10.30	10.80	10.50
1.31	0.52	1.94	2.40	2.49	2.40
4.97	8.38	7.73	7.25	7.10	8.19
0.67	1.53	0.95	1.01	1.05	1.16
3.24	8.63	4.78	5.23	5.18	5.64
0.59	1.72	0.89	0.99	1.00	1.03
1.80	4.83	2.66	2.73	2.87	2.95
0.27	0.78	0.37	0.40	0.40	0.43
1.71	4.84	2.21	2.49	2.44	2.70
0.25	0.68	0.31	0.36	0.36	0.39
0.59	0.63	0.45	0.24	0.61	0.53

A.Table 2 (con't.)

BML 48	FTO6-1	TPS-1	NAWZ53	HAW 80	HAW 84
SBMVC Trachydacite	SBMVC Ignimbrite	SBMVC Tuff	Chilled Granites Aztec Wash chilled margin	Chilled Granites Aztec Wash chilled margin	Chilled Granites Aztec Wash chilled margin
62.51	65.23	68.74	73.22	74.07	72.70
16.24	14.76	13.89	14.14	13.73	14.42
5.56	5.79	4.31	1.74	1.63	1.79
0.10	0.07	0.05	0.04	0.03	0.04
2.59	1.57	1.01	0.54	0.57	0.55
4.57	3.68	2.96	1.43	0.51	1.61
4.07	3.78	1.87	3.37	3.35	3.51
2.87	3.68	6.09	5.19	5.79	5.05
1.04	1.03	0.77	0.26	0.25	0.25
0.45	0.42	0.31	0.07	0.07	0.08
1859	1410	1137	1321	1347	1376
6.60	0.30	4.30			
22.0	20.0	20.0			
9.3	8.4	6.7	5.19	4.88	4.85
18.0	18.3	14.3	15.14	16.14	14.61
19.0	17.0	11.0			
134	57	116	154	141	133
11.5	12.4	7.36			
912	639	551	331	227	360
1.2	1.2	0.9	1.10	1.21	1.52
15.2	13.5	10.7	15.55	14.80	14.80
2.63	2.47	3.12	1.83	1.80	2.09
89.0	106.0	63.0			
29	29	20			
84.0	127.0	50.0			
90	81	59	169.48	186.79	173.17
175.0	159.0	120.0	53.26	57.50	53.30
20	18	14	89.48	105.00	93.20
64.4	58.9	43.7	8.91	9.90	9.07
64.4	58.9	43.7	28.63	33.40	31.40
10.20	9.91	6.81	4.57	5.13	4.62
2.30	2.33	1.60	0.89	0.89	0.91
7.73	7.64	5.38	3.19	3.50	3.23
1.05	1.06	0.75	0.49	0.50	0.50
5.13	5.33	3.47	2.61	2.97	2.76
0.98	1.03	0.66	0.51	0.58	0.53
2.64	2.81	1.93	1.54	1.69	1.64
0.38	0.41	0.28	0.25	0.26	0.25
2.43	2.47	1.79	1.69	1.78	1.74
0.37	0.38	0.27	0.26	0.27	0.26
0.97	0.33	0.73			

A.Table 2 (con't.)

SL200Z	BD3	BD9	BD16	BD18	BD35
Chilled Granites Dike, Searchlight Pluton	Chilled Granites Dike, Spirit Mountain Batholith	Chilled Granites Dike, Spirit Mountain Batholith	Chilled Granites Dike, Spirit Mountain Batholith	Chilled Granites Dike, Spirit Mountain Batholith	Chilled Granites Dike, Spirit Mountain Batholith
73.04	72.67	72.42	71.50	73.21	73.12
13.94	14.51	14.39	14.36	14.25	14.20
2.01	2.01	2.08	2.49	1.91	1.93
0.04	0.04	0.04	0.04	0.04	0.04
0.62	0.63	0.53	0.86	0.52	0.48
1.29	1.78	1.68	2.12	1.56	1.59
3.61	3.49	3.64	3.62	3.48	3.57
5.00	4.52	4.79	4.53	4.68	4.72
0.35	0.27	0.33	0.36	0.27	0.27
0.10	0.09	0.08	0.10	0.08	0.08
582	980	956	1099	796	848
6.30	4.19	5.43	4.37	4.56	4.33
28.10	12.31	17.60	11.97	13.48	13.31
157	155	155	125	144	147
196	287	209	271	225	246
1.90	1.05	1.56	0.93	1.17	1.18
33.10	13.83	19.15	12.43	15.83	14.94
4.92	1.91	2.60	1.67	1.88	2.14
218.00	140.00	192.00	175.00	159.00	139.00
60.80	42.22	60.88	44.34	49.30	42.53
113.00	77.33	110.67	80.62	89.63	79.27
11.30	7.54	10.52	7.77	8.56	7.70
33.70	27.24	36.92	28.05	30.45	27.51
5.45	4.68	6.06	4.66	5.04	4.65
0.89	0.87	1.07	0.93	0.85	0.84
4.15	3.49	4.50	3.40	3.63	3.50
0.60	0.57	0.75	0.56	0.58	0.59
3.22	2.89	3.85	2.85	2.95	3.05
0.61	0.54	0.72	0.53	0.54	0.58
1.82	1.72	2.36	1.74	1.75	1.93
0.29	0.26	0.35	0.26	0.28	0.29
1.85	1.58	2.30	1.65	1.77	1.85
0.28	0.23	0.33	0.23	0.25	0.28

A.Table 2 (con't.)

BD39	BW11	BW62	BW63	BGZ	BW33
Chilled Granites Dike, Spirit Mountain Batholith	Chilled Granites Sill, Spirit Mountain Batholith	Chilled Granites Sill, Spirit Mountain Batholith	Chilled Granites Sill, Spirit Mountain Batholith	Chilled Granites Sill, Spirit Mountain Batholith	Chilled Granites Sill, Spirit Mountain Batholith
72.44	72.12	71.36	72.98	73.83	70.93
14.42	14.38	14.83	14.28	14.23	15.00
2.10	2.39	2.40	1.90	1.56	2.47
0.04	0.04	0.05	0.04	0.04	0.05
0.59	0.80	0.69	0.51	0.34	0.63
2.06	2.10	2.09	1.64	1.48	2.00
3.57	3.77	3.65	3.48	3.63	3.59
4.38	3.97	4.47	4.87	4.62	4.82
0.30	0.34	0.35	0.23	0.23	0.38
0.10	0.10	0.11	0.08	0.05	0.11
685	1063	1183	1053	1009	1291
4.80	4.44	4.68	4.92	4.40	4.99
15.64	13.04	13.74	14.25	15.30	16.13
132	110	148	171	169	125
235	268	332	240	243	315
1.19	1.18	1.09	1.16	0.84	1.33
14.96	12.85	11.75	16.73	14.80	11.75
2.15	1.66	1.57	1.68	1.14	0.79
169.00	167.00	172.00	180.00	150.00	186.00
44.08	45.26	50.20	58.61	54.09	58.27
81.64	85.95	94.87	107.91	100.94	108.27
8.01	8.76	9.79	10.67	9.75	10.45
29.60	28.82	32.16	35.11	34.51	38.71
5.11	4.97	5.51	5.82	6.07	6.61
0.93	0.95	1.02	0.92	1.04	1.28
4.08	3.88	4.20	4.19	4.35	5.11
0.67	0.61	0.65	0.66	0.75	0.87
3.49	3.27	3.47	3.35	3.86	4.60
0.65	0.62	0.65	0.62	0.78	0.90
2.10	1.87	1.92	1.92	2.46	2.80
0.32	0.28	0.29	0.29	0.37	0.40
1.97	1.83	1.81	1.82	2.29	2.51
0.29	0.27	0.26	0.25	0.34	0.34

A.Table 2 (con't.)

TAW113	TAW114	TAW112	NAW-Z 13	AW 542	AW 557
Chilled Granites Sill, Aztec Wash	Chilled Granites Sill, Aztec Wash	Chilled Granites Sill, Aztec Wash	Chilled Granites Sill, Aztec Wash	Chilled Granites Sill, Aztec Wash	Chilled Granites Sill, Aztec Wash
74.80	72.55	71.65	73.89	74.19	73.94
13.84	14.46	14.88	14.31	13.99	13.99
0.94	1.74	1.85	1.31	1.27	1.40
0.03	0.04	0.02	0.03	0.02	0.03
0.16	0.40	0.61	0.47	0.42	0.33
0.52	0.85	1.85	1.55	1.16	1.14
3.86	4.37	3.88	3.83	3.39	3.60
5.68	5.16	4.82	4.37	5.32	5.29
0.16	0.34	0.33	0.19	0.18	0.20
0.02	0.09	0.11	0.06	0.06	0.06
208	539	1136	1284	1199	1195
6.20	8.20	5.92	3.64	3.90	4.45
27.82	28.32	18.33	12.80	12.73	9.73
214	168	112	129	170	117
158	238	473	417	278	368
2.30	1.80	1.20	1.18	1.27	0.64
39.20	35.00	24.00	13.96	13.45	18.29
8.70	6.50	5.50	3.07	2.32	2.13
166.00	277.00	202.00	114.00	134.00	158.00
54.33	72.65	58.39	36.51	41.19	52.97
79.39	120.59	95.01	62.83	72.90	89.86
5.49	9.77	7.95	6.82	7.07	8.28
15.01	32.82	27.61	22.37	23.63	26.89
1.93	5.09	4.53	3.62	3.74	3.65
0.24	0.89	0.93	0.69	0.68	0.78
0.85	2.72	2.74	2.75	2.97	2.48
0.19	0.47	0.45	0.44	0.48	0.32
1.28	2.65	2.46	2.38	2.64	1.54
0.27	0.49	0.44	0.48	0.50	0.28
0.95	1.52	1.31	1.46	1.54	0.86
0.18	0.25	0.21	0.25	0.26	0.13
1.31	1.76	1.42	1.68	1.65	0.95
0.22	0.27	0.22	0.25	0.25	0.16

A.Table 2 (con't.)

AW 566	SK 46D	S1	NMD-05B	NM24-04	NMD-05D2
Chilled Granites Sill, Aztec Wash	Chilled Granites Sill, Aztec Wash	NCREC Volcanics	NCREC Volcanics	NCREC Volcanics	NCREC Volcanics
73.62	70.10	64.41	65.03	65.14	65.19
14.09	15.46	16.06	16.00	15.16	16.00
1.52	2.63	4.25	4.21	4.32	4.22
0.02	0.04	0.07	0.06	0.07	0.06
0.46	0.80	3.77	2.32	2.37	2.26
1.43	2.21	2.64	2.89	3.49	2.91
3.60	3.73	4.00	4.48	3.94	4.45
4.95	4.49	3.85	4.03	4.52	3.98
0.23	0.40	0.67	0.67	0.70	0.65
0.08	0.14	0.29	0.30	0.28	0.29
1277	1508	1465	1545	1169	1489
		0.57	1.08	1.11	0.98
4.23	5.91	5.50	5.57	6.92	5.37
12.79	15.85	12.50	12.56	19.01	12.10
		26.98	16.77	32.51	16.49
117	109	81.73	88.64	114.28	87.08
		8.66	9.22	9.16	8.96
361	486	1039	1105	772	1115
1.03		0.83	0.82	1.36	0.81
16.80	12.89	10.78	10.93	17.19	10.35
3.05	1.88	1.94	1.99	3.02	1.92
		71	78.3	71.63219	76.7
		16.10	16.32	20.74	15.77
151.00	196.00	201.2	207.2	265.3	202.9
47.90	49.61	59.57	62.02	67.10	57.08
84.13	91.27	105.30	108.50	120.75	100.99
8.01	7.61	11.20	11.50	12.69	10.74
26.66	29.03	41.35	42.52	46.12	40.05
3.97	4.83	7.03	7.29	7.97	6.95
0.81	1.13	1.70	1.83	1.68	1.69
3.03	3.61	4.78	5.03	5.45	4.77
0.45	0.49	0.61	0.63	0.73	0.61
2.52	2.51	3.29	3.22	3.93	3.12
0.48	0.47	0.59	0.60	0.73	0.58
1.49	1.47	1.51	1.51	1.96	1.43
0.24	0.21	0.21	0.21	0.27	0.20
1.59	1.42	1.27	1.30	1.66	1.24
0.25	0.22	0.20	0.20	0.26	0.18

A.Table 2 (con't.)

NM22B-04	KD13	NNV5	SL201Z	NM-5-04	SL200Z
NCREC Volcanics	NCREC Volcanics	NCREC Volcanics	NCREC Volcanics	NCREC Volcanics	NCREC Volcanics
65.91	65.68	65.35	66.22	70.54	73.04
16.58	15.46	15.66	15.70	15.14	13.94
3.72	4.33	4.53	4.33	2.03	2.01
0.06	0.07	0.04	0.06	0.07	0.04
0.88	2.39	2.43	1.84	0.45	0.62
2.58	2.71	3.73	3.55	1.18	1.29
4.18	4.14	4.06	3.93	4.72	3.61
5.13	4.18	3.31	3.33	5.38	5.00
0.69	0.70	0.63	0.76	0.43	0.35
0.26	0.33	0.26	0.28	0.07	0.10
2170	1410	730	1724	1323	582
1.54	0.40		1.40	1.24	0.80
10.65	5.60		7.70	10.22	6.30
20.42	13.40	14.00	27.20	32.67	28.10
27.04	46.00		24.00	25.89	19.00
100.88	90.00	66.00	115.00	134.50	157.00
6.85	7.93		7.55	5.61	4.24
619	662	1010	1017	185	196
1.21	0.99		2.00	2.04	1.90
13.64	13.20		17.20	16.74	33.10
1.59	2.84		3.09	2.70	4.92
27.58791	79		68	18.47721	24
27.10	15.00		22.00	31.38	20.00
491.0	209.0		274.0	409.5	218.0
68.62	72.80		52.20	86.44	60.80
124.37	131.00		103.00	157.78	113.00
13.37	14.10		11.60	16.52	11.30
50.08	50.00		38.80	58.95	33.70
8.87	7.63		6.50	10.11	5.45
2.21	1.82		1.73	1.93	0.89
6.68	5.48		5.55	7.24	4.15
0.93	0.68		0.69	1.04	0.60
5.08	3.30		3.69	5.82	3.22
0.99	0.56		0.71	1.13	0.61
2.60	1.65		2.00	3.05	1.82
0.38	0.23		0.30	0.45	0.29
2.38	1.45		1.90	2.77	1.85
0.38	0.21		0.27	0.43	0.28

A.Table 2 (con't.)

KD15-6	KD8Z	KD6Z	S4	KD15-3	SL76
NCREC Volcanics	NCREC Volcanics	NCREC Volcanics	NCREC Volcanics	NCREC Volcanics	NCREC Volcanics
78.75	80.06	71.32	73.97	74.75	75.89
11.80	10.96	14.46	13.19	13.87	12.81
0.56	0.59	2.38	1.97	1.31	1.32
0.02	0.03	0.05	0.05	0.03	0.02
0.04	0.09	0.71	1.02	0.32	0.29
0.12	0.78	1.61	0.98	0.35	1.03
3.60	2.90	3.55	5.10	3.39	3.33
4.99	4.48	5.35	3.28	5.68	5.01
0.09	0.09	0.44	0.34	0.26	0.24
0.02	0.02	0.12	0.11	0.05	0.06
56	169	980	663	1039	280
0.70	0.80	0.50	2.42	0.70	
3.30	3.40	6.70	5.24	5.80	
26.10	24.10	23.60	18.67	21.70	22.00
23.00	28.00	24.00	20.24	27.00	
177.00	143.00	130.00	144.26	164.00	193.00
1.35	1.46	4.73	3.05	2.36	
56	76	287	184	148	145
2.24	1.90	1.60	1.50	1.79	
21.70	22.10	18.00	18.97	19.00	
3.66	3.14	2.75	2.54	2.65	
6	< 5	27	28	13	
7.00	10.00	24.00	17.66	17.00	22.00
75.0	78.0	250.0	181.9	209.0	190.0
29.40	28.70	64.00	60.91	70.90	
45.30	46.60	121.00	98.65	122.00	
3.62	3.89	13.20	9.18	11.70	
8.51	9.08	41.00	29.42	36.00	
1.08	1.21	6.69	5.00	5.17	
0.08	0.12	1.28	0.82	0.95	
0.65	1.07	5.45	3.56	3.69	
0.13	0.16	0.71	0.52	0.55	
0.89	1.08	3.96	3.07	3.03	
0.21	0.26	0.77	0.61	0.58	
0.89	0.94	2.26	1.75	1.83	
0.18	0.18	0.36	0.27	0.28	
1.36	1.35	2.24	1.77	1.89	
0.22	0.22	0.32	0.28	0.29	

A.Table 2 (con't.)

KD4	NM10-04	NM22C-04	NM22A-04	S9A	NM25-04
NCREC Volcanics	NCREC Volcanics	NCREC Volcanics	NCREC Volcanics	NCREC Volcanics	NCREC Volcanics
76.39	76.40	63.87	64.50	64.61	64.97
12.53	12.26	15.67	15.90	16.37	16.69
1.21	1.27	5.01	4.63	4.55	4.42
0.02	0.02	0.08	0.08	0.07	0.08
0.28	0.37	2.14	1.93	4.19	1.29
0.85	0.77	3.99	3.42	1.65	3.05
3.64	2.83	3.90	4.04	4.05	4.37
4.80	5.77	4.14	4.38	3.48	4.04
0.22	0.25	0.88	0.81	0.73	0.66
0.06	0.07	0.32	0.30	0.30	0.43
351	757	1226	1446	1380	1612
0.80	0.74	1.54	1.68	3.01	1.24
4.70	4.28	6.84	8.11	6.82	6.63
22.70	21.57	18.70	19.53	16.34	20.62
16.00	14.43	23.90	28.71	21.95	18.60
130.00	160.96	103.69	121.32	94.97	85.77
2.23	2.70	10.45	9.30	7.56	7.56
99	410	685	650	834	1170
1.78	1.74	1.28	1.24	1.11	1.14
19.90	25.46	16.05	15.50	14.13	17.43
3.31	4.03	2.63	1.95	2.40	1.81
11	17.69943	86.89325	67.66068	63	28.92731
15.00	14.28	21.97	24.20	18.90	16.36
159.0	130.7	265.0	335.2	262.0	282.8
53.10	52.07	63.38	66.45	66.77	94.74
93.00	81.75	114.46	120.39	116.79	167.23
8.81	7.40	12.24	12.79	12.43	17.29
26.10	23.38	44.75	47.06	44.60	61.59
4.18	3.85	7.92	8.31	7.51	9.74
0.55	0.62	1.79	1.93	1.74	2.25
3.18	2.79	5.76	6.04	5.22	6.07
0.49	0.40	0.78	0.84	0.70	0.71
2.70	2.41	4.26	4.62	3.71	3.42
0.54	0.47	0.81	0.87	0.68	0.58
1.74	1.35	2.07	2.34	1.76	1.45
0.29	0.21	0.30	0.33	0.25	0.21
1.91	1.47	1.84	2.08	1.50	1.29
0.28	0.24	0.29	0.33	0.24	0.20

A.Table 2 (con't.)

NM27-04	NM15-04	HR1	HR5	HR16	HR18
NCREC Volcanics	NCREC Volcanics	NCREC Volcanics	NCREC Volcanics	NCREC Volcanics	NCREC Volcanics
66.28	66.61	66.68	67.64	77.05	77.15
15.75	15.28	15.06	16.05	11.85	12.46
3.88	3.97	4.02	2.96	0.63	0.77
0.08	0.06	0.05	0.08	0.01	0.04
1.69	1.82	2.06	2.31	0.12	0.11
2.83	2.70	3.56	1.21	0.24	0.74
4.26	3.74	3.84	4.86	1.00	3.25
4.30	4.87	3.87	4.11	8.97	5.33
0.70	0.70	0.60	0.61	0.11	0.14
0.23	0.24	0.28	0.16	0.02	0.01
1328	1183	1557	1590	80	109
1.12	0.95	1.63	2.51	4.60	2.81
7.62	6.01	5.38	8.75	3.53	3.67
21.39	18.15	11.34	25.52	25.36	24.99
25.14	19.77	28.49	24.38	27.85	27.95
103.88	115.96	82.42	130.54	422.29	179.07
8.75	7.74	8.26	6.75	1.67	1.54
579	444	1156	491	77	46
1.41	1.28	0.74	1.65	2.10	2.05
14.42	15.41	10.21	13.17	27.14	21.94
2.29	2.22	1.91	2.32	4.52	3.83
59.87654	59.2333	71.54917	35	4.46334	5.25855
23.10	19.91	15.77	26.03	12.73	17.88
296.0	231.6	199.5	354.7	81.5	93.9
67.16	56.77	64.11	76.19	36.32	38.89
121.54	100.81	111.49	135.83	53.56	63.57
12.91	10.49	11.75	14.44	4.32	5.79
46.80	37.71	43.02	52.25	11.62	17.67
8.26	6.63	7.30	9.00	1.82	3.13
1.84	1.48	1.77	1.99	0.19	0.38
5.99	4.97	4.92	6.36	1.45	2.55
0.82	0.69	0.61	0.90	0.26	0.43
4.41	3.74	3.15	4.99	1.62	2.70
0.82	0.72	0.57	0.95	0.38	0.57
2.24	1.90	1.47	2.51	1.25	1.72
0.31	0.27	0.20	0.35	0.21	0.28
1.95	1.73	1.24	2.30	1.56	1.86
0.31	0.27	0.19	0.36	0.26	0.29

A.Table 2 (con't.)

HR17	NM16-04	MDL-HR38	GG9	SL43	MDL-HR58
NCREC Volcanics	NCREC Volcanics	NCREC Volcanics	NCREC Volcanics	NCREC Volcanics	NCREC Volcanics
79.07	71.14	70.06	75.74	77.35	76.76
11.13	15.28	15.74	13.38	12.39	11.74
0.63	1.92	2.38	0.99	0.77	0.64
0.03	0.09	0.05	0.02	0.00	0.01
0.20	0.40	1.90	0.24	0.12	0.75
0.82	0.99	3.56	0.90	0.31	0.60
3.09	4.71	2.32	3.60	3.12	8.47
4.88	5.01	3.44	4.94	5.82	0.88
0.11	0.40	0.43	0.16	0.12	0.10
0.03	0.06	0.11	0.03	0.00	0.04
64	1292	785	640	80	123
2.06	1.03	2.03	2.10		4.65
3.43	10.44	7.40	4.20		3.35
23.26	32.34	28.06	14.00	15.00	24.09
26.51	25.33	26.58	32.00		27.85
160.69	115.27	76.61	168.00	124.00	373.69
1.09	5.50	4.49			1.53
40	252	711	149	23	87
1.97	2.03	2.15	0.90		1.98
19.14	16.52	31.68	27.00		24.61
3.60	2.74	3.48	3.60		4.17
3.87021	15.44045	35.2158	10		1
12.65	31.04	26.03	22.00	21.00	11.93
81.7	421.5	255.9	140.0	100.0	75.6
35.65	90.45	69.27	38.90		34.48
43.33	163.58	129.69	56.70		50.97
4.56	17.07	13.00	4.80		4.17
12.61	60.49	44.67	13.70		11.43
2.01	10.27	8.20	1.90		1.80
0.23	2.05	1.15	0.22		0.18
1.53	7.23	5.96	1.80		1.33
0.27	1.05	0.89	0.20		0.24
1.83	5.87	5.02	1.10		1.60
0.40	1.14	0.95	0.21		0.36
1.27	3.09	2.50	0.70		1.15
0.21	0.44	0.36	0.10		0.20
1.51	2.82	2.18	0.90		1.52
0.24	0.43	0.33	0.15		0.24

A.Table 2 (con't.)

MDL-HR62	NM3C-04	93-73 thy dike	Tct2-41	93-75 rhy dike	Tct2-DSS-1
NCREC Volcanics	NCREC Volcanics	NCREC Volcanics	NCREC Volcanics	NCREC Volcanics	NCREC Volcanics
72.58	64.72	77.70	77.54	77.44	77.42
12.89	17.14	12.45	12.43	12.48	12.69
3.59	3.50	0.72	0.75	0.65	1.18
0.05	0.10	0.04	0.05	0.02	0.05
1.04	1.13	0.02	0.19	0.00	0.18
2.12	3.15	1.40	0.60	0.55	1.26
2.63	5.43	1.51	2.53	3.95	1.68
4.25	3.94	6.02	5.73	4.78	5.40
0.60	0.69	0.12	0.11	0.13	0.13
0.25	0.20	0.01	0.06	0.01	0.01
1039	1602	96	0	223	169
1.30	3.41	6		2	
5.79	5.10	2.88		3.14	
14.31	21.03	20.7	29	21.5	22
19.50	17.46		28.7		
121.47	107.36	231	204	152	156
6.62	6.35				
581	765	142	20	66	79
0.97	1.50	1.52		1.6	
12.45	11.47	23		19	23
1.28	2.37				
42.84901	45.27562				
15.40	22.01	15	14	20	22
221.6	178.7	83	76	98	87
55.36	57.39	35		52	
96.33	100.78	54		68.5	
10.38	10.87				
37.43	40.17				
6.40	7.15	2.1		3.87	
1.46	2.42	0.24		0.49	
4.40	5.27				
0.58	0.76	2.33		2.15	
3.04	4.30				
0.57	0.81				
1.49	2.11				
0.21	0.30				
1.24	1.79	0		0	
0.19	0.27	0.2		0.3	

A.Table 2 (con't.)

MP2 rhy dike	MP4 rhy dike	93-80 rhy vit	93-80/flow	E-4	Tct2-37
NCREC Volcanics	NCREC Volcanics	NCREC Volcanics	NCREC Volcanics	NCREC Volcanics	NCREC Volcanics
77.37	77.29	77.24	77.19	76.68	76.53
12.43	12.54	12.50	12.49	13.05	12.10
0.61	0.63	0.60	0.67	0.80	0.74
0.02	0.04	0.04	0.04	0.04	0.04
0.03	0.00	0.00	0.00		0.43
0.46	0.85	0.78	0.78	1.03	1.93
3.76	3.35	3.52	3.52	4.10	2.56
5.20	5.18	5.20	5.20	4.16	5.38
0.10	0.11	0.11	0.11	0.14	0.12
0.01	0.01	0.01	0.01	0.00	0.18
73	105	110	110		0
6	4	5	5		1
3.06	3.16	3.08	3.08		3.7
24.6	23.7	21.4	21.67	34	27
			29.29	35	
166	194	188	184.86	305	192
111	56	50	50	136	50
1.54	1.59	1.55	1.55		2.21
20	19	23	18.9	40	22
			2.49		
13	14	16	14.04	20	16
78	85	86	86	119	73
32	36.8	38	37.82	33	35
50	57.4	60	59.56	84	54
			5.17		
			14.9	18	
1.72	2.14	2.32	2.32		1
0.22	0.3	0.3	0.3		0.12
			1.56		
2.95	2.15	2.5	0.29		0.08
			1.82		
			0.4		
			1.31		
			0.21		
0	0	0	1.49		1.79
0.3	0.2	0.3	0.25		0.26

A.Table 2 (con't.)

Tct2-DS1.1	93-86 rhy vit	93-26 rhy dike	Tct2-DS7-1	Tct2-DS6-6	Tct2-DS6-5
NCREC Volcanics	NCREC Volcanics	NCREC Volcanics	NCREC Volcanics	NCREC Volcanics	NCREC Volcanics
76.47	76.43	75.60	75.59	75.49	75.49
12.69	12.79	13.57	12.96	14.43	14.12
0.87	0.98	0.95	1.22	1.21	1.75
0.04	0.04	0.01	0.04	0.05	0.06
0.37	0.01	0.08	0.53	0.01	0.00
1.58	0.98	0.22	1.09	0.73	0.73
2.38	3.85	3.95	2.89	1.73	1.70
5.45	4.72	5.41	5.43	6.13	5.95
0.15	0.18	0.19	0.19	0.22	0.22
0.00	0.02	0.02	0.06	0.01	0.00
236	408	638	240	678	582
	6	5			
	3.45	4.71			
17	19.4	26.6	19	23	23
149	168	138	143	143	160
103	106	46	125	80	70
	1.43	1.85			
16	20	25	16	21	17
22	21	26	22	24	25
88	116	150	101	174	164
	52	57			
	83	117			
	4	5.74			
	0.58	0.85			
	2.05	1.74			
	0	0			
	0.3	0.3			

A.Table 2 (con't.)

93-81 rhy vit	93-87a rhy vit	93-82 rhy vit	93-29 rhy vit	93-77 rhy dike	Tcr-80
NCREC Volcanics	NCREC Volcanics	NCREC Volcanics	NCREC Volcanics	NCREC Volcanics	NCREC Volcanics
75.01	74.90	74.78	74.73	74.71	74.69
13.48	13.53	13.61	13.56	12.41	13.97
0.90	0.89	0.96	1.18	0.83	1.14
0.04	0.04	0.04	0.04	0.02	0.05
0.00	0.00	0.00	0.31	0.00	0.11
0.86	0.89	0.95	1.22	0.28	0.71
3.58	3.74	3.60	3.36	2.91	3.47
5.92	5.79	5.85	5.33	8.64	5.57
0.20	0.20	0.21	0.23	0.17	0.24
0.01	0.02	0.02	0.04	0.02	0.06
733	737	755	746	331	192
5	4	7	3	4	
4.58	4.56	4.57	4.29	3.79	
22.6	22	22.3	22.2	21.9	21
164	160	170	205	196	158
103	111	115	170	129	83
1.65	1.62	1.6	1.55	1.55	
21	21	20	20	21	
26	26	25	19	18	29
152	155	161	147	120	169
51.9	60	62	57.7	45	
106	104	107	96	72	
6.21	6.29	6.29	4.85	3.6	
0.88	0.84	0.86	0.73	0.47	
2.25	2.14	2.11	1.9	2.15	
0	0	0	0	0	
0.3	0.3	0.3	0.3	0.3	

A.Table 2 (con't.)

93-65 rhy flow	Tct2-DS7-3	Tct-DS7-2	RM83-348	93-76 rhy dike	93-84 rhy vit
NCREC Volcanics	NCREC Volcanics	NCREC Volcanics	NCREC Volcanics	NCREC Volcanics	NCREC Volcanics
74.16	74.03	74.01	73.79	73.02	72.47
13.20	12.79	13.06	12.75	14.08	14.13
1.49	1.58	1.66	2.73	1.70	1.72
0.03	0.06	0.05	0.00	0.04	0.05
0.26	0.47	0.78	0.20	0.31	0.51
1.38	2.54	2.21	0.51	0.78	1.93
3.26	2.89	3.26	2.23	4.29	3.89
5.87	5.28	4.65	7.59	5.39	4.86
0.28	0.23	0.24	0.20	0.32	0.35
0.07	0.12	0.08	0.00	0.07	0.09
667	331	356	650	944	820
4			1.47	7	9
4.04			4.92	5.21	4.99
19.5	17	19	25.67	20.2	19.6
158	108	124	166	158	195
191	165	196	110	251	270
1.32			1.51	1.44	1.4
18	13	14	0	20	16
			0		
19	21	21	0	21	22
165	114	122	0	202	196
53			55.6	59	60
88			124.5	99	100
			0		
			22.4		
4.6			3.7	5.35	5.44
0.8			1	0.94	0.97
			0		
1.85			0.4	2.07	1.88
			0		
			0		
			0		
			0		
0			2.2	0	0
0.3			0.3	0.3	0.3

A.Table 2 (con't.)

93-84/flow	BM-13	Ttmt-18	NWHT-69	E-9	Tcr-9310
NCREC Volcanics	NCREC Volcanics	NCREC Volcanics	NCREC Volcanics	NCREC Volcanics	NCREC Volcanics
72.32	71.67	71.28	71.10	70.93	70.79
14.10	13.23	13.87	12.92	15.11	15.49
2.14	2.78	1.79	3.07	1.69	3.25
0.05	0.30	0.05	0.12	0.06	0.06
0.51	0.64	0.60	0.46	0.00	0.45
1.72	0.68	1.95	3.32	0.86	1.58
3.88	0.56	3.80	0.28	4.68	3.35
4.85	9.42	6.19	7.85	6.22	4.55
0.35	0.52	0.37	0.39	0.38	0.39
0.09	0.20	0.10	0.48	0.08	0.10
811	1562	0	2300	514	709
9		3	3	3.4	4
4.99		11.19		9.98	6.86
20.52	23	48		43	19
26.37	21	29.8		38	25.8
191.82	632	226	110	182	136
270	501	77		145	230
1.4		2.99	1.12	2.33	1.41
15.54	12	41	15	41	19
1.88					
20.18	29	36		32	23
196	319	265		374	210
59.89	70	96	58	108.7	77
99.64	161	182	94	176.6	136
9.65					
31.88	55			64.5	
5.44		14	6	10.15	7
0.97		1.21	1.26	1.49	1.29
3.47					
0.57		1.38		1.05	0.66
3.31					
0.66					
1.93					
0.28					
1.79		3.15	1.8	2.44	1.77
0.29		0.37	0.23	0.47	0.27

A.Table (con't.)

NWHT-144	NWHT-73	M1-5-95	A8-6-94	M23-1-95	NWHT-142
NCREC Volcanics	NCREC Volcanics	NCREC Volcanics	NCREC Volcanics	NCREC Volcanics	NCREC Volcanics
70.67	70.29	70.01	69.96	69.83	69.73
13.99	14.18	15.36	14.94	14.42	13.03
3.71	3.85	2.74	2.69	1.80	4.84
0.14	0.15	0.05	0.05	0.04	0.14
1.30	0.75	0.83	0.89	0.18	1.38
3.56	2.27	2.27	1.74	1.08	3.57
1.98	0.83	5.36	3.88	3.82	2.84
3.83	7.01	2.76	5.14	8.44	3.48
0.42	0.46	0.50	0.44	0.35	0.48
0.40	0.21	0.10	0.26	0.05	0.52
1790	601	785	1190	276	1100
4	4				6
6.34	9.28	8.41	7.62	8.52	5.25
		22	24	31	
123	129	203	163	198	
2330		687	340	130	
1.02	1.9	1.69	2.12	2.48	0.99
12	26	22.01	26.39	29.64	11
		4.6	5.1	6.3	
		28		30	
		340	232	281	
52	84	91.5	68.1	99.9	50
86	144	159.1	131.3	169.5	84
		54.33		58.12	
5	8	8.9	7.6	9.6	5
1.05	1.14	1.67	1.54	1.55	1.19
		0.81	0.74	0.88	
1.9	2.8	2.21	2.57	2.27	1.62
0.29	0.37	0.4	0.4	0.4	0.23

A.Table 2 (con't.)

NWHT-73	93-78 dac dike	RM78-223	NWHT-81	NWHT-102	NWHT-70
NCREC Volcanics	NCREC Volcanics	NCREC Volcanics	NCREC Volcanics	NCREC Volcanics	NCREC Volcanics
69.69	69.23	69.14	69.03	68.98	68.86
14.70	15.42	14.61	15.39	15.98	14.77
3.17	2.51	3.60	3.77	3.52	4.34
0.15	0.05	0.10	0.14	0.16	0.15
0.57	0.97	2.37	0.57	2.18	0.08
0.82	2.19	0.93	0.32	2.35	1.13
1.51	4.30	3.70	0.60	2.17	0.82
8.76	4.68	5.04	9.41	4.22	9.15
0.41	0.51	0.41	0.50	0.21	0.50
0.22	0.14	0.10	0.27	0.24	0.19
	1193	1472	647	480	444
2	11	3.75	4	3	5
10.1	5.62	4.76	10.3	4.02	9.36
	17.8	20.23			
175	128	187	174	108	171
	501	131		6760	
1.96	1.17	1.19	2.23	1.16	1.9
38	14	0	30	21	28
		0			
	21	0			
	244	0			
90	54.4	52.4	100	39	100
168	94	90.7	187	72	172
		0			
		34.2			
10	5.7	4.2	9	5	9
1.1	1.26	1.2	1.51	0.52	1.39
		0			
	1.44	0.3			
		0			
		0			
		0			
		0			
3.43	0	1.3	3.1	2.29	3.13
0.47	0.3	0.2	0.35	0.36	0.39

A.Table 2 (con't.)

NWHT-54	BM-16	E-8	NWHT-101	A7-6-94	NWHT-98
NCREC Volcanics	NCREC Volcanics	NCREC Volcanics	NCREC Volcanics	NCREC Volcanics	NCREC Volcanics
68.30	67.49	67.48	67.28	66.63	66.47
14.68	16.24	16.58	15.04	16.21	15.11
3.94	2.78	2.44	5.25	3.58	4.56
0.14	0.70	0.08	0.16	0.07	0.14
0.92	0.75	0.32	1.90	1.67	0.91
1.24	1.58	1.44	0.47	3.19	1.18
1.74	3.96	4.50	2.76	2.96	2.00
8.29	5.97	6.45	6.32	4.88	8.58
0.51	0.40	0.58	0.61	0.55	0.60
0.25	0.12	0.14	0.22	0.27	0.45
169	2032	1362	1390	1187	1350
2			5		5
10.2			9.13	1.1	9.78
	16	28		21	
	51	39			
	160	136	127	139	193
4	847	357	3970	751	
559			1.34	1.13	1.23
27	21	35	20	16.74	18
				3.6	
	21	30			
	422	635		434	
93	90	158	80	91	87
170	211	396	161	170.9	153
	69	28			
8			8	10.6	8
1.63			1.77	2.45	1.79
				0.92	
2.65			2.16	2.73	2.37
0.28			0.29	0.4	0.3

A.Table 2 (con't.)

BM-8	A6-6-94	93-87b dac flow	Tra-33	NWHT-84	93-79 dac flow
NCREC Volcanics	NCREC Volcanics	NCREC Volcanics	NCREC Volcanics	NCREC Volcanics	NCREC Volcanics
66.44	66.27	66.24	66.23	66.05	65.55
15.39	16.81	15.57	16.11	16.04	14.37
5.07	3.70	3.84	3.59	4.09	3.89
0.05	0.12	0.05	0.06	0.13	0.08
1.22	1.57	1.89	1.29	0.60	2.05
4.16	2.03	2.94	2.80	0.00	3.94
3.28	4.08	4.14	3.79	2.00	3.14
3.17	4.46	4.37	5.14	10.49	5.89
0.86	0.58	0.66	0.60	0.52	0.71
0.36	0.38	0.30	0.38	0.08	0.37
1308	1973	1502	931	1260	1519
8.4		9	5	4	11
5.33	11.08	5.13	12.7	8.74	5.63
13	22	12.8	32		13.3
23			37.7		
78	130	90	220	205	148
829	776	736	1013		591
0.83	1.31	0.92	2.51	1.53	0.72
14	16.91	11	68	23	14
1.9	3				
19		17	16		17
236	441	224	141		263
58.1	94.7	58.6	133	93	59
110.9	176.6	104	243	161	107
45.8	70.17				
7.78	11.1	7.14	12	8	7.32
1.85	2.44	1.61	2.28	1.66	1.69
0.72		1.51	0.83		1.49
1.53	2.95	0	1.57	2.51	0
0.29	0.4	0.2	0.27	0.26	0.2

A.Table 2 (con't.)

BM-12	BM-7	93-79/flow	NWHT-110
NCREC Volcanics	NCREC Volcanics	NCREC Volcanics	NCREC Volcanics
65.49	65.47	65.29	65.22
16.20	15.14	14.31	16.02
4.48	5.22	4.30	4.26
0.52	0.11	0.06	0.14
1.19	1.16	2.04	1.32
3.56	5.70	3.92	2.30
3.47	3.96	3.13	4.14
4.11	1.96	5.87	5.76
0.71	0.93	0.72	0.59
0.27	0.36	0.37	0.24
1336	1227	1373	1130
		11	6
		5.63	10.4
14	13	13.38	
23	15	23.96	
121	52	132.92	115
574	966	591	897
		0.72	1.42
9	12	9.26	22
		1.49	
18	21	15.51	
226	213	263	
48		58.92	94
107		106.85	174
		11.53	
35		42.34	
		7.32	9
		1.69	1.96
		4.49	
		0.6	
		2.92	
		0.53	
		1.37	
		0.19	
		1.11	2.4
		0.18	0.32

A.Table 3. NCREC Plutonic and Volcanic isotope data (excluding Southern Black Mountain volcanic center [see text, Table 1] and PST [see text, Table 7]). Data compiled from Metcalf (2004; and personal commun., 2012), Miller (personal commun., 2012), Bachl et al. (2001), and Falkner (1995).

Sample	AW13	HAW 5 (11/6 #3)	SK46D (11/6 #7)	TAW 102A (11/6 #6)	DAW 11 (11/18 #18)	DAW 2 (11/2 #18)	DAW 38 (11/18 #14)
Group	NCREC Plutonics	NCREC Plutonics	NCREC Plutonics	NCREC Plutonics	NCREC Plutonics	NCREC Plutonics	NCREC Plutonics
Description	Aztec Wash	Aztec Wash	Aztec Wash	Aztec Wash	Aztec Wash	Aztec Wash	Aztec Wash
$^{87}Sr/^{86}Sr$	0.7101	0.7102	0.7108	0.7097	0.7099	0.7116	0.7092
εNd		-11.1	-13.5	-9.4	-10.5	-14.4	-9.1
$^{206}Pb/^{204}Pb$	18.128	18.176	17.826	18.159	18.102	17.963	18.206
$^{207}Pb/^{204}Pb$	15.559	15.580	15.513	15.542	15.579	15.539	15.583
$^{208}Pb/^{204}Pb$	38.894	38.960	38.566	38.893	39.119	38.786	39.059

A.Table 3 (con't.)

DAW 9 (11/2 #16) NCREC Plutonics Aztec Wash	TAW 113 (11/2 #15) NCREC Plutonics Aztec Wash	AW4 NCREC Plutonics Aztec Wash	AWZ1A NCREC Plutonics Aztec Wash	AWZ1B NCREC Plutonics Aztec Wash	NAWZ 53 (11/2 #19) NCREC Plutonics Aztec Wash	CAWZ106 (11/6 #4) NCREC Plutonics Aztec Wash	DAW 6 (11/2 #17) NCREC Plutonics Aztec Wash
0.7089	0.7095	0.7102	0.7105	0.7114	0.7110	0.7105	0.7105
-8.7	-9.6	-10.1	-10.5		-13.4	-10.3	-11.3
18.186	18.055	18.124			17.942		17.990
15.563	15.501	15.581			15.564		15.558
38.868	38.702	38.986			39.100		39.155

A.Table 3 (con't.)

IR3	AW38C	AW73D	BS1	AWAG 2	AWAG 3	AWAG 7	AWAG 4
NCREC Plutonics	NCREC Plutonics	NCREC Plutonics	NCREC Plutonics	NCREC Plutonics	NCREC Plutonics	NCREC Plutonics	NCREC Plutonics
Aztec Wash	Aztec Wash	Aztec Wash	Aztec Wash	Aztec Wash	Aztec Wash	Aztec Wash	Aztec Wash
0.7105	0.7100	0.7097	0.7085	0.7096	0.7101 -9.7	0.7100 -9.2	0.7099
18.080	18.046	18.148	18.169				
15.560	15.546	15.559	15.555				
38.910	38.934	38.856	38.883				

A.Table 3 (con't.)

NAW 13	AWAG 6	NAW 26	NAW 50	CS-G/PST	CS-B/PST	SL69	SL63
NCREC Plutonics	NCREC Plutonics	NCREC Plutonics	NCREC Plutonics	NCREC Plutonics	NCREC Plutonics	NCREC Plutonics	NCREC Plutonics
Aztec Wash	Aztec Wash	Aztec Wash	Aztec Wash	Aztec Wash	Aztec Wash	Searchlight Pluton	Searchlight Pluton
0.7119	0.7101	0.7115	0.7104	0.7112	0.7117	0.7094	0.7093
-10.5	-10.3	-10.6	-10.4	-12.0	-12.0	-10.5	-10.1

A.Table 3 (con't.)

92-140	SL33	RIOZF	RM14	RM18	GG3B	GG8A	GG20B
NCREC Plutonics	NCREC Plutonics	NCREC Plutonics	NCREC Plutonics	NCREC Plutonics	NCREC Plutonics	NCREC Plutonics	NCREC Plutonics
Searchlight Pluton	Searchlight Pluton	Searchlight Pluton	Searchlight Pluton	Searchlight Pluton	Searchlight Pluton	Searchlight Pluton	Searchlight Pluton
0.7097	0.7096	0.7096	0.7097	0.7093	0.7065	0.7083	0.7084
-9.5	-9.6	-10.9	-11.5	-8.6	-3.7	-7.1	-8.5
		18.090	18.110	18.170			
		15.560	15.580	15.590			
		38.800	38.850	38.910			

A.Table 3 (con't.)

RM5	RM15	SL35	GC9	BGZ	BCOZ	BC101Z	BW47
NCREC Plutonics	NCREC Plutonics	NCREC Plutonics	NCREC Plutonics	NCREC Plutonics	NCREC Plutonics	NCREC Plutonics	NCREC Plutonics
Searchlight Pluton	Searchlight Pluton	Searchlight Pluton	Searchlight Pluton	Spirit Mountain Batholith	Spirit Mountain Batholith	Spirit Mountain Batholith	Spirit Mountain Batholith
0.7078	0.7086	0.7086	0.7087	0.7135	0.7115	0.7108	0.7159
-5.7	-7.2	-9.0	-12.4	-14.6	-13.1	-10.6	-11.5
18.250							
15.620							
39.030							

A.Table 3 (con't.)

BD35	SML49Z	SML59Z	SML120Z	MPL53Z	Tct2-DS4-1	Tct2-41	Tct2-DS1.1
NCREC Plutonics	NCREC Plutonics	NCREC Plutonics	NCREC Plutonics	NCREC Plutonics	NCREC Volcanics	NCREC Volcanics	NCREC Volcanics
Spirit Mountain Batholith	Spirit Mountain Batholith	Spirit Mountain Batholith	Spirit Mountain Batholith	Spirit Mountain Batholith			
0.7122	0.7220	0.7161	0.7128	0.7124	0.7082	0.7193	0.7101
-14.7	-9.9	-11.5	-12.8	-14.4	-10.0	-9.4	-9.6
					18.032	18.01	18.1
					15.577	15.56	15.58
					38.834	38.79	38.95

A.Table 3 (con't.)

Tcr-DS6-5	93-77 rhy dike	RM83-348	93-76 rhy dike	93-84 rhy vit	Ttmt-18	Tcr-9310	A8-6-94
NCREC Volcanics	NCREC Volcanics	NCREC Volcanics	NCREC Volcanics	NCREC Volcanics	NCREC Volcanics	NCREC Volcanics	NCREC Volcanics
0.7095		0.7100			0.7096	0.7101	0.7102
-10.1		-12.3			-9.3	-10.1	-8.9
18.01	17.95	18.156	17.93	17.89	18.03	17.95	17.98
15.56	15.55	15.578	15.55	15.55	15.54	15.53	15.54
38.89	38.9	38.906	39.01	38.9	38.96	38.8	39.05

A.Table 3 (con't.)

RM78-223	A7-6-94	A6-6-94	Tra-33	93-79 dac flow	93-84/flow	M1-5-95	M23-1-95
NCREC Volcanics	NCREC Volcanics	NCREC Volcanics	NCREC Volcanics	NCREC Volcanics	NCREC Volcanics	NCREC Volcanics	NCREC Volcanics
0.7092	0.7096	0.7095	0.7103	0.7099	0.7112	0.7094	0.7093
-11.4	-8.7	-8.6	-8.6	-10.6	-10.9	-8.9	-8.5
17.885	18.36	18.16	18.56	18.22			
15.553	15.58	15.58	15.6	15.61			
38.982	38.98	39.04	39.26	38.94			

A.Table 3 (con't.)

NM10-04	NM25-04	NM27-04	NM15-04	HR1	HR16	HR18	HR17
NCREC Volcanics	NCREC Volcanics	NCREC Volcanics	NCREC Volcanics	NCREC Volcanics	NCREC Volcanics	NCREC Volcanics	NCREC Volcanics
0.7100	0.7102	0.7094	0.7096	0.7099	0.7100	0.7100	0.7107
-10.07	-10.17	-10.06	-9.94	-11.08	-10.27	-10.28	-10.29

Appendix Table 4. Example of AFC modeling results for an enriched basalt assimilating 1.7 Ga crustal melt while undergoing fractional crystallization controlled by intermediate bulk distribution coefficients. Values in blue represent model results that return [Sr] below the PST's bulk compositional range, while values in green are those that are above the range of [Sr]. Values in black are model results for which the [Sr] falls within the PST range, but do not reproduce the PST isotopic composition. Values in red are the models which best reproduce both the elemental and isotopic composition of the PST.

r	F	0.9	0.8	0.7	0.6	0.5	0.4	0.3	0.2	0.1
0.1	$^{87}Sr/^{86}Sr$	0.7065	0.7066	0.7066	0.7068	0.7069	0.7073	0.7082	0.7106	0.205
	$^{143}Nd/^{144}Nd$	0.51232	0.51231	0.51230	0.51229	0.51228	0.51226	0.51224	0.51221	0.51217
	[Sr]	704	536	393	275	181	109	57	24	7
	[Nd]	50.13	50.27	50.43	50.61	50.82	51.06	51.38	51.80	52.48
0.2	$^{87}Sr/^{86}Sr$	0.7066	0.7067	0.7069	0.7071	0.7077	0.7088	0.7113	0.7180	0.7327
	$^{143}Nd/^{144}Nd$	0.51231	0.51229	0.51227	0.51224	0.51221	0.51218	0.51215	0.51210	0.51203
	[Sr]	675	490	341	225	139	78	38	16	7
	[Nd]	50.29	50.60	50.94	51.32	51.75	52.25	52.86	53.64	54.81
0.3	$^{87}Sr/^{86}Sr$	0.7066	0.7068	0.7072	0.7079	0.7090	0.7115	0.7172	0.7280	0.7382
	$^{143}Nd/^{144}Nd$	0.51230	0.51226	0.51223	0.51219	0.51215	0.51210	0.51205	0.51199	0.5192
	[Sr]	639	437	284	175	100	52	25	13	9
	[Nd]	50.49	51.00	51.56	52.16	52.83	53.57	54.43	55.48	56.90
0.4	$^{87}Sr/^{86}Sr$	0.7067	0.7071	0.7077	0.7089	0.7115	0.7168	0.7262	0.7360	0.7397
	$^{143}Nd/^{144}Nd$	0.51228	0.51223	0.51218	0.51213	0.51207	0.51202	0.51200	0.51190	0.51182
	[Sr]	594	375	224	126	66	33	18	12	11
	[Nd]	50.75	51.52	52.33	53.17	54.07	55.03	56.07	57.24	58.63
0.5	$^{87}Sr/^{86}Sr$	0.7068	0.7074	0.7087	0.7113	0.7166	0.7258	0.7350	0.7393	0.7400
	$^{143}Nd/^{144}Nd$	0.51226	0.51219	0.51212	0.51205	0.51199	0.51193	0.51187	0.51182	0.51177
	[Sr]	537	303	162	82	40	22	15	13	13
	[Nd]	51.10	52.20	53.30	54.40	55.50	56.60	57.70	58.80	59.90
0.6	$^{87}Sr/^{86}Sr$	0.7070	0.7082	0.7108	0.7166	0.7263	0.7354	0.7392	0.7399	0.7400
	$^{143}Nd/^{144}Nd$	0.51222	0.51213	0.51205	0.51197	0.51191	0.51185	0.51180	0.51176	0.51173
	[Sr]	461	222	102	47	24	17	15	15	15
	[Nd]	51.61	53.13	54.56	55.89	57.11	58.22	59.19	60.02	60.65
0.7	$^{87}Sr/^{86}Sr$	0.7074	0.7100	0.7166	0.7280	0.7367	0.7395	0.7400	0.7400	0.7400
	$^{143}Nd/^{144}Nd$	0.51217	0.51205	0.51195	0.51188	0.51182	0.51178	0.51175	0.51173	0.51172
	[Sr]	359	135	52	25	18	17	16	16	16
	[Nd]	52.40	54.46	56.21	57.66	58.82	59.70	60.34	60.74	60.95
0.8	$^{87}Sr/^{86}Sr$	0.7086	0.7167	0.7315	0.7387	0.7399	0.7400	0.7400	0.7400	0.7400
	$^{143}Nd/^{144}Nd$	0.51209	0.51194	0.51184	0.51178	0.51175	0.51173	0.51172	0.51172	0.51172
	[Sr]	220	57	24	19	18	18	18	18	18
	[Nd]	53.78	56.50	58.36	59.57	60.21	60.72	60.91	60.98	70
0.9	$^{87}Sr/^{86}Sr$	0.7167	0.7378	0.7400	0.7400	0.7400	0.7400	0.7400	0.7400	0.7400
	$^{143}Nd/^{144}Nd$	0.51193	0.51178	0.51174	0.51172	0.51172	0.51172	0.51172	0.51172	0.51172
	[Sr]	61	21	20	20	20	20	20	20	20
	[Nd]	56.74	59.52	60.56	60.89	60.98	61	61	61	61

A.Figure 1. Major element Harker diagrams for the PST showing the distinction between the trachyte, low-silica rhyolite, and high-silica rhyolite compositional groups.

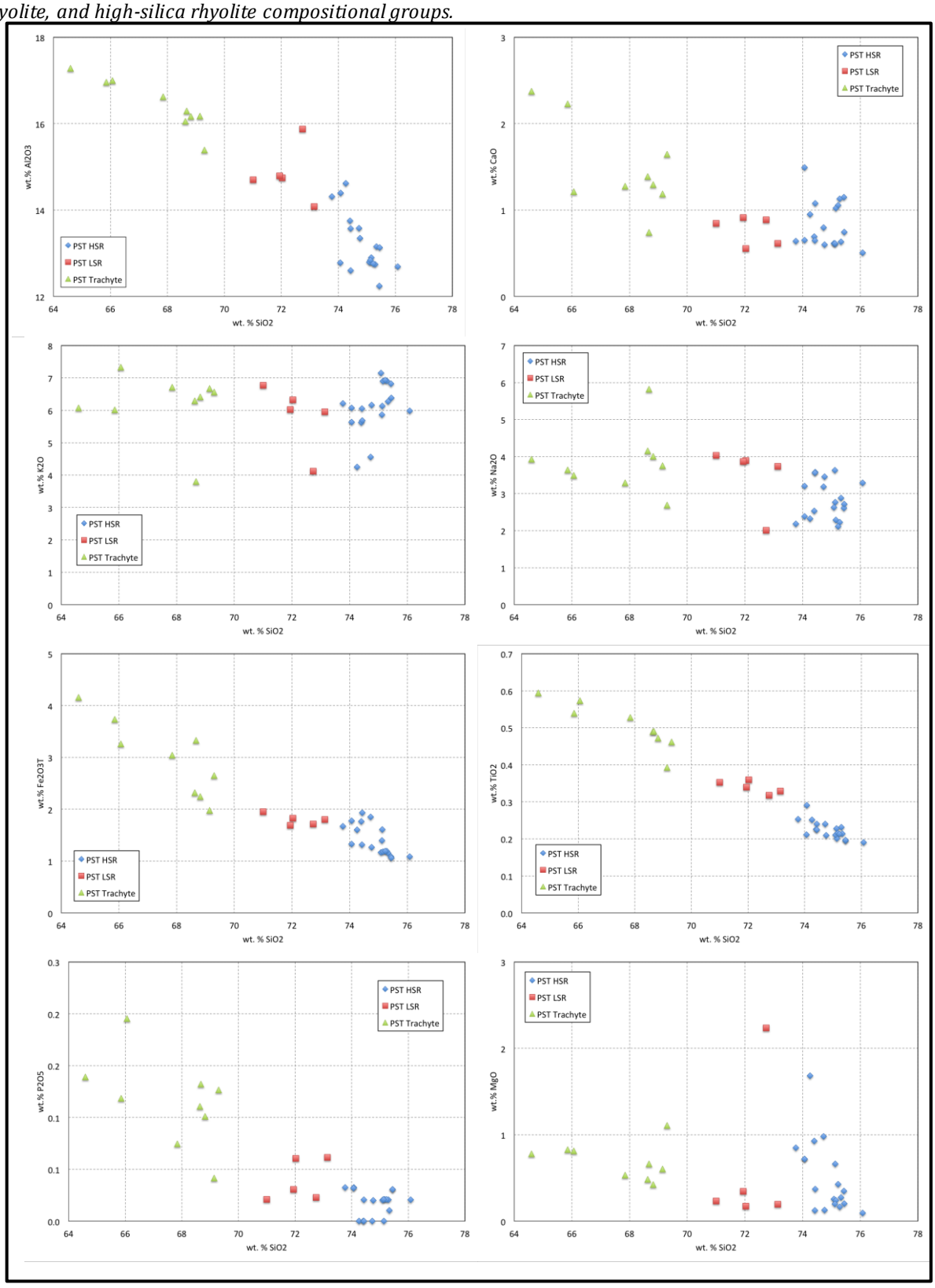

REFERENCES

Albarède, F., Telouk, P., Blichert-Toft, J., Boyet, M., Agranier, A., and Nelson, B., 2004. Precise and accurate isotopic measurements using multiple- collector ICPMS. Geochim. Cosmochim. Acta **68**, 2725–2744.

Anderson D.L., 2005. Large Igneous Provinces, Delamination, and Fertile Mantle. *Elements* **1**, 271-275.

Annen, C., Blundy, J.D., and Sparks, R.S.J., 2006. The genesis of intermediate and silicic magmas in deep crustal hot zones. *Journal of Petrology* **47**, 505-539.

Bachl, C.A., Miller, C.F., Miller, J.S., and Faulds, J.E., 2001. Construsction of a pluton: evidence from an exposed cross section of the Searchlight Pluton, Eldorado Mountains, Nevada. *Geological Society of America Bulletin* **113**, 1213-1228.

Bachmann, O., Dungan, M.A., and Bussy, F., 2005. Insights into shallow magmatic processes in large silicic magma bodies: the trace element record in the Fish Canyon magma body, Colorado. *Contributions to Mineralogy and Petrology* **149**, 338-349.

Bennett, V.C. and DePaolo, D.J., 1987. Proterozoic crustal history of the western United States as determined by neodymium isotopic mapping. *Geological Society of America Bulletin* **99**, 674-685.

Bowen, N.L., 1915. The crystallization of haplobasaltic, haplodioritic, and related magmas. *American Journal of Science* **40**, 161-185.

Bouvier, A., Vervoort, J.D., and Patchett, P.J., 2008. The Lu-Hf and Sm-Nd isotopic composition of CHUR: constraints from unequilibrated chondrites and implications for the bulk composition of terrestrial planets. *Earth and Planetary Science Letters* **273**, 48-57.

Bradshaw, T.K., Hawkesworth, C.J., and Gallagher, K., 1993. Basaltic volcanism in the southern Basin and Range: no role for a mantle plume. *Earth and Planetary Science Letters* **16**, 45-62.

Brophy, J.G., 2008. A study of rare earth element (REE)–SiO2 variations in felsic liquids generated by basalt fractionation and amphibolite melting: a potential test for discriminating between the two different processes. *Contributions to Mineralogy and Petrology* **156**, 337-357.

Bryan, S.E., Peate, I.U., Peate, D.W., Self, S., Jerram, D.A., Mawby, M.R., Marsh, J.S., and Miller, J.A., 2010. The largest volcanic eruptions on earth. *Earth-Science Review* **102**, 207-229.

Buesch, D.C., 1992. Incorporation and redistribution of locally derived lithic fragments within a pyroclastic flow. *Geological Society of America Bulletin* **104**, 1193-1207.

Christiansen, E.H. and McCurry, M., 2008. Contrasting origin of Cenozoic silicic volcanic rocks from the western Cordillera of the United States. *Bulletin of Volcanology* **70**, 251-267.

Colombini, L.L., Miller, C.F., Gualda, G.A.R., Wooden, J.L., and Miller, J.S., 2011. Sphene and zircon in the Highland Range volcanic sequence (Miocene, southern Nevada, USA): elemental partitioning, phase relations, and influence on evolution of silicic magma. *Mineralogy and Petrology* **102**, 29-50.

Condie, K.C., 2001. Mantle plumes and their record in Earth's history. Cambridge University Press.

Daley, E.E. and DePaolo, D.J., 1992. Isotopic evidence for lithospheric thinning during extension: southeastern Great Basin. *Geology* **20**, 104-108.

DePaolo, D.J., 1981. Trace element and isotopic effects of combined wall rock assimilation and fractional crystallization. *Earth and Planetary Science Letters* **53**, 189-202.

de Silva, S.L., 2008. Arc magmatism, calderas, and supervolcanoes. *Geology* **36**, 671-672.

de Silva, S.L. and Gosnold, W.D., 2007. Episodic construction of batholiths: insights from the spatiotemporal development of an ignimbrite flare-up. *Journal of Volcanology and Geothermal Research* **167**, 320-335.

DeWitt, E., Thorson, J.P., and Smith, R.C., 1986. Geology and gold deposits of the Oatman District, northwestern Arizona. *USGS Bulletin* **1857** I1-I27.

Falkner, C.M., Miller, C.F., Wooden, J.L., and Heizler, M.T., 1995. Petrogenesis and tectonic significance of the calc-alkaline bimodal Aztec Wash pluton, Eldorado Moutains, Colorado River extensional corridor. *Journal of Geophysical Research* **100**, 10453-10476.

Farmer, G.L., Perry, F.V., Semken, S., Crowe, B., Curtis, D., and DePaolo, D.J., 1989. Evidence on the structure and origin of subcontinental lithospheric mantle in southern Nevada. *Journal of Geophysical Research* **94**, 7885-7898.

Faulds, J.E., Feuerbach, D.L., Miller, C.F., and Smith, E.I., 2001. Cenozoic evolution of the northern Colorado River extensional corridor, southern Nevada and northwest Arizona. *Guidebook – Pacific Section, American Association of Petroleum Geologists* **78**, 239-271.

Ferguson, C.A., 2008. Silver Creek caldera, probable source of the Miocene Peach Spring Tuff, Oatman Mining District, Arizona. *Abstracts with Programs – Geological Society of America* **40**, 33.

Ferguson, C.A., McIntosh, W.C., and Miller, C.F., 2013. Silver Creek caldera—the tectonically dismembered source of the Peach Spring Tuff. *Geology* **41**, 3-6.

Ferrari, L., Lopez-Martinez, M., and Rosas-Elguera, J., 2002. Ignimbrite flare-up and deformation in the southern Sierra Madre Occidental, western Mexico: Implications for the late subduction history of the Farallon plate. *Tectonics* **21**: TC001302.

Feuerbach, D.L., Reagan, M.K., and Faulds, J.E., 1998. Lead isotopic evidence for synextensional lithospheric ductile flow in the Colorado River extensional corridor, western United States. *Journal of Geophysical Research* **103**, 2515-2528.

Fujimaki, H., 1986. Partition-Coefficients of Hf, Zr, and Ree between Zircon, Apatite, and Liquid. *Contributions to Mineralogy and Petrology* **94**, 42-45.

Galer, S.J.G., 1999. Optimal double and triple spiking for high precision lead isotopic measurement. *Chemical Geology* **157**, 255-274.

Glazner, A.F., Nielson, J.E., Howard, K.A., and Miller, D.M., 1986. Correlation of the Peach Springs Tuff, a large-volume Miocene ignimbrite sheet in California and Arizona. *Geology* **14**, 840-843.

Glazner, A.F., Farmer, G.L., Hughes, W.T., Wooden, J.L., and Pickthorn, W., 1991. Contamination of basaltic magma by mafic crust at Amboy and Pisgah craters, Mojave Desert, California. *Journal of Geophysical Research* **96**, 13673-13691.

Gualda, G. A. R., Ghiorso, M. S., Lemons, R. V. & Carley, T. L. (2012a). Rhyolite-MELTS: a modified calibration of MELTS opti- mized for silica-rich, fluid-bearing magmatic systems. *Journal of Petrology* **53**, 875-890.

Gusa, S., Nielsen, J.E., and Howard, K.A., 1987. Heavy-mineral suites confirm the wide extent of the Peach Springs Tuff in California and Arizona, U.S.A. *Journal of Volcanology and Geothermal Research* **33**, 343-347.

Hanchar, J.M. and Watson, B.E., 2003. Zircon saturation thermometry. *Reviews in Mineralogy and Geochemistry* **53**, 89-112.

Harper, B.E., Miller, C.F., Koteas, G.C., Cates, N.L., Wiebe, R.A., Lazzareschi, D.S., and Cribb, J.W., 2004. Granites, dynamic magma chamber processes and pluton construction: the Aztec Wash pluton, Eldorado Mountains, Nevada, USA. *Transactions of the Royal Society of Edinburgh: Earth Sciences* **95**, 277-295.

Harrison, M.T. and Watson, B.E., 1984. The behavior of apatite during crustal anatexis: equilibrium and kinetic considerations. *Geochimica et Cosmochimica Acta* **48**, 1467-1477.

Hildreth, W. and Moorbath, S., 1988. Crustal cotributions to arc magmas in the Andes of central Chile. *Contributions to Mineralogy and Petrology* **98**, 455-489.

Hillhouse, J.W. and Wells, R.E., 1991. Magnetic fabric, flow directions, and source area of the lower Miocene Peach Springs Tuff in Arizona, California, and Nevada. *Journal of Geophysical Research* **96**, 12443-12460.

Hughes, G.R. and Mahood, G.A., 2008. Tectonic controls on the nature of large silicic calderas in volcanic arcs. *Geology* **36**, 627-630.

Humphreys, E.D., 1995. Post-Laramide removal of the Farallon slab, western United States. *Geology* **23**, 987-990.

Ionov, D.A. and Hofmanm, 1995. Nb-Ta-rich mantle amphiboles and micas: Implications for subduction-related metasomatic trace element fractionations. *Earth and Planetary Science Letters* **131**, 341-356.

Jacobsen, S.B. and Wasserburg, G.J., 1980. Sm-Nd isotopic evolution of chondrites. *Earth and Planetary Science Letters* **50**, 139-155.

Johannes, W. and Holtz, F., 1996. Petrogenesis and experimental petrology of granitic rocks. *Minerals and Rocks* **22**.

Kapp, J.D., Miller, C.F., and Miller, J.S., 2002. Ireteba Pluton, Eldorado Mountains, Nevada: Late, Deep-Source, Peraluminous Magmatism in the Cordilleran Interior. *The Journal of Geology* **110**, 649-669.

Kempton, P.D., Fitton, J.G., Hawkesworth, C.J., and Ormerod, D.S., 1991. Isotopic and trace element constraint on the composition and evolution of the lithosphere beneath the southwestern United States. *Journal of Geophysical Research* **96**, 13713-13735.

Keskin, M., 2012. AFC-Modeler: a Microsoft® Excel© Workbook Program for Modelling Assimilation combined with Fractional Crystallization (AFC) Process in Magmatic Systems by Using Equations of DePaolo (1981). *Turkish Journal of Earth Sciences* **21**, 1-18.

Kuiper, K. F., Deino, A., Hilgen, F. J., Krijgsman, W., Renne, P. R. and Wijbrans, J. R., 2008. Synchronizing rock clocks of Earth history. *Science* **320**, 500-504.

Lang, N.P., Walker, B.J., Claiborne, L.E., Miller, C.F., Hazlett, R.W., and Heizler, M.T., 2008. The Spirit Mountain batholith and Secret Pass Canyon volcanic center: A cross-sectional view of the magmatic architecture of the uppermost crust of an extensional terrain, Colorado River, Nevada-Arizona. The Geological Society of America Field Guide **11**.

Lidzbarski, M., Miller, J.S., Miller, C.F., Wooden, J.L., Vazquez, J.A., Pamukcu, A.S., Carley, T.L., and Gualda, G.A.R., 2012. Geochronology and trace element analysis of the Peach Spring Tuff zircons and their bearing on growth of the Peach Spring Tuff magma chamber and eruption. *Abstracts with Programs—Geological Society of America* **40**, 60.

Lipman, P.W., 1984. The Roots of Ash Flow Calderas in Western North America' Windows Into the Tops of Granitic Batholiths. *Journal of Geophysical Research* **89**, 8801-8841.

Lipman, P.W., 2007. Incremental assembly and prolonged consolidation of Cordilleran magma chambers: Evidence from the Southern Rocky Mountain volcanic field. *Geosphere* **3**, 42-70.

Mason, B.G., Pyle, D.M., and Oppenheimer, C., 2004. The size and frequency of the largest explosive eruptions on Earth. *Bulletin of Volcanology* **66**, 735-748.

McCracken, R., Miller, C.F., Dufek, J., Gualda, G., Buesch, D., and Brooks, C.E., 2012. Understanding the Peach Spring supereruption through its basal layer deposits (southwestern USA). *American Geophysical Union* **2011**, #V51F-2572.

McDowell, S.M., Miller, C.F., and Ferguson, C.A., 2011. Post-supereruption (18-19 Ma) magmatic reactivation beneath the Silver Creek Caldera, Black Mountains, AZ. *American Geophysical Union* **2011**, #V21C-2516.

McDowell, S.M., Miller, C.F., Ferguson, C.A., Fisher, C., Frazier, W.O., Miller, J.S., Mundil, R., Overton, S., and Vervoort, G., 2012. Geochemical insights in the evolution of a supereruptive volcanic center: magmatic precursors and successors of the Miocene Peach Spring Tuff, southern Black Mountains, western AZ. *Abstracts with Programs—Geological Society of America* **44**, 320.

McDowell et al., in prep

Metcalf, R.V., 2004. Volcanic-plutonic links, plutons as magma chambers and crust-mantle interaction: a lithospheric scale view of magma systems. *Transactions of the Royal Society of Edinburgh: Earth Sciences* **95**, 357-374.

Metcalf, R.V., Smith, E.I., Walker, J.D., Reed, R.C., and Gonzales, D.A., 1995. Isotopic disequilibrium among commingled hybrid magmas: evidence for a two-stage magma mixing-commingling process in the Mt. Perkins pluton, Arizona. *The Journal of Geology* **103**, 509-527.

Miller, J.S. and Glazner, A.F., 1995. Jurassic plutonism and crustal evolution in the central Mojave Desert, California. *Contributions to Mineralogy and Petrology* **118**, 379-395.

Miller, C.F. and Wooden, J.L., 1994. Anatexis, hybridization, and the modification of ancient crust: Mesozoic plutonism in the Old Woman Mountains area, California. *Lithos* **32**, 111-113.

Munker, C., Weyer, S., Scherer, E., and Mezger, K., 2001. Separation of high field strength elements (Nb, Ta, Zr, Hf) and Lu from rock samples for MC-ICPMS measurements. *Geochemistry Geophysics Geosystems* **vol. 2**, **no. 12**. Pp. 19.

Newhall, C.G. and Self, S., 1982. The volcanic explosivity index (VEI): an estimate of explosive magnitude for historical volcanism. *Journal of Geophysical Research* **87**, 1231-1238.

Nielsen, J.E., Lux, D.R., Dalrymple, B., and Glazner, A.F., 1990. Age of the Peach Springs Tuff, southeastern California and western Arizona. *Journal of Geophysical Research* **95**, 571-580.

Pamukcu, A.S., Carley, T.L., Gualda, G.A.R., Miller, C.F., and Ferguson, C.A., 2013. The evolution of the Peach Spring Tuff giant magma body: evidence from accessory mineral textures and compositions, bulk pumice and glass geochemistry, and rhyolite-MELTS modeling. *Journal of Petrology*, online advanced access.

Patchett, P.J. and Ruiz, J., 1987. Nd isotopic ages of crust formation and metamorphism in the Precambrian of eastern and southern Mexico. *Contributions to Mineralogy and Petrology* **96**, 523–528.

Patchett, J.P., Kouvo, O., Hedge, C.E., and Tatsumoto, M., 1981. Evolution of Continental Crust and Mantle Heterogeneity: Evidence from Hf Isotopes. *Contributions to Mineralogy and Petrology* **78**: 279-297.

Pearce, J.A., Harris, N.B.W., and Tindle, A.G., 1983. Trace element discrimination diagrams for the tectonic interpretation of granitic rocks. *Journal of Petrology* **25**, 956-983.

Perry, F.V., DePaolo, D.J., and Baldridge, W.S., 1993. Neodymium isotopic evidence for decreasing crustal contributions to Cenozoic ignimbrites of the western United States: Implications for the thermal evolution of the Cordilleran crust. *Geological Society of America Bulletin* **105**, 872-882

Pearthree, P.A., 2007. Geologic map of the Needles NE 7 1/2' quadrangle, Mohave County, Arizona. *Arizona Geological Survey Digital Geologic Map DGM-53*.

Pearthree, P. A., Ferguson, C. A., Johnson, B. J. & Guynn, J. (2009). Geologic map and report for the proposed State Route 95 Realignment Corridor, Mohave County, Arizona, version 1.0. *Arizona Geological Survey Digital Geologic Map DGM-65.*

Prytulak, J., Vervoort, J.D., Plank, T., and Yu, C., 2006. Astoria Fan sediments, DSDP site 174, Cascadia Basin: Hf-Nd-Pb constraints on provenance and outburst flooding. *Chemical Geology* **233**, 276-292.

Rollinson, H. (1993). *Using Geochemical Data: Evaluation, Presentation and Interpretation*. Harlow: Addison Wesley-Longman.

Rudnick, R.L. and Gao, S., 2003. *Composition of the Continental Crust.*

Self, S., Gertisser, R., Thordarson, T., Rampino, M.R., and Wolff, J.A., 2004. Magma volume, volatile emissions, and stratospheric aerosols from the 1815 eruption of Tambora. *Geophysical Research Letters* **31**, L20608.

Self, S., 2006. The effects and consequences of very large explosive volcanic eruptions. *Philosophical Transactions of the Royal Society* **364**, 2073-2097.

Sisson, T.W., 1991. Pyroxene-High Silica Rhyolite Trace-Element Partition-Coefficients Measured by Ion Microprobe. *Geochimica et Cosmochicia Acta* **55**, 1575-1585.

Sisson, T.W. and Bacon, C.R., 1992. Garnet High-Silica Rhyolite Trace-Element Partition-Coefficients Measured by Ion Microprobe. *Geochimica et Cosmochicia Acta* **56**, 2133-2136.

Spera, F.J. and Bohrson, W.A., 2001. Energy-constrained open-system magmatic processes I: general model and enegy-constrained assimilation and fractional crystallization (EC-AFC) formulation. *Journal of Petrology* **42**, 999-1018.

Thorson, J. P. (1971). Igneous petrology of the Oatman District, Mojave County, Arizona, PhD thesis, University of California, Santa Barbara.

Tuttle, O.F., and Bowen, N.L., 1958. Origin of granite in the light of experimental studies in the system $NaAlSi_3O_8$-$KAiSi_3O_8$-SiO_2-H_2O. *Geol. Soc. America Mem*. **74**, pp. 153.

Varga, R. J., Faulds, J. E., Snee, L. W., Harlan, S. S. and Bettison-Varga, L, 2004. Miocene extension and extensional folding in an anticlinal segment of the Black Mountains accommodation zone, Colorado River extensional corridor, southwestern United States. *Tectonics* **23**, TC1019

Vervoort, J.D., and Blichert-Toft, J., 1999. Evolution of the depleted mantle: Hf isotope evidence from juvenile rocks through time. *Geochimica Cosmochimica Acta* **63**, 533–556.

Vervoort, J.D., and Patchett, P.J., 1996. Behavior of hafnium and neodymium isotopes in the crust: constraints from Precambrian crustally derived granites. *Geochimica Cosmochimica Acta* **60**, 3717–3733.

Watson, E. B. and Harrison, T. M. (1983). Zircon saturation revisited: temperature and composition effects in a variety of crustal magma types. *Earth and Planetary Science Letters* **64**, 295-304.

Wenrich, K.J., Billingsley, G.H., and Blackerby, B.A., 1995. Spatial migration and compositional changes of Miocene-Quaternary magmatism in western Grand Canyon. *Journal of Geophysical Research* **100**, 10417-10440.

White, W.M., Albarède, F., and Telouk, P., 2000. High-precision analysis of Pb isotope ratios by multi-collector ICP-MS. *Chemical Geology* **167**, 257–270.

Wooden, J.L. and Miller, D.M., 1990. Chronologic and isotopic framework for early Proterozoic crustal evolution in the eastern Mojave Desert region, SE California. *Journal of Geophysical Research* **95**, 20133-20146.

Young, R.A. and Brennan, W.J., 1974. Peach Springs Tuff: its bearing on structural evolution of the Colorado Plateau and development of Cenozoic drainage in Mohave County, Arizona. *Geological Society of America Bulletin* **85**, 83-90.